UC San Diego

UC San Diego Electronic Theses and Dissertations

Title

Regulation of GPCR-Mediated Inflammatory Signaling by Deubiquitinases

Permalink

https://escholarship.org/uc/item/3h19x641

Author

Cheng, Norton

Publication Date

2024

Supplemental Material

https://escholarship.org/uc/item/3h19x641#supplemental

Peer reviewed|Thesis/dissertation

eScholarship.org Powered by the California Digital Library
University of California

UNIVERSITY OF CALIFORNIA SAN DIEGO

Regulation of GPCR-Mediated Inflammatory Signaling by Deubiquitinases

A Dissertation submitted in partial satisfaction of the requirements
for the degree Doctor of Philosophy

in

Biomedical Sciences

by

Norton Cheng

Committee in charge:

Professor JoAnn Trejo, Chair
Professor Eric J. Bennett
Professor Tracy M. Handel
Professor Jin Zhang

2024

Copyright

Norton Cheng, 2024

All rights reserved.

The Dissertation of Norton Cheng is approved, and it is acceptable in quality and form for publication on microfilm and electronically.

University of California San Diego

2024

DEDICATION

This dissertation is dedicated to my parents, Roc and Jennifer, for their continuous support and guidance. They have been there for me since the moment I decided to pursue this long and challenging path. I would not be able to reach this far without them and I hope that I have made them proud.

I would also like to dedicate this work to my husband, Keng-Chi, for being an example of perseverance, determination, and an outstanding academic. He is one of the people that I look up to. It has been a truly memorable journey through this PhD with him.

This work is also dedicated to the memories of my grandmother, Hui-Fang. Although she could not witness where I am and what I have managed to achieve, I believe that she would be the person who cheered the loudest had she stayed longer with us.

TABLE OF CONTENTS

DISSERTATION APPROVAL PAGE iii

DEDICATION iv

TABLE OF CONTENTS v

LIST OF FIGURES vii

LIST OF TABLES ix

LIST OF SUPPLEMENTAL FILES x

LIST OF ABBREVIATIONS xi

ACKNOWLEDGEMENTS xiii

VITA xv

ABSTRACT OF THE DISSERTATION xvi

INTRODUCTION 1

GPCR posttranslational modifications and endosomal signaling 1

Ubiquitination and deubiquitination of substrate proteins 2

General roles of DUB in cellular signal transduction and Regulation of DUBs 3

DUBs regulate GPCR trafficking 5

DUBs regulate GPCR signaling at endosomes 6

Chapter 1 AN SIRNA LIBRARY SCREEN IDENTIFIES CYLD AND USP34 AS DEUBIQUITINASES THAT REGULATE GPCR-STIMULATED P38 MAPK SIGNALING AND DISTINCT INFLAMMATORY RESPONSES 11

Abstract 11

Introduction 12

Results 14

Discussion 23

Figures 28

Material and Methods 41

Acknowledgements 46

Supplemental Information 47

Chapter 2 USP34 REGULATES ENDOTHELIAL PAR1 MRNA TRANSCRIPT EXPRESSION AND CELLULAR SIGNALING 51

Abstract 51

Introduction 51

Results 54

Discussion 59

Figures 63

Material and Methods 75

Acknowledgements 83

Supplemental Information 84

Chapter 3 CYLD DEUBIQUITINASE REGULATES ENDOTHELIAL PAR1 UBIQUITINATION AND SIGNALING 90

Introduction 90

Results 91

Discussion 99

Figures 102

Material and Methods 111

Acknowledgements 119

Supplemental Information 120

Chapter 4 CONCLUSIONS 131

REFERENCES 134

LIST OF FIGURES

Figure 1-1. An siRNA library screen identifies nine DUBs that regulate thrombin-stimulated p38 signaling. 28

Figure 1-2. A subset of DUBs regulate thrombin-stimulated p38 MAPK signaling over time. 30

Figure 1-3. DUB mRNA expression, protein domains and phosphorylation sites. 32

Figure 1-4. DUB candidate subcellular localization. 33

Figure 1-5. Depletion of CYLD, USP34 and USP47 by individual SMART pool siRNAs alter thrombin-induced p38 phosphorylation. 34

Figure 1-6. Depletion of CYLD or USP34 using multiple individual siRNAs enhance thrombin-stimulated p38 phosphorylation but not ERK1/2 phosphorylation. 36

Figure 1-7. Depletion of CYLD but not USP34 enhances thrombin-induced endothelial barrier permeability. 38

Figure 1-8. Thrombin-induced IL-6 expression is differentially regulated by CYLD and USP34. 39

Figure 1-9. Model of thrombin-activated PAR1 ubiquitin-driven p38-mediated inflammatory signaling regulation by CYLD versus USP34. 40

Figure 2-1. Knockdown of USP34 increases thrombin-induced p38 phosphorylation. 63

Figure 2-2. USP34 is a nucleus- and cytoplasm-residing protein in endothelial EA.hy926 cells. 65

Figure 2-3. Loss of USP34 does not alter expression and ubiquitination of the key components mediating PAR1-p38 signaling. 67

Figure 2-4. Knockdown of USP34 significantly increases PAR1 cell surface expression but does not affect PAR1 constitutive internalization or agonist-induced endocytosis rate. 69

Figure 2-5. Knockdown of USP34 upregulates PAR1 protein expression but does not alter PAR1 ubiquitination. 70

Figure 2-6. Loss of USP34 does not affect PAR1 basal degradation. 72

Figure 2-7. Loss of USP34 significantly upregulates PAR1 mRNA expression. 73

Figure 2-8. Hypothesized model describing regulation of PAR1 signaling by USP34. 74

Figure 3-1. CYLD regulates thrombin-induced, PAR1-stimulated p38 signaling. 102

Figure 3-2. CYLD does not regulate PAR1 surface expression or internalization. 104

Figure 3-3. CYLD does not regulate PAR1-stimulated p38 pathway components expression, but may modulate post-translational modifications of TAB1. 105

Figure 3-4. CYLD regulates thrombin-induced PAR1 ubiquitination without modulating PAR1 protein abundance. 107

Figure 3-5. CYLD is localized to cytoplasm in endothelial cells and may interact with PAR1. 108

Figure 3-6. Thrombin induced phosphorylation of p38 kinase activity biosensors at endosomes and nuclei. 109

Supplemental Figure 1-1. HeLa cell DUB siRNA library screen immunoblots of thrombin-stimulated p38 phosphorylation. 47

Supplemental Figure 1-2. Endothelial EA.hy926 cells DUB siRNA library screen immunoblots of thrombin-stimulated p38 phosphorylation. 48

Supplemental Figure 3-1. TAB1 post-translational modification. 120

Supplemental Figure 3-2. PerKy-EV p38 activity biosensor was phosphorylated when stimulated by thrombin. 121

Supplemental Figure 3-3. CYLD may regulate p38 kinase activity at endosomes. 122

LIST OF TABLES

Table 0.1. DUBs that regulate GPCR trafficking and Signaling 10

Supplemental Table 1-1. ANOVA results 49

Supplemental Table 2-1. ANOVA results for Figure 2-1 84

Supplemental Table 2-2. Multiple linear regression models for Figure 2-4 85

Supplemental Table 2-3. ANOVA results for Figure 2-5 87

Supplemental Table 2-4. Student's t test result and multiple linear regression model for Figure 2-6 88

Supplemental Table 2-5. ANOVA results for Figure 2-7 89

Supplemental Table 3-1. ANOVA results for Figure 3-1. 123

Supplemental Table 3-2. ANOVA results for Figure 3-2. 126

Supplemental Table 3-3. ANOVA results for Figure 3-3. 128

Supplemental Table 3-4. ANOVA results for Figure 3-4. 130

LIST OF SUPPLEMENTAL FILES

Supplemental File 1. Original quantification of DUB siRNA library screen in HeLa cells.
Supplemental File 2. Original quantification of DUB siRNA library screen in Ea.hy926 cells.

LIST OF ABBREVIATIONS

ANOVA	Analysis of variance
BSA	Bovine serum albumin
CHX	Cycloheximide
CRISPR	Clustered regularly interspaced short palindromic repeats
Ct	Cycles until threshold
CYLD	Cylindromatosis
DMSO	Dimethyl sulfoxide
DUB	Deubiquitinase
ECIS	Electric cell-substrate impedance sensing
EEA1	Early endosome antigen 1
ERK	Extracellular signal-regulated kinase
ESCRT	Endosomal sorting complexes required for transport
FDA	US Food & Drug Administration
FRET	Förster resonance energy transfer
GAPDH	Glyceraldehyde 3-phosphate dehydrogenase
GPCR	G protein-coupled receptor
HRP	Horseradish peroxidase
HUVEC	Human umbilical-vein endothelial cell
IL	Interleukin
LAMP1	Lysosomal associated membrane protein 1
MAPK	Mitogen-activated protein kinase
mRNA	Messenger RNA

NA	Numerical aperture
NEDD4-2	Neural precursor cell expressed developmentally down-regulated 4-like
NS (ns)	Non-specific, or not significant
NLS	Nuclear localization signal(s)
OD	Optical density
PAR	Protease-activated receptor
PBS	Phosphate-buffered saline
PCR	Polymerase chain reaction
PTM	Posttranslational modification
RT-qPCR	Real-time quantitative polymerase chain reaction
S.D.	Standard deviation
SDS-PAGE	Sodium dodecyl sulfate-polyacrylamide gel electrophoresis
siRNA	Small interfering ribonucleic acid
TAB	Transforming growth factor-β-activated protein kinase-1-binding protein
TF	Transcription factor
Th	Thrombin
TBST	Tris-buffered saline with Tween-20
TUBE	Tandem ubiquitin-binding entities
USP	Ubiquitin-specific protease

ACKNOWLEDGEMENTS

This work would not have seen the light of day without the mentorship from my mentor, Dr. JoAnn Trejo. I started my PhD program with an expectation that it would be as difficult as crossing a stormy sea, but JoAnn is an experienced captain who showed me how to read the currents and waves, and how to work with the crew. I have been able to grow as a scientist with her support and I feel fortunate to have such a great mentor that paid close attention to my training during the first phase of this journey and provided tailored mentorship when I gradually became more independent.

I would like to also acknowledge the lab members, who are instrumental in helping me to learn the way of science and to enjoy life both inside and outside of the laboratory. They created a space where I feel safe and included. I would like to particularly thank Helen, Mika, and Oye: we shared many wonderful moments and inspiring conversations, and they fueled me through this journey.

My thesis committee members, Drs. Eric Bennett, Tracy Handel, and Jin Zhang, have also been supportive by providing useful feedbacks and warm encouragement. I also would like to thank the Biomedical Sciences Graduate Program and Pharmacology Department for their continuous support. UCSD Pharmacology Training Grant, NHLBI Predoctoral NRSA Fellowship, and SHORE program also played vital roles in the completion of my PhD.

The introduction, in part, is currently being prepared for submission for publication of the material. Norton Cheng, Julio M. Pimentel and JoAnn Trejo. The dissertation author was the primary investigator and author of this paper.

Chapter 1, in full, is a reprint of the material as it appears in Journal of Biological Chemistry. Norton Cheng, JoAnn Trejo, Elsevier Inc, 2023. The dissertation author was the

primary investigator and author of this paper.

Chapter 2, in part, is currently being prepared for submission for publication of the material. Norton Cheng, Monica L. Gonzalez Ramirez, Chloe Edwards and JoAnn Trejo. The dissertation author was the primary investigator and author of this paper.

VITA

2014 Bachelor of Science in Life Sciences, National Chung Hsing University

2016 Master of Science in Life Science, National Taiwan University

2024 Doctor of Philosophy in Biomedical Sciences, University of California San Diego

PUBLICATIONS

Rahajeng, J., Kuna, R. S., Makowski, S. L., Tran, T. T. T., Buschman, M. D., Li, S., **Cheng, N.**, Ng, M. M., and Field, S. J. (2019) Efficient Golgi Forward Trafficking Requires GOLPH3-Driven, PI4P-Dependent Membrane Curvature. *Developmental Cell*. **50**, 573-585.e5

Patwardhan, A., **Cheng, N.**, and Trejo, J. (2021) Post-Translational Modifications of G Protein–Coupled Receptors Control Cellular Signaling Dynamics in Space and Time. *Pharmacological Reviews*. **73**, 120–151

Molinar-Inglis, O., Wozniak, J. M., Grimsey, N. J., Orduña-Castillo, L. B., **Cheng, N.**, Lin, Y., Ramirez, M. L. G., Birch, C. A., Lapek, J. D., Gonzalez, D. J., and Trejo, J. (2022) Phosphoproteomic analysis of thrombin- and p38 MAPK-regulated signaling networks in endothelial cells. *Journal of Biological Chemistry*. 10.1016/j.jbc.2022.101801

Cheng, N., and Trejo, J. (2023) An siRNA library screen identifies CYLD and USP34 as deubiquitinases that regulate GPCR-p38 MAPK signaling and distinct inflammatory responses. *Journal of Biological Chemistry*. 10.1016/j.jbc.2023.105370

Cheng, N., Pimentel, J. M., and Trejo, J. (2024). Ubiquitin-driven G protein-coupled receptor inflammatory signaling at the endosome. *American Journal of Physiology-Cell Physiology*. 10.1152/ajpcell.00161.2024

ABSTRACT OF THE DISSERTATION

Regulation of GPCR-Mediated Inflammatory Signaling by Deubiquitinases

by

Norton Cheng

Doctor of Philosophy in Biomedical Sciences

University of California San Diego, 2024

Professor JoAnn Trejo, Chair

Cardiovascular disease (CVD) is a leading cause of deaths in the United States, however the underlying inflammatory pathways that contribute to CVD are poorly understood. Endothelial dysfunction is a hallmark of CVD and induced by various inflammatory mediators, many of which signal through G-protein coupled receptor (GPCRs). Thrombin, an inflammatory mediator, is generated in response to vascular injury and disrupts endothelial barrier integrity and promotes

vascular leakage, a hallmark of inflammation. Thrombin activates endothelial protease-activated receptor-1 (PAR1) to disrupt endothelial barrier through the RhoA/myosin light chain (MLC) pathway. However, thrombin/PAR1-stimulated p38 mitogen-activated protein kinase (MAPK) signaling also promotes barrier permeability through a pathway that does not integrate with the RhoA/MLC signaling, suggesting that p38 acts through an uncharacterized pathway to promote inflammatory responses in endothelial cells. Our previous work showed that thrombin-activated PAR1 ubiquitination drives the recruitment of TAB2-TAB1 protein complexes on endosomes to trigger non-canonical p38 activation and endothelial barrier disruption. The mechanisms that regulate PAR1 ubiquitination/de-ubiquitination are not known. This proposal aims to understand the molecular processes that regulate PAR1-ubiquitin-driven p38 signaling and most importantly its impact on endothelial barrier integrity. The central hypothesis is that de-ubiquitination of PAR1 leads to termination of p38-mediated pro-inflammatory signaling. Using advanced biochemical, microscopy and genome-wide RNAi screening methods, we for the first time investigate molecular determinants that regulate the dynamics of PAR1-ubiquitination and the impact on endothelial proinflammatory responses *in vitro* using human endothelial cells. We reveal new information regarding the function of PAR1 ubiquitination in driving non-canonical endosomal p38 MAPK signaling in endothelial barrier disruption, a hallmark of inflammation, which will provide an opportunity for the development new strategies for the treatment of inflammatory responses associated with CVD.

INTRODUCTION

GPCR posttranslational modifications and endosomal signaling

G protein-coupled receptors (GPCRs) are a large family of cell surface receptors in the mammalian genome that participate in many physiological functions (1,2). Dysregulation of GPCR signaling is linked to human diseases and caused by gain of function resulting in overabundance of signaling, or loss of function causing a deficiency in signaling. The critical role and function of GPCRs in normal physiology and disease combined with unique receptor structural attributes has advanced the status of GPCRs as therapeutic targets. GPCRs currently represent 34% of all Food and Drug Administration approved drugs (3,4).

Significant advances in knowledge of GPCR structure and pharmacology have occurred over the past decades, however the mechanisms that regulate GPCR signaling remain poorly characterized, especially the contribution of posttranslational modifications. GPCR posttranslational modifications control the spatial and temporal aspects of receptor signaling from the cell surface and intracellular compartments and are critical for eliciting proper cellular responses (5). A vast literature has revealed fundamental roles for phosphorylation in regulating GPCR signaling and trafficking (5), however far less is known about ubiquitination. Posttranslational modification of proteins with ubiquitin is a highly complex and dynamic process that controls protein degradation and numerous non-proteolytic critical cellular activities like cellular signaling (5,6). As expected, several early studies established a role for ubiquitination in GPCR trafficking within the endosomal-lysosomal pathway and proteasomal degradation (7-10). However, new emerging studies have directly linked GPCR ubiquitination to signaling from endosomes (11-15). Ubiquitination is a reversible and dynamic process balanced by the covalent attachment of ubiquitin to substrate proteins mediated by ubiquitin modifying enzymes with

deubiquitinases (DUBs), enzymes that remove ubiquitin from substrate proteins (16-20). In this introductory chapter, we discuss recent advances in our understanding of the role of ubiquitination in regulation of GPCR trafficking and signaling with an emphasis on DUBs, key regulatory proteins that control the dynamics of protein ubiquitination.

Ubiquitination and deubiquitination of substrate proteins

Substrate ubiquitination occurs through formation of an isopeptide bond between a lysine (K) residue of a substrate protein and the C-terminal glycine residue of the 76 amino acid ubiquitin protein (21). The covalent linkage of ubiquitin to substrate proteins is a multistep, highly regulated process that involves sequential actions of three distinct ubiquitin modifying enzymes (22). They include the ubiquitin-activating (E1), conjugating (E2), and several hundred E3 ligase enzymes, which modify proteins at different lysine residues through attachment of one ubiquitin moiety (mono-ubiquitination) or with multiple ubiquitins (poly-ubiquitination) at different sites generating branched or mixed ubiquitin chains (22-24). Ubiquitin conjugation occurs most frequently at lysines, however non-lysine residues, such as methionine, cysteine, serine, and threonine, can also be ubiquitinated (25). The type and abundance of ubiquitination dictates its' function. For example, modification of proteins with K48-linked ubiquitin is known to target proteins for proteasomal degradation (22-24,26-28), whereas K63-linked ubiquitination mediates protein-protein interaction that can trigger signaling cascades, like the nuclear factor-kB (NF-kB) and p38 mitogen-activated protein kinase (MAPK) pathways, induce autophagy and regulate receptor trafficking (29-31).

Ubiquitination and deubiquitination control important physiological functions and dysregulation of ubiquitination is associated with human disease including cancer, inflammatory and neuronal disorders (31-34). Deubquitination is catalyzed by a family of deubiquitinating

enzymes or deubiquitinases (DUBs) which cleave peptide bonds or isopeptide bonds between linked ubiquitin or between ubiquitin and substrate proteins (20). DUBs also maintain homeostasis of the cellular ubiquitome by cleaving newly synthesized linear ubiquitin chains to replenish the cellular ubiquitin pool (35). There are approximately one hundred DUBs expressed in the human genome that can be grouped into seven subfamilies (36-38). DUB subfamilies include the ubiquitin-specific proteases (USPs), ubiquitin C-terminal hydrolases (UCHs), ovarian tumor proteases (OTUs), Machado-Josephin domain proteases (MJDs), JAB1/MPN+/MOV34 (JAMM) domain proteases, monocyte chemotactic protein-induced proteins (MCPIPs), and motif interacting with ubiquitin-containing DUB family (MINDY) (36-38). DUBs have cellular functions that involve removing, editing, and recycling ubiquitin from substrate proteins (39). Deubiquitination also serves to rescue proteins destined for ubiquitin-mediated degradation and modulates protein-protein interactions important cellular signaling and protein trafficking, which is relevant to GPCR biology.

General roles of DUB in cellular signal transduction and Regulation of DUBs

DUBs regulate a number of biological processes, the most important of which are gene expression and protein subcellular localization (40-43). To accomplish this, DUBs supply ubiquitin monomers to ubiquitin enzymes, which they obtain by deubiquitinating proteins and replenish the free ubiquitin pool (35,44). Some of these ubiquitinated proteins are then translocated into endosomes, where they combine with lysosomes and are destroyed (45-47). However, some DUBs, including RPN11 and USP8, can deubiquitinate proteins and rescue them from endosomal degradation (35,41,48-50). This includes surface receptors and Rab small G proteins, such as USP8 and USP32 have been shown to regulate the trafficking of EGFRs and Rab7, respectively. Thus, these features underline the importance of DUBs as mediators of protein trafficking and cell

surface receptor expression in cells (40-43,51,52).

DUBs also have a role in regulating gene and protein expression, as indicated by their ability to regulate DNA damage repair and protein translation pathways (53-59). Consequently, these crucial pathways can be linked to other key signaling pathways regulated by DUBs. They include the NF-κB (CYLD, A20, OTUD7B, USP11, USP15), TGFβ (USP9X. UCHL-5), HIPPO (DUB3, USP9X, USP21, OTUB2, OTUD1), WNT (USP15, USP4), and p53 (USP7) signaling pathways (60-80). In addition, earlier research has revealed that the location of a DUB, whether free in the cytosol and nucleus or bound to organelles, might influence its regulation on the aforementioned pathways. USP30, for example, contains a mitochondrial targeting motif for the outer membrane of the mitochondria (81,82). This motif allows it to be drawn to the mitochondria, where it deubiquitinates the substrates of Parkin-mediated mitophagy and inhibits it (81,82). In contrast, USP19 can be expressed in the endoplasmic reticulum (ER), where it can rescue substrates from ER-associated degradation (ERAD) during skeletal muscle catabolism (83,84).

Because DUBs are required for many physiological functions, their activity is regulated by several molecular mechanisms. These include post-translational modifications such as phosphorylation, ubiquitination, and SUMOylation (85-89). Phosphorylation is generally recognized to activate several DUBs, including A20, OTUD5, USP1, USP14, USP16, and USP37, although it inhibits the activation of CYLD and USP8 (87-98). In addition, phosphorylation may affect the subcellular localization of several DUBs. OTUB16, USP10, and ATXN3 are examples of proteins that become phosphorylated and translocate from the cytosol to the nucleus, while USP4 does the reverse (99-102). Some DUBs, however, have been found to regulate their own activity through ubiquitin and auto-deubiquitination (85,86,103,104). UCH-L1 and USP30, for example, are monoubiquitinated, which prevents them from activating. Other examples include

the auto-deubiquitination and activation of USP25 and BAP1, which causes BAP1 to translocate to the nucleus from the cytoplasm (85,86,103-105). Similarly, the ubiquitin-like protein SUMO binds to and inhibits the activation of USP25, USP28, and CYLD (106,107). Still, it is unclear whether SUMOylation activates DUBs as much as phosphorylation and ubiquitination (106,107). Furthermore, DUBs binding to regulatory proteins may amplify the effects of the previous post-translational modifications, resulting in greater function or substrate affinity (108,109). This is evidenced by USP1, USP2, USP12, and USP46 interacting with the WD40-repeat protein (WDR48), resulting in increased protein deubiquitination (108,109). E3 ubiquitin ligases, such as SIAH1 and SIAH2, can also affect the expression of DUBs, including USP19 (110). Despite recent breakthroughs in understanding the role and regulation of DUBs, additional research is still needed to fully understand their function and regulation.

DUBs regulate GPCR trafficking

Previous studies have documented roles for DUBs in regulating GPCR trafficking as discussed in a comprehensive review on GPCR posttranslational modifications (5) and summarized below. Deubiquitination of the adenosine A_{2A} receptor by USP4 (111) was reported to enhance transport to through the endoplasmic reticulum and surface expression, whereas deubiquitination of the Frizzled-4 receptor by USP8 increased recycling and surface expression (112). USP33 and USP20 were shown to deubiquitinate agonist-activated β1- and β2-adrenergic receptors rescuing the receptor from lysosomal degradation by promoting recycling (113-116). Similarly, deubiquitination of protease-activated receptor-2 (PAR2) by USP8, also known as ubiquitin isopeptidase Y, and associated molecule with the SH3 domain of STAM (AMSH) slowed lysosomal degradation (117). USP14 was demonstrated to deubiquitinate the metabotropic $GABA_B$ receptor (118) and to regulate the ubiquitination status of the chemokine receptor CXCR4

(119) resulting in accelerated lysosomal degradation of the former, yet prevents agonist-induced degradation of the latter. In addition, USP8 appeared to regulate CXCR4 lysosomal degradation indirectly by altering ubiquitination of a component of the endosomal sorting complex required for transport (ESCRT)-0 machinery (120). A more recent study showed that agonist-activated ubiquitinated glucagon receptors undergo deubiquitination at endosomes by two DUBs, USP33 and signal transduction adaptor molecule binding protein (STAMBP), also known as AMSH, which enhanced glucagon receptor recycling via a Rab4a-dependent pathway (14). Collectively these studies provide evidence that certain DUBs and deubiquitination function as key regulators of GPCR trafficking (see **Table 0.1**), based on a candidate approach surveying one or small subset of DUBs to identify the critical functional DUB. Given the ubiquitous nature of protein ubiquitination, most if not all GPCRs are likely to be ubiquitinated at least once during their lifetime. A major challenge is to employ unbiased approaches to identify DUBs that function specifically to control GPCR biology in physiologically relevant cellular contexts.

DUBs regulate GPCR signaling at endosomes

In parallel to the canonical G protein-mediated signaling transduction modules from plasma membrane, some GPCR has also been found to mediate signaling at the endosomes (121,122). Several DUBs have established roles in regulating GPCR ubiquitination and endosomal-lysosomal trafficking (see **Table 0.1**), whereas DUB may also play unique roles in GPCR endosomal signaling. For instance, USP8 has emerged as an important DUB for endosomal regulation. USP8 has been shown to deubiquitinate GPCRs and growth factor receptors enhancing endosomal recycling (112,117,120,123) and endosomal resident ESCRT protein components (124), but Endo *et al.* recently showed that depletion of USP8 caused pronounced accumulation of K63-linked ubiquitin chains on early endosomes leading to the recruitment of transforming growth

factor-β-activated protein kinase-1-binding protein-2 (TAB2), TAB3 and p62 K63-linked ubiquitin-binding proteins and downregulation of ESCRT proteins (125). USP8 depletion further increased signaling by transforming growth factor-β-activated kinase 1 (TAK1), p38 MAPK and NF-kB, that was dependent on the ubiquitin binding capacity of TAB2, since a mutant TAB2 not able to bind K63-linked ubiquitin failed to activate the signaling pathways. Although the role of USP8 in regulating GPCR endosomal signaling has not been fully explored, this study supports the notion that DUBs function as key regulators of endosomal signaling induced by multiple receptor types including GPCRs.

A new study by Kaur *et al.* demonstrated that ubiquitination and deubiquitination of the glucagon receptor controls signal bias (15). A mutant glucagon receptor deficient in ubiquitination exhibited diminished G_S protein coupling and downstream signaling, whereas the ubiquitin deficient mutant receptor displayed enhanced β-arrestin recruitment and p38 MAPK activation. Ubiquitin-deficient glucagon receptor preferential activation of p38 MAPK signaling was similarly observed in a physiologically relevant B-cell line. The ubiquitously expressed β-arrestin-1 and -2 isoforms are multifunctional adaptor proteins that promote GPCR desensitization, internalization and function as signaling scaffolds and display redundant functions (126). However, the β-arrestin-1 isoform appears to function preferentially to regulate glucagon receptor-induced p38 MAPK activation via the canonical three-tiered kinase cascade. Ubiquitin-deficient glucagon receptor internalization and colocalization with β-arrestin-1 on endosomes was also enhanced and exhibited prolonged p38 MAPK signaling compared to wildtype receptor. Interestingly, neither β-arrestin-1 or -2 are required for glucagon receptor recruitment of USP33 or STAMBP, the DUBs that mediate glucagon receptor deubiquitination at the endosome (14). Together these data suggest that ubiquitination precludes glucagon receptor-stimulated β-arrestin-

1-dependent p38 MAPK signaling, which may occur at the endosome.

Unlike the glucagon receptor, we showed that ubiquitination of a subset of endogenous GPCRs expressed in endothelial cells drives p38α MAPK activation on endosomes via a non-canonical pathway. This is best exemplified by protease-activated receptor-1 (PAR1), a GPCR for thrombin, and the purinergic P2Y1 receptor (11,13,127). Agonist induced K63-linked ubiquitination of PAR1 mediated by the NEDD4-2 E3 ligase, initiates ubiquitin-driven recruitment of TAB2 (12,13). TAB2 co-associates with TAB1 on endosomes (13,128). And TAB1 binds directly to p38α MAPK isoform promoting a conformational change resulting in autophosphorylation and activation (129,130). Ubiquitin-driven GPCR stimulated p38 MAPK signaling has been linked to endothelial barrier disruption and cytokine interleukin-6 (IL-6) induction *in vitro* and vascular leakage *in vivo* (11,131).

Like other target proteins, GPCR ubiquitination is dynamic and regulated by DUBs. We hypothesized that deubiquitination is an important step for turning off GPCR-induced ubiquitin-driven p38 MAPK endosomal signaling. In this dissertation, I conducted an unbiased siRNA library screen targeting 96 DUBs in different cell types to identify the physiologically relevant DUBs that control GPCR-p38 MAPK endosomal signaling and inflammatory responses (132). The dual screens resulted in the identification of two DUBs, cylindromatosis (CYLD) and USP34, that specifically regulated thrombin-activated PAR1-stimulated p38 MAPK signaling in endothelial and HeLa cells. Moreover, CYLD depletion by siRNA not only enhanced thrombin/PAR1-stimulated p38 MAPK signaling, but also increased endothelial barrier permeability and IL-6 cytokine production. Interestingly, depletion of USP34 expression increased thrombin/PAR1-promoted p38 MAPK activation, whereas loss of UPS34 diminished IL-6 cytokine production and had no effect on endothelial barrier integrity. This study indicates that

different DUBs distinctly regulate GPCR-p38 MAPK induced inflammatory responses. The mechanisms by which CYLD and USP34 differentially regulate thrombin/PAR1-induced p38 MAPK mediated inflammatory responses is not known. Here, I also show that USP34 plays a role in negatively regulating PAR1 surface expression via regulating *F2R* transcript expression. Along with other observations showing USP34 depletion affects *IL-6* and *F2RL1* mRNA expression, I propose that USP34 may be involved in the regulation mechanisms of transcription factor activity or chromatin remodeling. Lastly, I show that CYLD may be responsible for regulating PAR1 ubiquitination, which is critical in understanding how ubiquitin regulates GPCR signaling and its physiological relevance in endothelial dysfunction.

Table 0.1. DUBs that regulate GPCR trafficking and Signaling

DUB Name	GPCR Name (GPCRdb)	Mechanism	Regulated Pathway(s)/Function(s)	Note
AMSH	PAR2	Deubiquitination of receptor	Lysosomal degradation and signaling (117)	
	Glucagon receptor	Deubiquitination of receptor	Agonist-induced recycling (14)	AMSH is also known as STAMBP
A20	μ receptor	Interaction with β-arrestin-2	Agonist-induced endocytosis (133)	
USP4	A_{2A} receptor	Deubiquitination of receptor	ER transport and surface expression (111)	
USP8	FZD_4	Deubiquitination of receptor	Receptor recycling and surface expression (112)	
	PAR2	Deubiquitination of receptor	Lysosomal degradation and signaling (117)	USP8 is also known as UBPY
	CXCR4	Regulation of ESCRT-0 ubiquitination	Lysosomal degradation and signaling (120)	
	MT_1 receptor	Unknown	Lysosomal degradation (62)	
	V_{1B} receptor	Regulation of receptor gene promoter	Receptor mRNA expression (134)	V_{1B} receptor is also known as AVPR1B
USP14	$GABA_{B1}$	Deubiquitination of receptor	Lysosomal degradation (118)	
	CXCR4	Interaction with receptor, regulation of receptor ubiquitination	Agonist-induced degradation and signaling (119)	
USP20	β1-adrenoceptor	Deubiquitination of receptor	Lysosomal degradation and signaling (116)	
	β2-adrenoceptor	Deubiquitination of receptor	Lysosomal degradation and recycling (114,115)	
USP33	β2-adrenoceptor	Deubiquitination of receptor	Lysosomal degradation and recycling (114)	
USP48	MrgC	Deubiquitination of receptor	Lysosomal degradation (135)	MrgC is a mouse GPCR. Human and mouse USP48 share >90% amino acid sequence homology.

Chapter 1 AN SIRNA LIBRARY SCREEN IDENTIFIES CYLD AND USP34 AS DEUBIQUITINASES THAT REGULATE GPCR-STIMULATED P38 MAPK SIGNALING AND DISTINCT INFLAMMATORY RESPONSES

Abstract

G protein-coupled receptors (GPCRs) are highly druggable and implicated in numerous diseases including vascular inflammation. GPCR signals are transduced from the plasma membrane as well as from endosomes and controlled by post-translational modifications. Activation of the GPCR protease-activated receptor-1 (PAR1) by thrombin promotes ubiquitin-driven p38 mitogen-activated protein kinase (MAPK) signaling via recruitment of transforming growth factor-β–activated kinase-1–binding protein 2 (TAB2). TAB2 co-associates with TAB1 on endosomes, which triggers p38 MAPK-dependent inflammatory responses in endothelial cells. Other endothelial GPCRs also induce p38 activation via a non-canonical TAB1-TAB2 dependent pathway. However, the regulatory processes that control GPCR ubiquitin-driven p38 inflammatory signaling remains poorly understood. We discovered mechanisms that turn on GPCR ubiquitin-dependent p38 signaling, however, the mechanisms that turn off the pathway are not known. We hypothesize that deubiquitination is an important step in regulating ubiquitin-driven p38 signaling induced by GPCRs. To identify specific deubiquitinating enzymes (DUBs) that control GPCR-p38 MAPK signaling, we performed a siRNA library screen targeting 96 different DUBs in endothelial cells and HeLa cells. We identified nine DUBs and validated the function two DUBs including cylindromatosis (CYLD) and ubiquitin specific protease-34 (USP34) that specifically regulate thrombin-induced p38 MAPK activation. Depletion of CYLD expression by siRNA enhanced thrombin-stimulated p38 signaling, endothelial barrier permeability and increased interleukin-6 (IL-6) cytokine expression. Conversely, siRNA knockdown of USP34 expression decreased

thrombin-promoted IL-6 expression and had no effect on thrombin-induced endothelial barrier permeability. These studies suggest that specific DUBs distinctly regulate GPCR-induced p38 mediated inflammatory responses.

Introduction

G protein-coupled receptors (GPCRs) are a large family of cell surface receptors with broad functions in physiology and disease and the target of 34% of FDA approved drugs (136,137). Recent advances in GPCR structure and pharmacology have been significant. However, an aspect of GPCR regulation that remains poorly understood is the role of post-translational modifications. Phosphorylation is well studied and critical for controlling GPCR signaling and trafficking via recruitment of the multifunctional β-arrestin-1 and 2 adaptor proteins (1). In addition to phosphorylation, ubiquitination has been implicated in regulation of GPCR signaling and trafficking (1). Like phosphorylation, ubiquitination is typically inducible and a reversible process. However, there is a limited understanding of how ubiquitination controls GPCR signaling.

Protein ubiquitination is best known to target proteins for degradation via the 26S proteasome and lysosome (138). Ubiquitin is covalently linked to lysine residues of substrate proteins through the sequential action of E1, E2 and E3 ubiquitin modifying enzymes. While proteins are predicted to be modified with ubiquitin at least once during their lifetime, ubiquitination has been studied only for a small subset of approximately forty GPCRs (1,139,140). In most studies, ubiquitin has been linked to GPCR endosomal-lysosomal trafficking or to the proteasome for degradation (141-143). However, emerging studies indicate that for certain GPCRs, ubiquitin promotes direct interaction with signaling effectors (144). Thus, the function of ubiquitination may vary depending on the GPCR, cell type and physiological function.

Several studies have examined the role of ubiquitin in propagating GPCR signaling from

the plasma membrane (145,146). We showed that agonist stimulation of a subset of endothelial GPCRs promotes ubiquitin-dependent p38 mitogen-activated protein kinase (MAPK) activation on endosomes via a non-canonical pathway (144,147,148). Activation of the GPCR protease-activated receptor-1 (PAR1) by thrombin induces ubiquitin-dependent recruitment of transforming growth factor-β-activated protein kinase-1 binding protein-2 (TAB2), which associates with TAB1 (144,148,149). TAB1 binds directly to the p38α isoform inducing a conformational change resulting in autophosphorylation and activation (150,151). The ubiquitin-driven PAR1 signaling is specific to p38 MAPK, as thrombin activation of extracellular signal-regulated kinase-1/2 (ERK1/2) proceeds through the canonical three-tiered kinase cascade (144). Like PAR1, the purinergic P2Y1 receptor also promotes ubiquitin-driven p38 activation through a TAB1-TAB2-dependent pathway (144,147), indicating that this pathway is used by multiple GPCRs. Indeed, other GPCR agonists including histamine (H1 or H2 receptors) and prostaglandin E2 (EP4 prostanoid receptor) activate p38α through a non-canonical TAB1-dependent pathway in endothelial cells (147).

Ubiquitination is a reversible process and deubiquitination is important for governing ubiquitin-dependent cellular responses such as endocytic trafficking and cell signaling. The human genome encodes approximately 100 deubiquitinating enzymes (DUBs). DUBs serve multiple functions including removal of ubiquitin from protein substrates, which can rescue proteins from degradation or modulate signaling, ubiquitin chain editing and recycling of ubiquitin, which ensures that ubiquitin re-enters the ubiquitin cellular pool (152,153). Although ubiquitination is important for regulating GPCR signaling and trafficking, the role of DUBs in controlling GPCR signaling and the impact on biological functions remains poorly understood. In this study we employed an RNA interference library screen in two cell types to identify deubiquitinating

enzymes that specifically regulate thrombin-stimulated p38 MAPK signaling and endothelial inflammatory responses.

Results

An siRNA library screen identifies a subset of deubiquitinating enzymes that regulate GPCR p38 MAPK signaling

Thrombin activation of PAR1 triggers ubiquitin-driven p38 MAPK inflammatory signaling via a non-canonical TAB1-TAB2 dependent pathway on endosomes to promote endothelial barrier disruption (131,144,147) (**Figure 1-1**, A). Although mechanisms that turn on ubiquitin-driven GPCR-p38 signaling have been identified (148), the mechanisms that turn off non-canonical p38 signaling are not known. We hypothesize that deubiquitination is a key step in terminating ubiquitin-dependent p38 signaling induced by GPCRs. To identify DUBs that specifically regulate thrombin-stimulated p38 MAPK signaling, an siRNA library screen targeting 96 different mammalian DUBs was conducted in two different cell types including human umbilical-vein endothelial cells (HUVEC)-derived EA.hy926 cells and HeLa cells. Endothelial EA.hy926 cells express endogenous PAR1 (154,155), whereas PAR1 is stably expressed in HeLa cells (156). A siRNA specifically targeting the p38α MAPK isoform reduced p38 expression and blocked thrombin-stimulated p38 phosphorylation detected with a pan anti-phospho-p38 antibody in HeLa cells and endothelial cells (**Figure 1-1**, B and D), indicating that the p38α isoform is a major effector of thrombin signaling (131,157). A similar inhibitory effect on thrombin-induced p38 activation was observed with SB203580, an inhibitor of the p38α and β isoforms, consistent with autoactivation as shown in our previous studies (144,147) (**Figure 1-1**, B and C). These data indicate that thrombin induces p38α isoform signaling via autoactivation in endothelial cells and HeLa cells (131,144,147,157).

The DUB siRNA library screen workflow performed in endothelial and HeLa cells transfected with non-specific siRNA and 96 different SMARTpool siRNAs targeting human DUBs is illustrated in **Figure 1-1**, E. After transfection, cells were left untreated or treated with thrombin at a single time point and the induction of p38 phosphorylation was measured by immunoblotting, quantified, and analyzed (**Figure 1-1**, E). Nine siRNA SMARTpools targeting different DUBs known to cleave mono- or K63-linked ubiquitin markedly increased thrombin-induced p38 phosphorylation in endothelial and HeLa cells compared to non-specific siRNA control cells (**Figure 1-1**, F and G), suggesting that a subset of DUBs control thrombin-stimulated p38 signaling. Six of the DUBs including cylindromatosis (CYLD), ubiquitin specific protease (USP)34, USP51, USP47, OTU deubiquitinase 7A (OTUD7A), and ubiquitin domain containing 2 (UBTD2) regulated thrombin-p38 signaling in both cell types, whereas USP18 and BRCA1 associated protein 1 (BAP1) were effective in endothelial cells and josephin domain containing 1 (JOSD1) in HeLa-PAR1 cells (**Figure 1-1**, H). Data from the complete SMARTpool siRNA DUB library screen performed in endothelial cells and HeLa cells are shown in **Supplemental Figure 1-1** and **Supplemental Figure 1-2** and Supplemental File 1 and Supplemental File 2. To our knowledge this study is the first comprehensive siRNA library screen of all mammalian DUBs conducted to identify modulators of GPCR signaling.

A subset of DUBs regulate thrombin-stimulated p38 MAPK signaling over time

Deubiquitinating enzymes that specifically regulate thrombin-activated p38 MAPK inflammatory signaling have not been identified. To verify the specificity of SMARTpool siRNAs targeting the candidate DUBs at modulating thrombin-stimulated p38 signaling, a time course analysis in endothelial cells was performed. Endothelial cells were transfected with non-specific siRNA or SMARTpool siRNA targeting the nine candidate DUBs and then stimulated with or

without thrombin over a 20 min time course. PAR1- and p38α-specific siRNA and the SB203580 inhibitor were used as controls. Thrombin induced a marked increase in p38 phosphorylation detectable as early as 5 min that remained elevated at 7.5 and 10 min in non-specific siRNA transfected cells (**Figure 1-2**, A lane 1, B and D). However, siRNA-mediated depletion of p38α or PAR1 expression markedly reduced thrombin-stimulated p38 phosphorylation at various times compared to non-specific control siRNA, (**Figure 1-2**, A lanes 1 and 11-12 and B). A similar effect was observed in endothelial cells pretreated with the p38 inhibitor SB203580 (**Figure 1-2**, A lanes 1 and 13-14 and B). We predicted that depletion of a critical DUB by siRNA may modulate PAR1-induced p38 signaling through loss-of-function exhibited as no signaling or gain-of-function displayed as either increased signaling or sustained signaling compared to non-specific siRNA as illustrated in **Figure 1-2**, C. Analysis of the effect of DUB depletion by SMARTpool siRNA on thrombin-p38 signaling showed that loss of USP47, USP51, CYLD and USP34 expression resulted in a marked sustained increase in p38 signaling compared to non-specific siRNA (**Figure 1-2**, A lanes 1, 2, 5-7 and D). In addition, siRNA-mediated loss of CYLD expression increased the magnitude of thrombin-induced p38 activation compared to control non-specific siRNA transfected cells (**Figure 1-2**, A lanes 1, 6 and D). However, SMARTpool siRNA mediated depletion of OTUD7A, UBTD2, USP18, BAP1, and JOSD1 failed to alter thrombin-stimulated p38 signaling compared to siRNA control cells over time (**Figure 1-2**, A lanes 1, 3-4 and 8-10). These data indicate that four different DUBs may function to regulate thrombin-induced p38 signaling.

CYLD, USP34, USP47 and USP51 expression in endothelial and HeLa cells

To interrogate the function of candidate DUBs implicated in thrombin-induced p38 signaling, we first examined the expression of endogenous CYLD, USP34, USP47 and USP51 in

endothelial cells and HeLa cells quantitatively using RT-qPCR. USP34 exhibited the highest expression in endothelial cells and HeLa cells compared to the other DUBs (**Figure 1-3**, A and B). Considerable expression of USP47 and CYLD were also detected in both cell types (**Figure 1-3**, A and B). However, USP51 displayed the lowest expression compared to the other DUBs and was barely detectable in HeLa cells (**Figure 1-3**, A and B) and therefore eliminated from further analysis.

CYLD, USP34 and USP47 belong to the cysteine protease class of DUBs that utilize an active site cysteine (C) residue as part of a catalytic triad containing an adjacent histidine (H) and a third acidic residue within the USP domain to facilitate hydrolysis of ubiquitin linkages (**Figure 1-3**, C, D, and E). CYLD has been highly studied and contains two N-terminal cytoskeleton-associated protein glycine-rich domains, two proline-rich motifs, a mucosa-associated lymphoid tissue lymphoma translocation protein-1 (MALT1) cleavage site at arginine (R)-324 and a C-terminal USP domain that mediates preferential cleavage of K63- and methionine-1-linked ubiquitin (**Figure 1-3**, C). In contrast to CYLD, USP34 is a poorly characterized DUB that contains an N-terminal ubiquitin-like domain, two nuclear export signals and a C-terminal USP domain that cleaves K11-, K48- and K63-linked ubiquitin (**Figure 1-3**, D) (158). USP47 contains a N-terminal USP domain that cleaves K48- and K63-linked ubiquitin (**Figure 1-3**, E), like USP34.

DUB activity is controlled by relative abundance, protein-protein interaction and subcellular localization (159,160). DUBs are also regulated by post-translational modifications. Numerous phosphorylation sites have been identified in CYLD, USP34 and USP47 in discovery mass spectrometry studies reported on PhosphoSitePlus (161). The sites of phosphorylation with greater than ten reports are shown for CYLD, USP34 and USP47 (**Figure 1-3**, C, D and E). CYLD phosphorylation serine (S)418 and S422 sites are well documented in independent studies (89,162)

and shown in **Figure 1-3**, C. USP34 phosphorylation S718 and S1751 sites have been identified in HeLa cells (163), and are not shown in Fig 3, D, since there were less than 10 reports, whereas no additional USP47 phosphorylation sites have been identified. Intriguingly, only USP34 ubiquitination at a single site K1968 has been reported on PhosphoSitePlus and detected in twelve discovery mass spectrometry studies (**Figure 1-3**, D).

Next, we examined the subcellular localization of the candidate DUBs including CYLD, USP34 and USP47. In UniProt (164), CYLD has been reported to reside in several subcellular compartments depending on the cell type including the plasma membrane, cytoplasm in HEK293 cells (165) and cytoskeleton in ciliated epithelial cells (166) (**Figure 1-4**, A). In HeLa cells, endogenous CYLD localized to the cytoplasm with some detection in the nucleus (**Figure 1-4**, B). USP34 is reported to reside in the cytoplasm and nucleus in UniProt (**Figure 1-4**, C) and shown to regulate the cytoplasmic Axin protein, and Wnt/β-catenin signaling (167). USP34 also reported to localize to the nucleus in HeLa cells (168) (**Figure 1-4**, C). Consistent with these studies, we found that USP34 resides in the cytoplasm and nucleus in HeLa cells (**Figure 1-4**, D). USP47 has been shown to localize mainly in the cytoplasm in HeLa cells (169) (**Figure 1-4**, E). We also detected USP47 predominantly in the cytoplasm (**Figure 1-4**, E). These findings suggest that multiple regulatory processes including posttranslational modifications, protein-protein interactions and subcellular localization exist to control DUB activity.

Depletion of CYLD, USP34 and USP47 by single siRNAs alter thrombin-induced p38 MAPK signaling in endothelial cells

To examine the specificity of SMARTpool siRNAs, we separately examined the effect of the four individual siRNAs constituting the SMARTpools on thrombin-stimulated p38 phosphorylation over time. In non-specific siRNA transfected endothelial cells, thrombin promoted a marked increase in p38 phosphorylation at 7.5 min that decreased by 10 min and

returned to basal levels by 20 min (**Figure 1-5**, A lanes 1-4). Similarly, a substantial increase in p38 activation peaked at 7.5 min following thrombin stimulation in endothelial cells transfected with all three of the four CYLD siRNAs (**Figure 1-5**, A lanes 5-20). However, in cells transfected with CYLD siRNA #5, #7 and #8 thrombin-stimulated p38 signaling was enhanced and sustained compared to non-specific siRNA control (**Figure 1-5**, A lanes 1-8 and 13-20). The CYLD #5, #7 and #8 siRNAs effectively depleted cells of endogenous CYLD protein expression detected by immunoblot compared to control cells (**Figure 1-5**, A lanes 1-8 and 13-20). However, siRNA #6 failed to reduce CYLD expression and as expected thrombin-p38 signaling was comparable to control siRNA transfected cells (**Figure 1-5**, A lanes 9-12 versus 1-4). Moreover, depletion of CYLD with siRNAs #5, #7, #8 appeared to modestly enhance basal p38 phosphorylation compared to siRNA control cells (**Figure 1-5**, A lanes 1 versus 5, 13 and 17). Unlike CYLD, none of the four individual siRNAs targeting either USP34 or USP47 affected basal p38 phosphorylation in endothelial cells (**Figure 1-5**, B and C). However, USP34 siRNA #5 and USP47 siRNA #6 were found to alter thrombin-p38 signaling. Cells transfected with USP34 siRNA #5 showed a marked and sustained increase in p38 phosphorylation following thrombin stimulation compared to control cells (**Figure 1-5**, B lanes 1-8), and a considerable loss of endogenous USP34 expression detected by immunoblot (**Figure 1-5**, B lanes 1-8). Similarly, thrombin enhanced p38 phosphorylation in endothelial cells transfected with USP47 siRNA #6, which also showed diminished USP47 expression by immunoblot compared to non-specific siRNA treated control cells (**Figure 1-5**, C lanes 1-4 and 9-12). The individual siRNAs including CYLD #7, USP34 #5 and USP47 #6 were also validated by examining their capacity to specifically knockdown gene expression in endothelial and HeLa cells using RT-qPCR. Consistent with the loss of DUB expression detected by immunoblot, endothelial cells transfected with the individual DUB specific siRNAs showed

substantial decrease in CYLD, USP34 and USP47 mRNA expression compared to non-specific siRNA control (**Figure 1-5**, D). The individual DUB specific siRNAs caused a similar marked reduction in CYLD, USP34 and USP47 mRNA expression in HeLa cells (**Figure 1-5**, E). These data suggest that CYLD, USP34 and USP47 may function as key regulators of thrombin-stimulated p38 MAPK signaling.

Depletion of CYLD or USP34 with multiple individual siRNAs significantly increased thrombin-induced p38 phosphorylation but not ERK1/2 phosphorylation

To ensure the responses observed with the individual DUB siRNAs are specific and not due to off-target effects, we examined the effect of two individual siRNAs targeting CYLD, USP34 and USP47 on thrombin-stimulated p38 and ERK1/2 phosphorylation. In non-specific siRNA transfected HeLa cells, thrombin induced a marked increase in p38 phosphorylation (**Figure 1-6**, A, lanes 1-3), which was significantly enhanced in cells depleted of CYLD expression using siRNA #7 or #8 (**Figure 1-6**, A lanes 4-9). In contrast, thrombin stimulated a marked increase in ERK1,2 phosphorylation at 7.5 min in non-specific siRNA transfected cells (**Figure 1-6**, A lanes 1-3) that was comparable in CYLD deficient cells (**Figure 1-6**, A lanes 1-9). Thrombin-promoted a significant increase in p38 phosphorylation in cells depleted of USP34 using siRNA #5 but had no effect on ERK1/2 phosphorylation compared to non-specific siRNA transfected cells (**Figure 1-6**, B lanes 1-6). A similar effect was observed with USP34 siRNA #8 compared to non-specific siRNA control transfected cells (**Figure 1-6**, C lanes 1-6). Unlike CYLD and USP34, only USP47 siRNA #5 significantly enhanced thrombin-stimulated p38 phosphorylation without effecting the ERK1/2 phosphorylation response compared to non-specific siRNA transfected control cells (**Figure 1-6**, D lanes 1-6), whereas USP47 siRNA #6 failed to alter the thrombin-p38 response (**Figure 1-6**, D lanes 1-3 and 7-9). Moreover, USP47 siRNA #6

and not siRNA #5 appears to modulate thrombin-induced p38 signaling in endothelial cells (**Figure 1-5**, C lanes 1-12), opposite of that observed in HeLa cells. Given the potential off-target effects of USP47 SMARTpool siRNAs, the function of USP47 in thrombin-promoted p38 mediated responses was not further evaluated. Whereas two different individual siRNAs targeting CYLD or USP34 enhanced thrombin-p38 phosphorylation without altering ERK1/2 phosphorylation, suggesting that the siRNA effects are specific.

CYLD and not UPS34 preferentially regulates thrombin-stimulated endothelial barrier permeability

To determine impact of CYLD and USP34 on thrombin-mediated inflammatory responses, endothelial cells were transfected with validated CYLD #7 and USP34 #5 siRNA and endothelial barrier disruption was examined using electric cell-substrate impedance sensing (ECIS). ECIS measures the dynamics of endothelial barrier function in living cells, the maximum peak change in impedance (resistance) and barrier recovery. Endothelial EA.hy926 cells form cell-cell junctions that maintain barrier function (170). In these studies, endothelial cells were transfected with CYLD siRNA #7 or USP34 siRNA #5 verified above (**Figure 1-5** and **Figure 1-6**) and non-specific control siRNA. In control siRNA transfected cells, thrombin induced a rapid and significant 25% reduction in resistance (barrier function) that peaked at 20 min followed by return to baseline by 60 min. In contrast, thrombin caused a significantly greater 34% reduction in peak maximum resistance in endothelial cells deficient in CYLD expression compared to control siRNA transfected thrombin-stimulated cells (**Figure 1-7**, A and C lanes 1-6), consistent with enhanced p38 signaling that we previously reported to promote thrombin-induced barrier disruption (144). However, depletion of USP34 with siRNA #5 had no significant effect on thrombin-induced endothelial barrier disruption compared to non-specific siRNA treated control cells (**Figure 1-7**,

B and C lanes 1-3 and 7-12), despite altering thrombin stimulated p38 signaling (**Figure 1-5**, B, and **Figure 1-6**, B). These findings suggest that distinct DUBs differentially regulate thrombin-stimulated inflammatory responses (**Figure 1-7**, D).

CYLD and USP34 differentially regulate thrombin-induced IL-6 cytokine production

Several endothelial GPCRs including PAR1 induce production of IL-6, a potent inflammatory cytokine (171,172), which occurs through non-canonical TAB1-TAB2 activation of p38 signaling (147) (**Figure 1-8**, A). To determine the function of DUBs in thrombin-stimulated IL-6 production, endothelial cells were transfected with CYLD siRNA #7, USP34 siRNA #5 or non-specific siRNA and IL-6 gene induction was measured quantitatively by RT-qPCR. In non-specific siRNA transfected cells, a marked increase in IL-6 mRNA abundance was detected following 1 to 2 h of thrombin stimulation (**Figure 1-8**, B). In CYLD depleted cells (**Figure 1-8**, B), basal levels of IL-6 mRNA were significantly greater than non-specific siRNA transfected control cells (**Figure 1-8**, B). However, despite higher basal IL-6 mRNA, thrombin induced a significant increase in IL-6 mRNA production in CYLD depleted cells compared to non-specific siRNA control cells (**Figure 1-8**, B). In contrast to CYLD, the basal levels of IL-6 mRNA were significantly lower in cells depleted of USP34 expression (**Figure 1-7**, C and **Figure 1-8**, B) compared to non-specific siRNA transfected cells (**Figure 1-8**, B). Nonetheless, thrombin caused a modest increase in IL-6 mRNA abundance in USP34 knockdown cells compared to untreated control cells (**Figure 1-8**, B). These data suggest that CYLD functions to attenuate thrombin-induced IL-6 production, whereas USP34 is important for promoting thrombin-stimulated IL-6 expression.

CYLD and USP34 regulate GPCR-stimulated p38 signaling, however, the different DUBs appear to function in unique pathways to control GPCR-induced inflammatory responses. CYLD

attenuates thrombin-p38-dependent stimulated barrier function and IL-6 production, whereas USP34 promotes IL-6 mRNA expression but does not alter endothelial barrier maintenance (**Figure 1-9**). These studies are the first to identify a subset of DUBs using a comprehensive DUB siRNA library screen that specifically regulate GPCR-p38 signaling and distinctly regulate endothelial inflammatory responses (**Figure 1-9**).

Discussion

The role and regulation of GPCR function by ubiquitination remains poorly understood. Most studies have linked ubiquitination to GPCR lysosomal or proteasomal degradation (1). However, ubiquitin can also directly modulate GPCR signaling. This has been well characterized for the GPCR PAR1, where thrombin triggers ubiquitin-dependent recruitment of TAB2-TAB1 and activation of p38 MAPK signaling on endosomes to promote endothelial inflammatory responses (144,147,148). Ubiquitination is a reversible process and deubiquitination is important for governing proper ubiquitin-dependent cellular responses. To identify deubiquitinating enzymes that regulate thrombin-stimulated p38 signaling in human cultured endothelial cells, a SMARTpool siRNA library screen targeting 96 different human DUBs was conducted. A similar siRNA library screen was performed in HeLa cells expressing PAR1. The dual screens identified nine DUBs including USP18, BAP1, CYLD, USP34, OTUD7A, UBTD2, USP51, USP 47 and JOSD1. We validated the function of two DUBs, CYLD and USP34, that altered thrombin-stimulated p38 signaling in both cell types. Our study indicates that CYLD functions as a key regulator of thrombin-induced p38 activation and controls endothelial barrier permeability and IL-6 cytokine expression. Like CYLD, USP34 knockdown enhanced thrombin-promoted p38 signaling and regulated IL-6 expression but did not alter endothelial barrier integrity. This study reveals the diversity of DUB function in regulating GPCR signaling and further suggests that

specific DUBs distinctly regulate GPCR-p38-mediated inflammatory responses.

In this study an unbiased siRNA library screen approach was used to identify the relevant DUBs that control thrombin-stimulated p38 signaling in two cell types. Other studies used different approaches to identify DUBs that regulate activated GPCR ubiquitination and lysosomal degradation. USP33 was identified in a yeast-two hybrid screen with β-arrestin (113). USP33 and its homolog USP20 were shown to decrease b2-adrenergic receptor ubiquitination, which reduced receptor lysosomal degradation, and enhanced recycling and cellular resensitization (114). USP14 was identified in a proteomics screen and shown to decrease ubiquitination of agonist activated CXCR4 chemokine receptor and lysosomal degradation (119,173). USP8 was identified in a far western cDNA library screen using signal-transducing adaptor molecule (STAM) (174) and appears to regulate CXCR4 lysosomal degradation indirectly via modulation of hepatocyte growth factor-regulated tyrosine kinase substrate (HRS) (120). STAM and HRS are components of the endosomal sorting complex required for transport-0 (ESCRT-0) that recognize and initiate ubiquitinated cargo sorting within the endosomal-lysosomal pathway. Thus, multiple strategies have been used to identify DUBs that regulate GPCR function. However, a DUB siRNA library screen conducted in two different cell lines with endogenous or ectopically expressed receptor is a powerful approach to identify new and relevant DUBs that regulate GPCR mediated cellular responses.

The regulation of DUB activity is important for proper cellular responses. DUB activity is controlled through relative abundance, protein-protein interactions, subcellular localization, and post-translational modifications (159,160). DUB phosphorylation impacts function as demonstrated for CYLD regulation of tumor necrosis factor (TNF) receptor associated factors 2 (TRAF2) and 6 (TRAF6) proteins (175,176). Phosphorylation of CYLD at S418 by NF-kB

signaling impairs CYLD catalytic activity enhancing TRAF2 and TRAF6 degradation (89,162). In addition, CYLD can modulate NF-kB signaling (177). Although thrombin activates NF-kB signaling in endothelial cells (178,179), it is not known if thrombin regulates CYLD function via phosphorylation. Moreover, CYLD has been implicated in thrombin-induced endothelial barrier permeability through a pathway mediated by MALT1 cleavage of CYLD that results in microtubule destabilization (180). In contrast to CYLD, the function of USP34 phosphorylation sites are not known. CYLD is also ubiquitinated by the Skp1-Cullin1-F-box protein β-transducin repeat-containing protein, which promotes proteosomal degradation (181). A ubiquitination site has also been identified for USP34 (**Figure 1-3**), however the role of ubiquitination in regulating USP34 function has yet to be determined.

In addition to posttranslational modifications, DUB function is regulated by subcellular localization which is often mediated by protein-protein interactions with components of large complexes such as the proteosome. Several DUBs are known to bind to the proteasome and function to deubiquitinate proteins that are destined for degradation, a process that facilitates recycling of ubiquitin (49,182,183). A systematic analysis of the subcellular localization of 66 different GFP-tagged DUBs including CYLD but not UPS34 or USP47 was conducted in HeLa cells (184). In this study, GFP-tagged CYLD was shown to reside in the cytoplasm and nucleus, consistent with endogenous CYLD subcellular localization as shown in **Figure 1-4**, B. However, other studies have reported endogenous and ectopically expressed CYLD localization to microtubules (185,186), which was not obvious in our HeLa cell studies. Similar to CYLD, subcellular localization of USP34 was detected in the cytoplasm and nucleus and is consistent with its known function to regulate the cytoplasmic protein Axin and DNA damage repair (167,168). These findings raise the intriguingly possibility that CYLD and USP34 differentially modulate

thrombin-induced p38 activity in distinct subcellular compartments including endosomes and the nucleus to promote differential regulation of endothelial barrier permeability versus IL-6 production.

The role of ubiquitin in driving GPCR signaling is an emerging concept. Several GPCRs including mGluR7, CXCR2 and parathyroid hormone receptor promote ubiquitin-dependent signaling via recruitment of β-arrestin to the plasma membrane (146,187,188). The CXCR4 receptor also drives ubiquitin-dependent signaling indirectly via modulation of STAM ubiquitination (145). GPCR ubiquitination is also influenced by biased agonists as demonstrated for the m-opioid receptor (189). Interestingly, biased ligands induce ubiquitination of the b-adrenoreceptor via distinct E3 ubiquitin ligases (190-192). We showed that thrombin induces PAR1 ubiquitination and recruitment of TAB2-TAB1 to endosomes, which promotes non-canonical p38 signaling and endothelial barrier disruption (144,148). Thrombin-stimulated p38 signaling does not integrate with the RhoA/myosin light chain (MLC) pathway to control endothelial barrier permeability (131). In a recent study, we sought to determine how thrombin-stimulated endosomal p38 signaling contributes to endothelial barrier disruption using quantitative mass spectrometry and identified a rich array of candidate proteins including ERK1/2 and α-catenin that may regulate p38-dependent barrier disruption independent of RhoA/MLC (157). Other subsets of GPCRs including P2Y1 receptor, histamine H1 and H2 and prostaglandin receptors also stimulate non-canonical ubiquitin- and TAB2-TAB1-dependent p38 activation (147). Currently, it is not known whether CYLD and/or USP34 directly modulates ubiquitination of the GPCR PAR1 and/or other p38 pathway components such as p38, TAB1, TAB2, NEDD4-2 and c-Src to control non-canonical p38 MAPK signaling. In fact, several GPCR ubiquitin-driven p38 pathway components are known to be ubiquitinated including TAB1 (193), NEDD4-2

(148,194) and c-Src (195), but it is unclear if any of the pathway components are direct targets of CYLD and/or USP34.

Our study also provides critical insight into the function of CYLD and USP34 in regulating GPCR-p38 signaling and cytokine IL-6 production. We found that depletion of CYLD enhanced basal IL-6 production and amplified thrombin-induced IL-6 production (**Figure 1-8**, B), which might be attributed to the increased basal p38 phosphorylation observed in CYLD knockdown at the 0 min time point (**Figure 1-5**, A). The mechanism responsible for enhancing p38 basal signaling in CYLD depleted cells is not known. In contrast, USP34 knockdown diminished basal IL-6 production and decreased thrombin-induced IL-6 production (**Figure 1-8**, B), even though both CYLD and USP34 enhance thrombin-p38 signaling. As mentioned above, subcellular localization of the DUB and impact on compartmentalized p38 signaling may contribute to differential regulation of thrombin-induced IL-6 production. Clearly, additional studies are needed to interrogate the mechanisms by which CYLD and USP34 differentially modulate thrombin-induced endothelial barrier disruption and IL-6 production.

Figures

Figure 1-1. An siRNA library screen identifies nine DUBs that regulate thrombin-stimulated p38 signaling.

A, Thrombin cleaves and activates PAR1 at an N-terminus arginine (R) 41 site. After activation, PAR1 is phosphorylated and ubiquitinated, ubiquitin drives TAB1-TAB2 dependent p38 activation from endosomes and disruption of endothelial barrier. *B* and *D*, HeLa and endothelial EA.hy926 cells transfected with either p38α-specific or non-specific (ns) siRNA were stimulated with thrombin (Th) and p38 phosphorylation detected by immunoblot (n=1). *C*, HeLa cells pretreated with p38 inhibitor SB203580 or DMSO vehicle control were stimulated with thrombin and p38 phosphorylation determined (n=1). *E,* Workflow diagram. Endothelial EA.hy926 cells and HeLa cells transfected with Human DUB siRNA SMARTpool library and ns siRNA control were stimulated with thrombin for either 7.5 min (endothelial) or 5 min (HeLa), performed in duplicate. Phosphorylation of p38 was detected by immunoblot and quantified (n=1) for the two different cell types. *F* and *G*, Endothelial and HeLa cell siRNA library screen data are expressed as the fold change in p38 phosphorylation normalized to total p38 expression relative to ns siRNA control (red dotted line). *H*, Venn diagram includes DUBs known to cleave K63-linked ubiquitin which resulted in upregulated thrombin-stimulated p38 phosphorylation in both endothelial and HeLa cell lines.

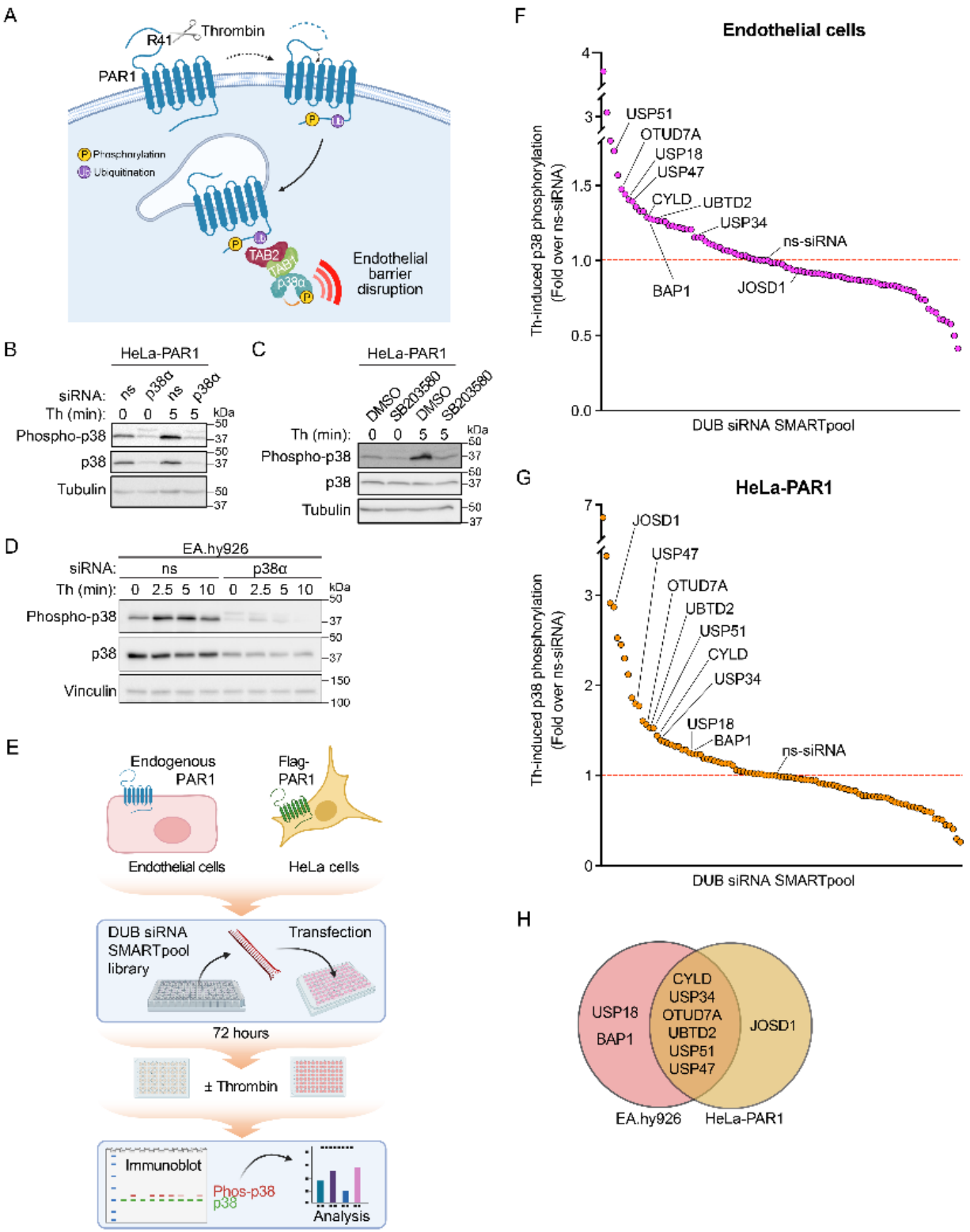
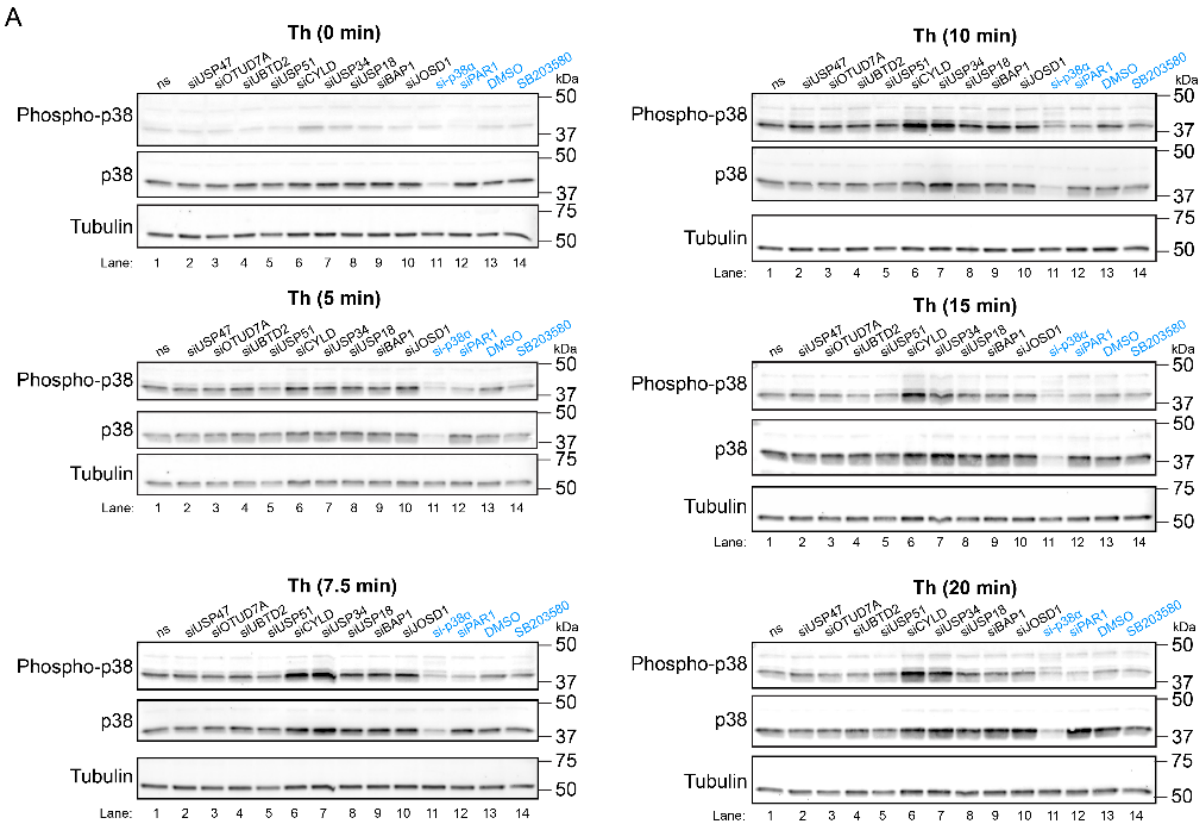
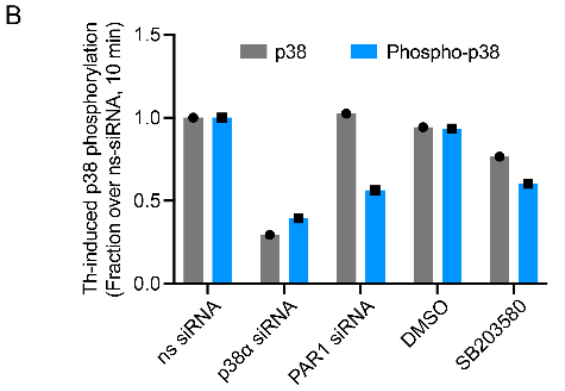
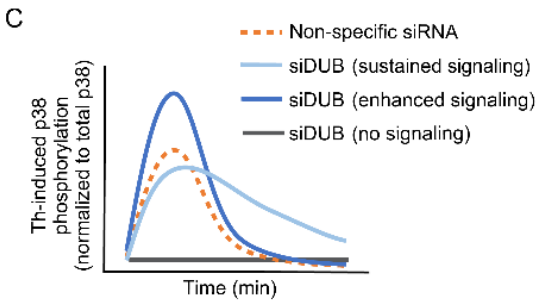

A
R41
Thrombin
PAR1
Phosphorylation
Ubiquitination
TAB2
TAB1
p38α
Endothelial barrier disruption
B
HeLa-PAR1
siRNA: ns p38α ns p38α
Th (min): 0 0 5 5
kDa
Phospho-p38
p38
Tubulin
C
HeLa-PAR1
DMSO SB203580 DMSO SB203580
Th (min): 0 0 5 5
Phospho-p38
p38
Tubulin
D
EA.hy926
siRNA: ns p38α
Th (min): 0 2.5 5 10 0 2.5 5 10
Phospho-p38
p38
Vinculin
E
Endogenous PAR1
Flag-PAR1
Endothelial cells
HeLa cells
DUB siRNA SMARTpool library
Transfection
72 hours
± Thrombin
Immunoblot
Phos-p38
p38
Analysis
F
Endothelial cells
Th-induced p38 phosphorylation (Fold over ns-siRNA)
USP51
OTUD7A
USP18
USP47
CYLD
UBTD2
USP34
ns-siRNA
BAP1
JOSD1
DUB siRNA SMARTpool
G
HeLa-PAR1
Th-induced p38 phosphorylation (Fold over ns-siRNA)
JOSD1
USP47
OTUD7A
UBTD2
USP51
CYLD
USP34
USP18
BAP1
ns-siRNA
DUB siRNA SMARTpool
H
USP18
BAP1
CYLD
USP34
OTUD7A
UBTD2
USP51
USP47
JOSD1
EA.hy926
HeLa-PAR1

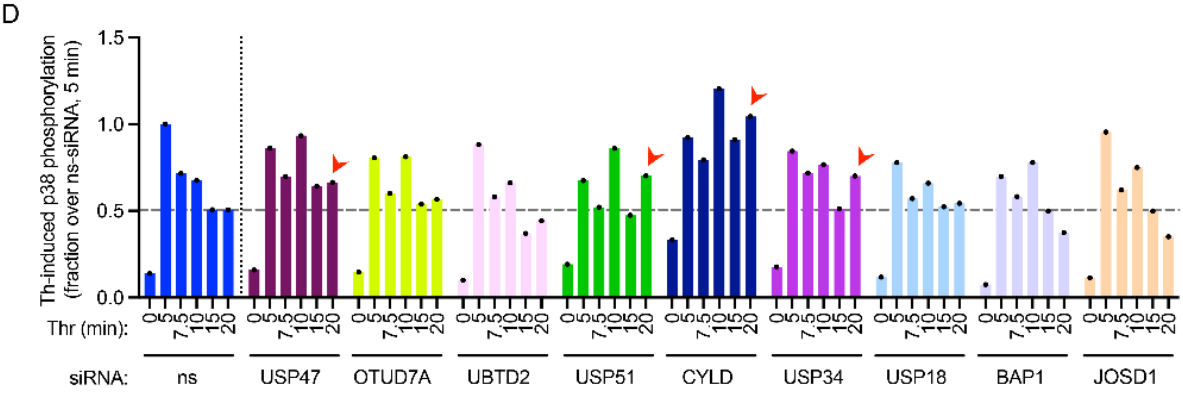
Figure 1-2. A subset of DUBs regulate thrombin-stimulated p38 MAPK signaling over time.

A, Endothelial EA.hy926 cells transfected with either non-specific (ns) siRNA, nine DUB SMARTpool siRNA, or p38α- or PAR1-specific siRNAs were serum-starved and stimulated with thrombin (Th) for the indicated times. Non-transfected endothelial cells were pre-treated with DMSO or the p38 inhibitor SB203580 and then stimulated with thrombin. Cell lysates were immunoblotted as indicated and quantified (n=1). *B*, Changes in thrombin-induced p38 phosphorylation in ns-, p38α-, PAR1-siRNA transfected cells or DMSO, SB203580 treated cells are shown as a fraction of ns siRNA control (n=1). *C*, Graphical illustration of anticipated impact of DUB depletion on p38 signaling over time. *D*, Changes in thrombin-stimulated p38 phosphorylation in DUB depleted endothelial cells are expressed as a fraction of ns siRNA at 0 min over time (n=1). Red arrowhead shows markedly elevated thrombin-stimulated p38 phosphorylation compared to ns siRNA control cells.


A
Th (0 min)
Th (5 min)
Th (7.5 min)
Th (10 min)
Th (15 min)
Th (20 min)
ns
siUSP47
siOTUD7A
siUBTD2
siUSP51
siCYLD
siUSP34
siUSP18
siBAP1
siJOSD1
si-p38α
siPAR1
DMSO
SB203580
kDa
Phospho-p38
p38
Tubulin
Lane: 1 2 3 4 5 6 7 8 9 10 11 12 13 14


B
Th-induced p38 phosphorylation
(Fraction over ns-siRNA, 10 min)
p38
Phospho-p38
ns siRNA
p38α siRNA
PAR1 siRNA
DMSO
SB203580


C
Non-specific siRNA
siDUB (sustained signaling)
siDUB (enhanced signaling)
siDUB (no signaling)
Th-induced p38 phosphorylation (normalized to total p38)
Time (min)


D
Th-induced p38 phosphorylation
(fraction over ns-siRNA, 5 min)
Thr (min):
siRNA:
ns
USP47
OTUD7A
UBTD2
USP51
CYLD
USP34
USP18
BAP1
JOSD1

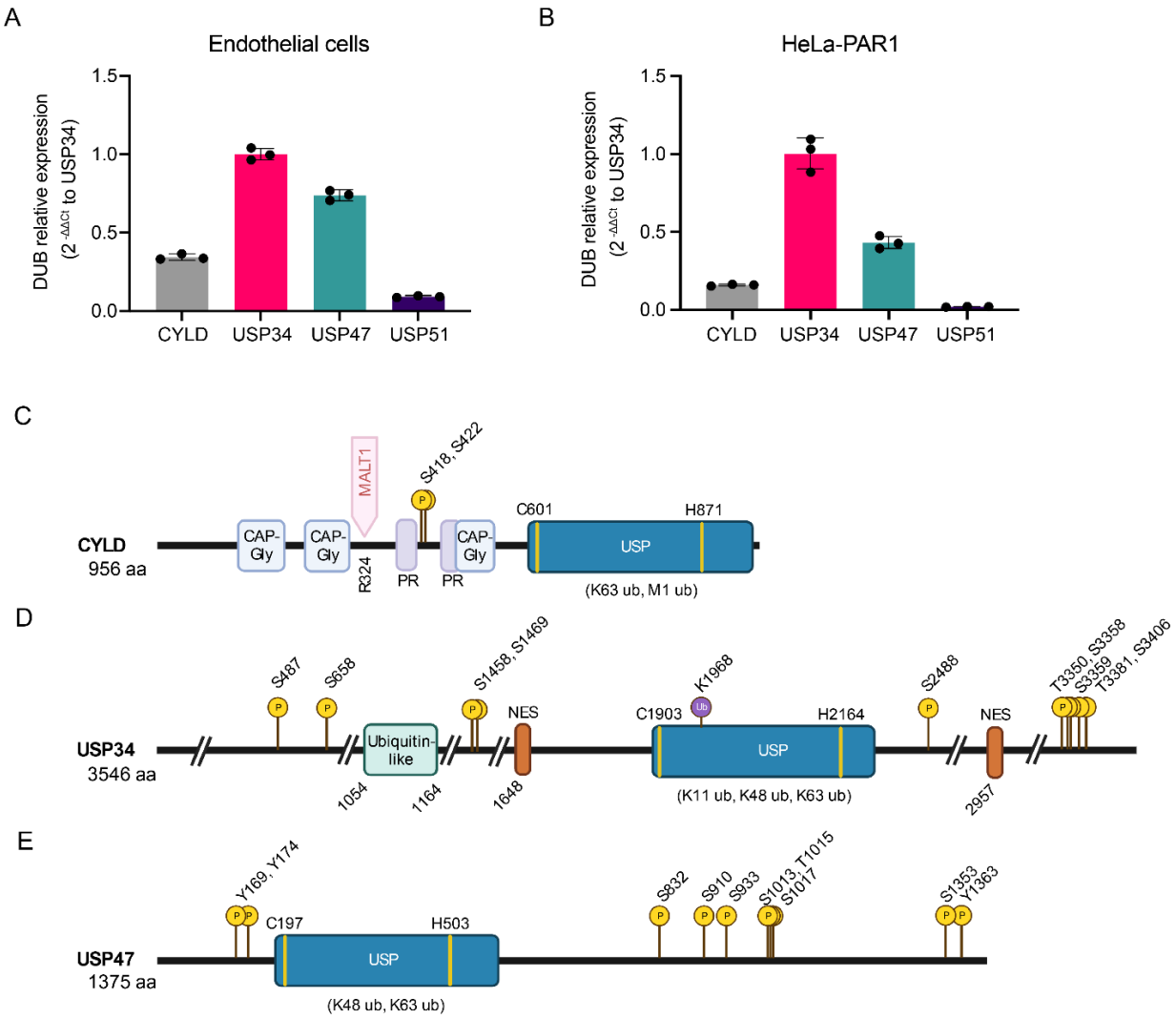


Figure 1-3. DUB mRNA expression, protein domains and phosphorylation sites.

CYLD, USP34, USP47 and USP51 expression was determined in endothelial EA.hy926 cells (*A*) and PAR1-expressing HeLa cells (*B*) by real time RT-qPCR. Data (mean ± S.D, n=3) normalized to 18S rRNA are expressed as ($2^{-\Delta\Delta Ct}$) relative to USP34 expression. CYLD (*C*), USP34 (*D*) and USP47 (*E*) cartoon illustrations of domains, phosphorylation, and ubiquitination sites. CYLD contains three cytoskeleton-associated protein-glycine-rich domain (CAP-Gly), two proline rich (PR) regions and ubiquitin-specific protease domain (USP). CYLD is cleaved by MALT1. USP34 contains a ubiquitin-like domain, USP domain and two nuclear export signals (NES). USP47 contains a USP domain. DUBs contain multiple sites of phosphorylation and USP34 possesses one ubiquitination site identified in PhosphositePlus.

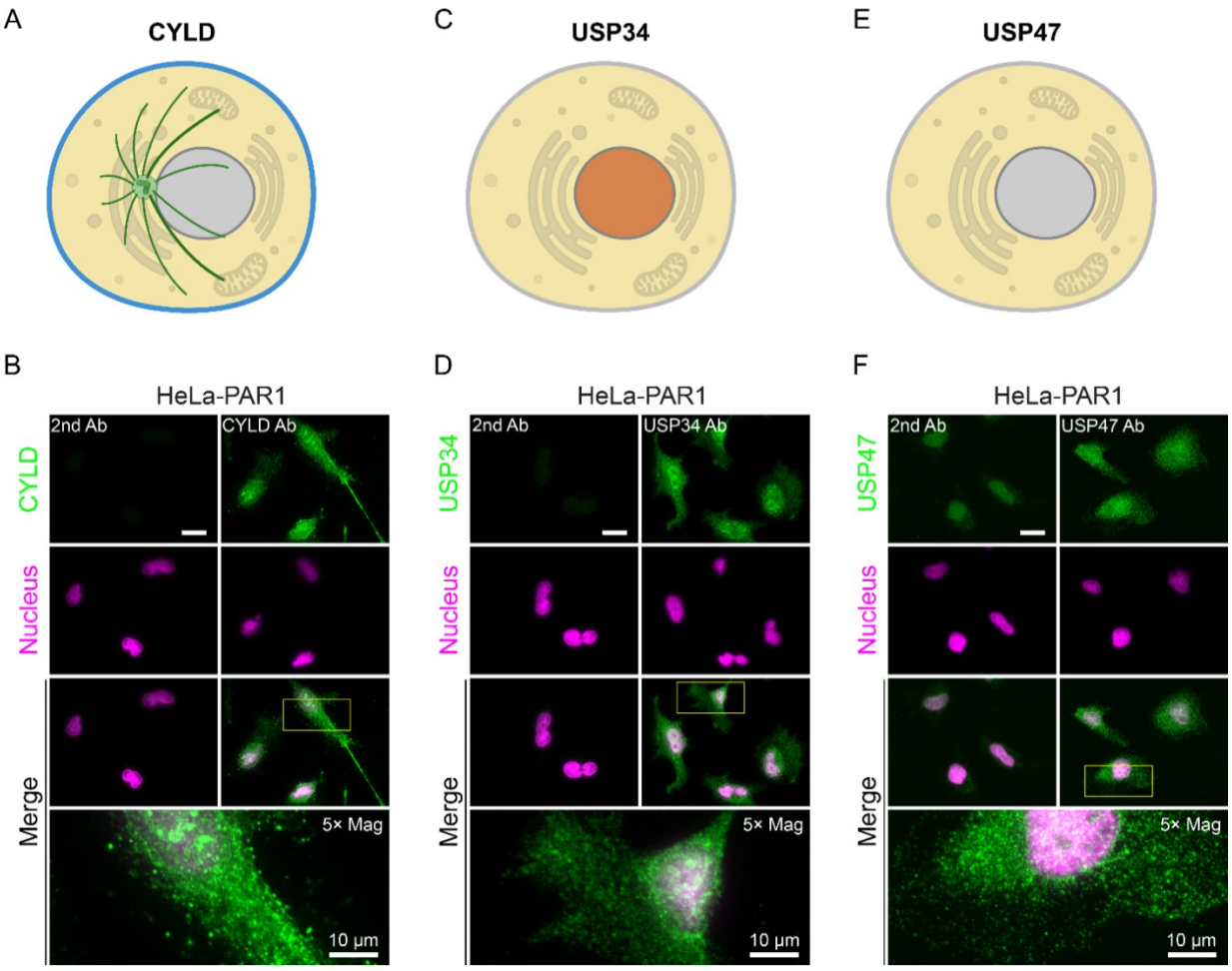


Figure 1-4. DUB candidate subcellular localization.

Cartoon illustrations of CYLD (*A*), USP34 (*C*) and USP47 (*E*) subcellular localization at the plasma membrane (blue), cytoskeleton (green), cytoplasm (yellow) and nucleus (orange). Gray indicates no localization. *B*, *D* and *F*, HeLa cells were fixed, processed, immunostained for endogenous CYLD, USP34 or USP47, stained with Hoechst to detect the nucleus and imaged by confocal microscopy. Scale bar=20 µm. Insets are 5X magnifications with scale bar=10 µm.

Figure 1-5. Depletion of CYLD, USP34 and USP47 by individual SMART pool siRNAs alter thrombin-induced p38 phosphorylation.

Endothelial EA.hy926 cells were separately transfected with four individual SMARTpool siRNAs for CYLD (*A*), USP34 (*B*) and USP47 (*C*) or non-specific (ns) siRNA control. Cells were then treated with or without thrombin (Th) for the indicated times. Cell lysates were immunoblotted as shown. Changes in thrombin-induced p38 phosphorylation were quantitated (n=1) and shown as phosphorylated-to-total ratios for each sample, which were then normalized as fraction over ns-siRNA at 0 min for each DUB knockdown experiment. The effect of selected individual DUB siRNAs on CYLD, USP34 and USP47 mRNA degradation was determined by RT-qPCR in endothelial EA.hy926 cells (*D*) and HeLa cells (*E*). The data (mean ± S.D., n=3) normalized to 18S rRNA are expressed as $2^{-\Delta\Delta Ct}$ relative to ns siRNA.

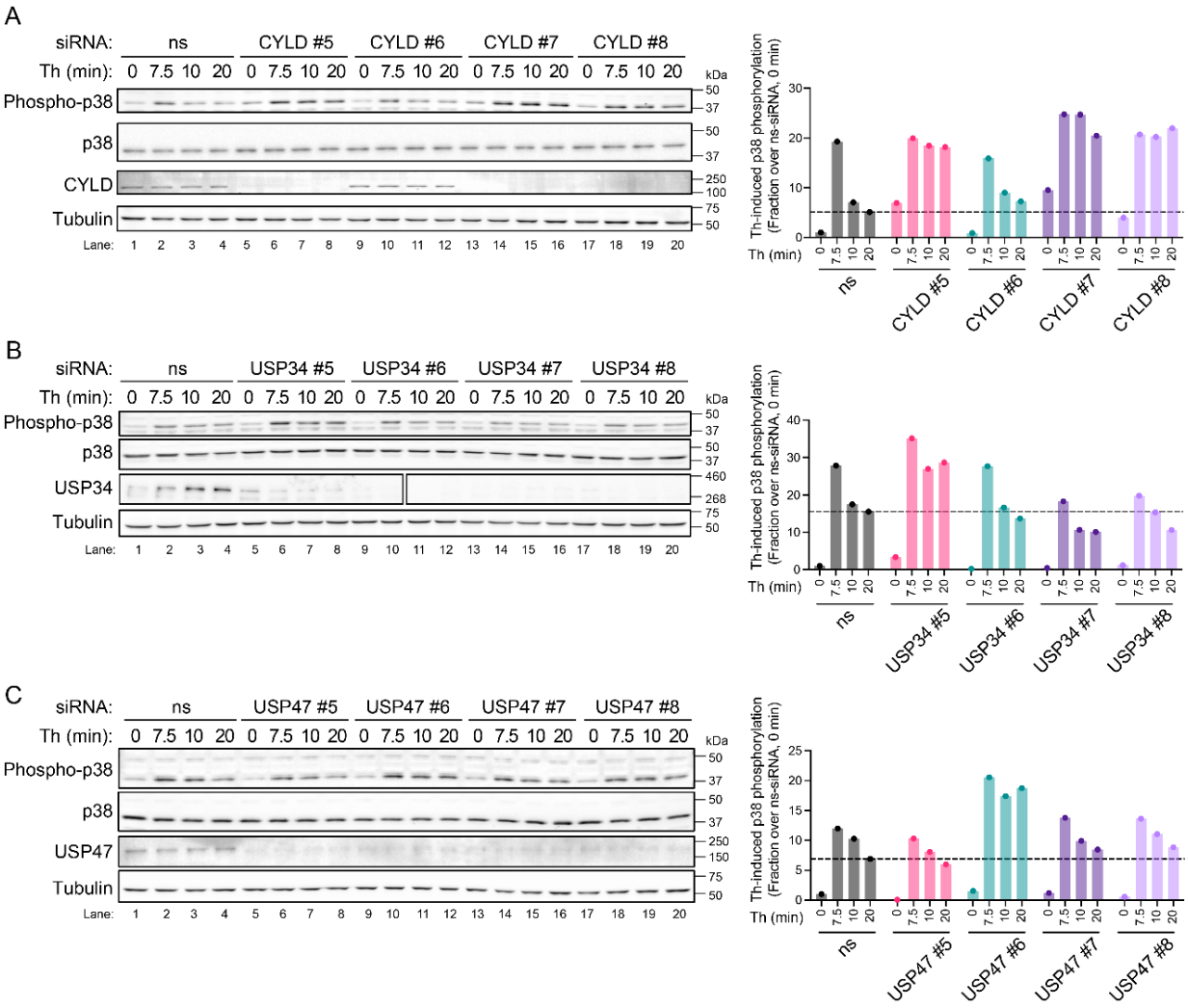
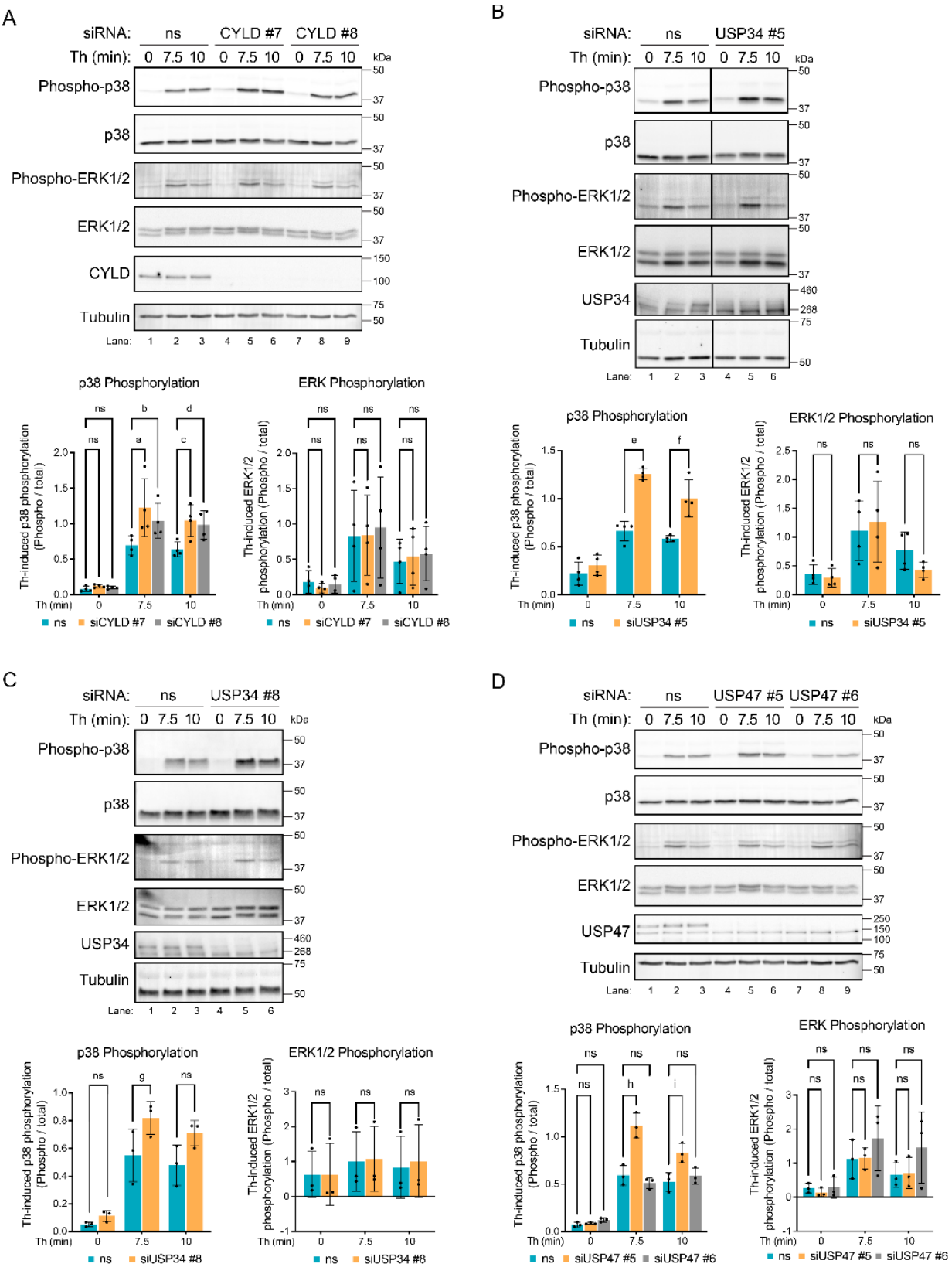

A
siRNA:
ns
CYLD #5
CYLD #6
CYLD #7
CYLD #8
Th (min):
0 7.5 10 20 0 7.5 10 20 0 7.5 10 20 0 7.5 10 20 0 7.5 10 20
kDa
Phospho-p38
p38
CYLD
Tubulin
Lane: 1 2 3 4 5 6 7 8 9 10 11 12 13 14 15 16 17 18 19 20
Th-induced p38 phosphorylation (Fraction over ns-siRNA, 0 min)
Th (min)
B
siRNA:
ns
USP34 #5
USP34 #6
USP34 #7
USP34 #8
USP34
C
siRNA:
ns
USP47 #5
USP47 #6
USP47 #7
USP47 #8
USP47
D
Endothelial cells
DUB relative expression (2 -ΔΔCt to ns-siRNA)
ns
siCYLD #7
siUSP34 #5
siUSP47 #6
CYLD
USP34
USP47
E
HeLa-PAR1

Figure 1-6. Depletion of CYLD or USP34 using multiple individual siRNAs enhance thrombin-stimulated p38 phosphorylation but not ERK1/2 phosphorylation.

A, HeLa cells transfected with CYLD or non-specific (ns) siRNAs were incubated with thrombin (Th) for various times, lysed and equivalent amounts of lysates were immunoblotted as indicated. HeLa cells were transfected with (B) USP34 or ns siRNA or (C) USP47 or ns siRNA, treated with thrombin and immunoblotted as described above. The data (mean ± S.D.) for CYLD siRNA #7 (n=4), CYLD siRNA #8 (n=4), USP34 siRNA #5 (n=4), USP34 siRNA #8 (n=3), USP47 siRNA #5 (n=3) and USP47 siRNA #6 (n=3) are represented as the ratio of phosphorylated p38 or ERK1/2 to total p38 or ERK1/2 from independent experiments. Data were analyzed by two-way ANOVA, followed by Šídák's post hoc test. P-values: a=0.0013, b=0.0378, c=0.0126, d=0.0365, e<0.0001, f=0.0002, g=0.0445, h<0.0001, i=0.0005; ns, not significant. See **Supplemental Table 1-1** for full results of ANOVA.


A
siRNA: ns CYLD #7 CYLD #8
Th (min): 0 7.5 10 0 7.5 10 0 7.5 10 kDa
Phospho-p38
p38
Phospho-ERK1/2
ERK1/2
CYLD
Tubulin
Lane: 1 2 3 4 5 6 7 8 9
p38 Phosphorylation
ERK Phosphorylation
Th-induced p38 phosphorylation (Phospho / total)
Th-induced ERK1/2 phosphorylation (Phospho / total)
ns siCYLD #7 siCYLD #8
B
siRNA: ns USP34 #5
Th (min): 0 7.5 10 0 7.5 10 kDa
Phospho-p38
p38
Phospho-ERK1/2
ERK1/2
USP34
Tubulin
Lane: 1 2 3 4 5 6
p38 Phosphorylation
ERK1/2 Phosphorylation
ns siUSP34 #5
C
siRNA: ns USP34 #8
Th (min): 0 7.5 10 0 7.5 10 kDa
Phospho-p38
p38
Phospho-ERK1/2
ERK1/2
USP34
Tubulin
Lane: 1 2 3 4 5 6
p38 Phosphorylation
ERK1/2 Phosphorylation
ns siUSP34 #8
D
siRNA: ns USP47 #5 USP47 #6
Th (min): 0 7.5 10 0 7.5 10 0 7.5 10 kDa
Phospho-p38
p38
Phospho-ERK1/2
ERK1/2
USP47
Tubulin
Lane: 1 2 3 4 5 6 7 8 9
p38 Phosphorylation
ERK Phosphorylation
ns siUSP47 #5 siUSP47 #6

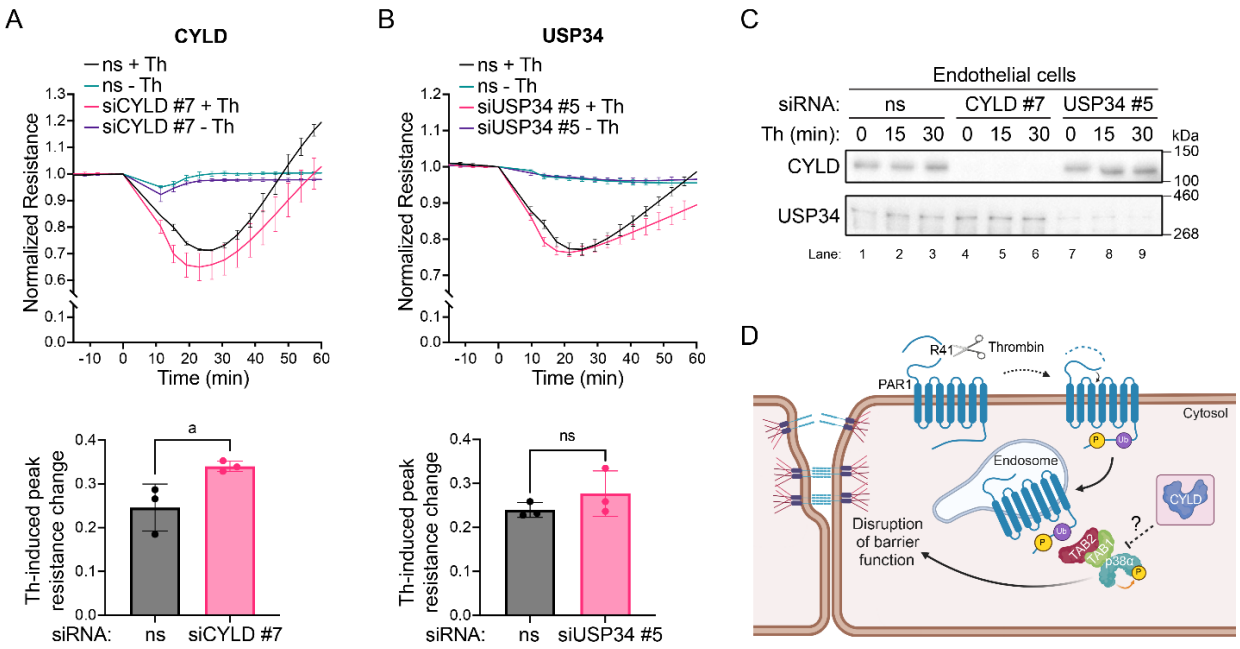


Figure 1-7. Depletion of CYLD but not USP34 enhances thrombin-induced endothelial barrier permeability.

Endothelial EA.hy926 cells transfected with non-specific (ns), CYLD (*A*) and USP34 (*B*) specific siRNA were stimulated with or without thrombin (Th) and endothelial barrier permeability (resistance) was measured by ECIS. Changes in endothelial barrier resistance were normalized to baseline for each condition, and data expressed relative to maximum thrombin-induced change in resistance quantified from three independent experiments for CYLD and USP34 siRNA knockdown. The line graphs are from a representative experiment (mean ± S.D., performed in triplicate, n=3) for each DUB knockdown. The bar graphs are the peak change in resistance (mean ± S.D.) from the three independent experiments (n=3) and were analyzed by two-tailed student's t test. P-value: a=0.0415; ns, not significant. *D*, Cell lysates were prepared from the non-specific, CYLD and USP34 siRNA transfected cells and immunoblotted as indicated. *E*, Cartoon illustration of thrombin-activated PAR1 ubiquitin-driven p38 mediated endothelial barrier disruption regulation by CYLD.

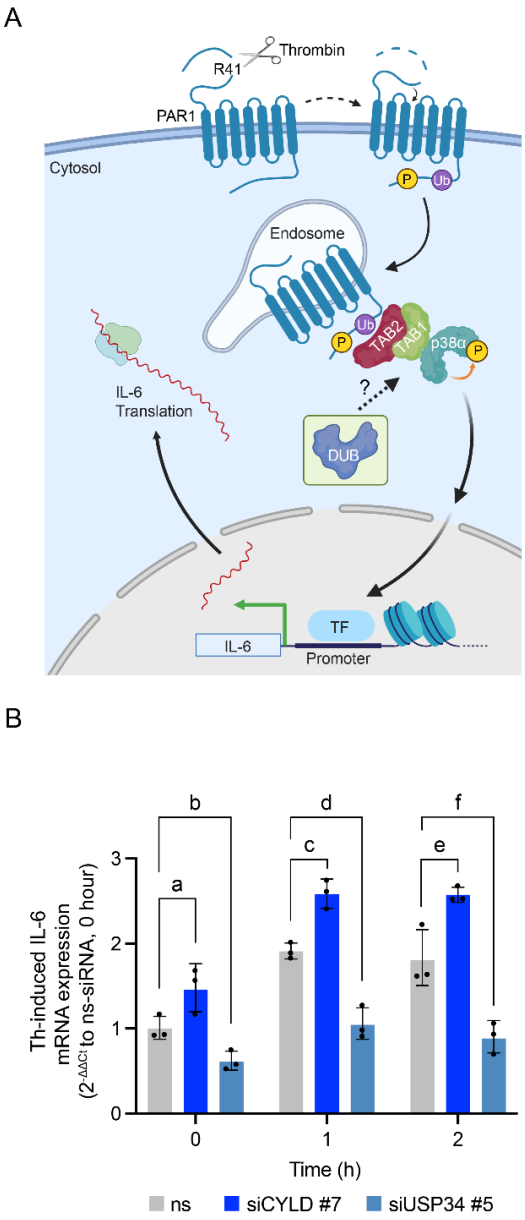


Figure 1-8. Thrombin-induced IL-6 expression is differentially regulated by CYLD and USP34.

A, Cartoon illustration of thrombin-activated PAR1-stimulated TAB1/TAB2-p38 mediated induction of interleukin-6 (IL-6) expression and potential regulation by deubiquitinating enzymes (DUBs). *B*, Endothelial EA.hy926 cells were transfected with non-specific (ns), CYLD or USP34 specific siRNAs. Cells were then stimulated with or without thrombin (Th) for the indicated times. The effect of CYLD and USP34 siRNA-mediated depletion compared to non-specific (ns) siRNA on thrombin-stimulated IL-6 expression was then quantified by RT-qPCR. Data (mean ± S.D., n = 3) normalized to 18S rRNA are expressed as $2^{-\Delta\Delta Ct}$ relative to ns siRNA and analyzed by two-way ANOVA, followed by Dunnett's post hoc test. *P*-values: a=0.0132, b=0.0017, c=0.0455, d=0.0002, e=0.0189, f<0.0001. See **Supplemental Table 1-1** for full results of ANOVA.

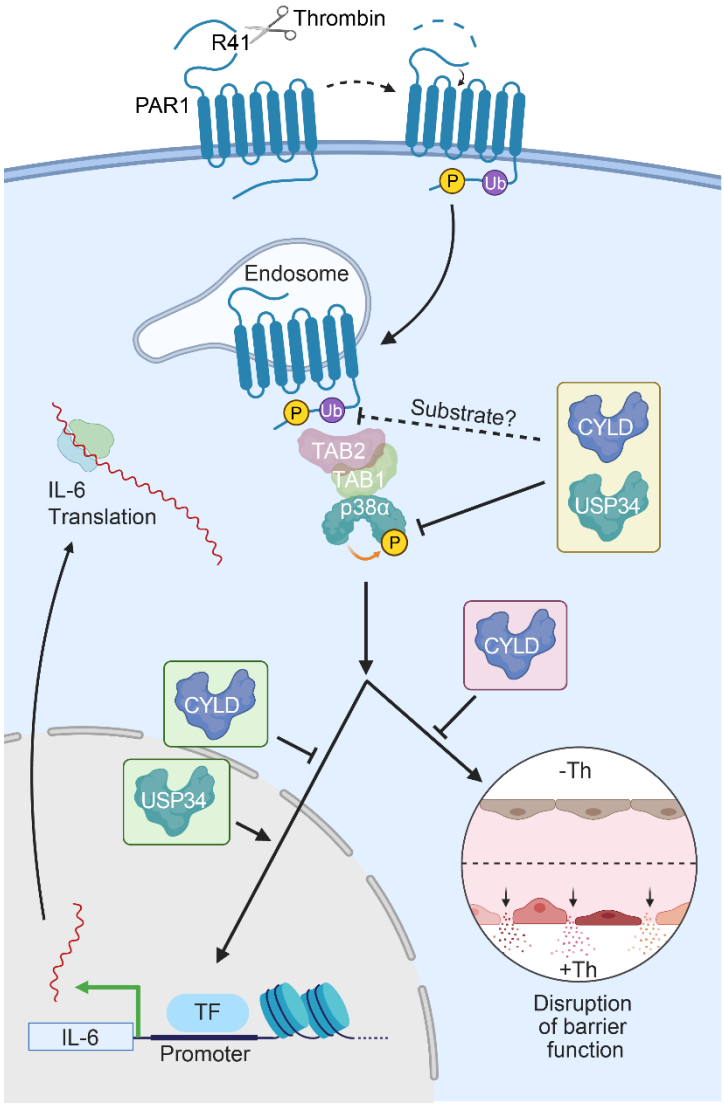


Figure 1-9. Model of thrombin-activated PAR1 ubiquitin-driven p38-mediated inflammatory signaling regulation by CYLD versus USP34.

Thrombin activation of PAR1 promotes ubiquitin-dependent TAB1-TAB2 stimulated p38 MAPK signaling from endosomes. Both CYLD and USP34 regulate thrombin-activated PAR1-induced p38 signaling. However, CYLD functions to control thrombin-induced endothelial barrier permeability, whereas both CYLD and USP34 regulate thrombin-stimulated IL-6 mRNA expression. The precise mechanisms by which CYLD and USP34 function to control GPCR ubiquitin-driven p38 signaling are not known.

Material and Methods

Reagents and antibodies

Human α-Thrombin was obtained from Enzyme Research Laboratories (#HT1002a). The following antibodies were obtained from Cell Signaling Technology p38 MAPK (#9212), phospho-p38 MAPK (#4511), p44/42 MAPK ERK1/2 (#9102), phospho-p44/42 MAPK ERK1/2 (#9106) and CYLD (#8462). Other antibodies included USP47 (#ab72143, Abcam), USP34 (#A300-824A, Bethyl Laboratories). The p38, CYLD, USP34 and USP47 antibodies were validated by siRNA as shown in Figure 1, B, and Figure 5, A, B, and C, respectively. The ERK1/ antibody #9102 was validated by siRNA as shown on the CST website. HRP-conjugated goat-anti rabbit (#1706515), HRP-conjugated goat-anti mouse (#1706516), StarBright Blue 520 goat anti-mouse (#12005867), StarBright Blue 700 goat anti-rabbit (#12004162), and hFAB Rhodamine Tubulin (#12004166) were from BioRad. Vinculin antibody (#V9131) and SB203580 (#S8307) were from Sigma-Aldrich.

Cell Culture

Human umbilical vein endothelial cell (HUVEC)-derived EA.hy926 cells were obtained from American Type Culture Collection (Manassas, VA), grown and propagated and used between P2 and P10 according to ATCC instructions and as described (155,157). HUVEC-derived EA.hy926 cells are authenticated by short tandem repeat (STR) profiling as noted by ATCC. HeLa cells stably expressing FLAG-tagged PAR1 wildtype cloned in pBJ were generated and cultured as previously described (156,196). All cell lines are routinely monitored for mycoplasma using Venor™ GeM Mycoplasma detection kit (Sigma-Aldrich, #MP0025-1KT) per the manufacturer's instructions.

Deubiquitinating enzyme siRNA library screen

Human ON-TARGETplus siRNA library targeting 96 deubiquitinating enzymes genes consisting of SMARTpool™ siRNA (4 individual siRNAs targeting each gene) in a 96-well format was purchased from Horizon Discovery (#G-104705-05). Endothelial EA.hy926 cells were seeded at 0.7×10^5 cells per well in 48-well plates and PAR1 HeLa cells were seeded at 7×10^3 cells per well in 96-well plates and grown overnight. Endothelial cells were transfected with 96 distinct DUB SMARTpool siRNAs at 28 nM using TransIT-X2 Dynamic Delivery System and PAR1 HeLa cells were transfected with the same DUB SMARTpool siRNAs at 50 nM using Oligofectamine Transfection Reagent according to the manufacturer's instructions. Endothelial and HeLa cells were also transfected with 50 nM p38〈 siRNA, 25 nM of PAR1-208 siRNA and 50 nM non-specific siRNA as controls. After 72 h of transfection, cells were serum-starved and then stimulated with 10 nM thrombin for 7.5 min (endothelial cells) or 5 min (PAR1 HeLa cells) at 37ºC or left untreated 0 min. Cells were also pretreated with 5 μM SB203580 or DMSO for 30 min before thrombin stimulation as a control. After stimulation, cells were placed on ice, washed and lysed in 2×Laemmli Sample Buffer supplemented with 200 mM dithiothreitol. Cell lysates were resolved by SDS-PAGE, transferred to PVDF membrane, and immunoblotted with antibodies as indicated. Immunoblots were developed and imaged using ChemiDoc Imaging System (BioRad) with appropriate filter set for StarBright 520, StarBright 700, and chemiluminescence. Signal was quantified by densitometry with NIH ImageJ software or Image Lab 6.1 (BioRad), and displayed as fold increase relative to non-specific siRNA control.

Individual siRNAs

AllStars negative control non-specific siRNA (#1027281) and p38α-specific siRNA 5'-AAC TGC GGT TAC TTA AAC ATA-3', and custom designed PAR1-208 siRNA 5′-AGA UUA

GUC UCC AUC AAU A-3′ (197) were purchased from Qiagen. The following individual DUB siRNAs were used in validation studies including: CYLD 5'-GGA CAU GGA UAA CCC UAU U-3' (#J-004609-05), 5'-AGA GAU AUC UAC AGA CUU U-3' (#J-004609-06), 5'- GGA GAG UAC UUG AAG AUG U-3 (#J-004609-07), 5'- GAA GGU UGG AGA AAC AAU A-3' (#J-004609-08), and UPS34 5'- GCA GGG AAG UUC UGA CGA A-3' (#J-006082-05), 5'- AAC AGA UCA GUA GUA AUU-3' (#J-006082-06), 5'- GCA GCU AUC CAG UAU AUU A-3' (#J-006082-07), 5'- CCA UGU GAC UGG AGA UUU A-3' (#J-006082-08) and USP47 5'- GCA ACG AUU UCU CCA AUG A-3 (#J-006093-05), 5'- CAA CAU GUC AGC AGG AUA A-3' (#J-006093-06), 5'- GCU GUC GCC UUG UUA AAU A-3' (#J-006093-07), 5'- CGC AAU ACA UGC AAG AUA A-3' (3 J-006093-08).

Quantitative real-time reverse transcription polymerase chain reaction (RT-qPCR)

RNA was isolated from endothelial EA.hy926 cells seeded at 9.6×10^5 cells per well in a 6-well plate and PAR1 HeLa cells seeded at 6×10^5 cells per well of a 6-well plate grown overnight using Direct-zol RNA Miniprep Plus Kit (#R2072, Zymo Research). Total RNA was quantified and 1 μg total RNA was utilized for cDNA synthesis reaction with the SuperScript IV VILO Master Mix with ezDNase enzyme kit (#111766050, Thermo Fisher Scientific). Quantitative RT-PCR was performed with TaqMan Fast Advanced Master Mix (#4444964, Thermo Fisher Scientific) and TaqMan Gene Expression Probes CYLD (#Hs01031576_m1), USP34 (#Hs00611330_m1), USP47 (#Hs00215725_m1), USP51 (#Hs01651394_s1), IL-6 (#Hs00174131_m1) and 18S (#Hs03003631_g1, primer-limited) using a QuantStudio™ 3 Real-Time PCR System (Thermo Fisher Scientific). DUB and IL-6 mRNA transcript levels were analyzed using the comparative CT (threshold cycle) method, normalized to 18S ribosomal RNA expression. Briefly, the number of cycles until threshold (Ct) was determined for each target, and

the Ct value for 18S was subtracted from the Ct value for each target, the differences in expression was then determined using the $2^{-\Delta\Delta Ct}$ method.

Signaling assays and immunoblotting

Signaling assays were performed essentially as described (144,147,148). Cells were serum-starved and pretreated with 5 μM SB203580 or DMSO vehicle control for 30 min at 37ºC. Cells were then stimulated with 10 nM thrombin for various times. Cells were lysed, protein concentrations determined using a BCA protein assay (ThermoFisher Scientific) and equivalent amounts of cell lysates were resolved by SDS-PAGE, transferred to PVDF membranes and immunoblotted with antibodies as indicated. Membranes were developed by chemiluminescence or fluorescence detection using a ChemiDoc Imaging System (BioRad), and quantified, analyzed by densitometry using with NIH ImageJ software or Image Lab 6.1 (BioRad). For p38 and ERK1/2 phosphorylation experiments, the integrated intensity of phosphorylated species is normalized (by division) to the integrated intensity of total p38 or total ERK1/2. Such ratio is either presented directly or further expressed as fraction over a designated control, as indicated in the legends.

Immunofluorescence Confocal Microscopy

HeLa cells stably expressing FLAG-tagged PAR1 wildtype were plated at 3×10^4 cells per well in a 12-well plate and grown on fibronectin-coated coverslips for 24 h. Cells were fixed and permeabilized with methanol at −20°C for 10 min, and blocked with 2% BSA/PBS for 60 min at room temperature. Primary antibodies rabbit anti-CYLD (#PA5-29795, Invitrogen) at 1:200 dilution, rabbit anti-USP34 (#A300-824A, Bethyl Laboratories) at 1:200 dilution, and rabbit anti-USP47 (#ab72143, Abcam) at 1:500 dilution were used for staining. Secondary antibody goat anti-Rabbit IgG (H+L) conjugated to Alexa Fluor 488 (A-11008, Invitrogen) at 1:2000 dilution was

used. All the antibodies were prepared in the blocking buffer and were incubated with coverslips for 60 min. Nuclei were stained with Hoechst 33342 solution prepared in blocking buffer. Coverslips were mounted with ProLong™ Gold Antifade Mountant (#P36934, Invitrogen).

Confocal microscopy image acquisition was perform using Olympus IX81 spinning-disk Microscope (Tokyo, Japan), equipped with a CoolSNAP HQ2 CCD Camera (Andor, Belfast, United Kingdom), a 60× 1.40 NA oil PlanApo objective lens (Olympus), and appropriate filters. At least three random fields of view for each coverslip were acquired using MetaMorph software (MDS Analytical Technologies, Sunnyvale, CA, USA) with multiple focal positions. Image stacks were processed to generate Z-projection (maximum-intensity method) images using NIH Fiji software.

Electrical Cell Impedance Sensing

Endothelial EA.hy926 cells were seeded onto cysteine- and collagen-coated gold microwell 8W10E+ ECIS array (Applied Biophysics). Cells were transfected with 28 nM non-specific, CYLD, USP34 and USP47 siRNA using TransIT X2 (MirusBio) according to the manufacturer's instructions. Cells were then allowed to reach confluence for 48 to 72 h until impedance reached 3000 ohms. The baseline barrier was recorded and established by multiple frequency time. Changes in resistance, a measure of barrier function, was determined after the addition of thrombin and recording continued until the barrier recovered to the previously established baseline impedance as we described (131).

Model and Prediction Analysis

Schematics and Figures were created in Adobe Illustrator and Photoshop. The cartoons were created with BioRender.com. UniProt Knowledgebase was used to query CYLD, UBP34 (USP34) and UBP47 (USP47) subcellular localization based on curated information (164).

Statistical Analysis

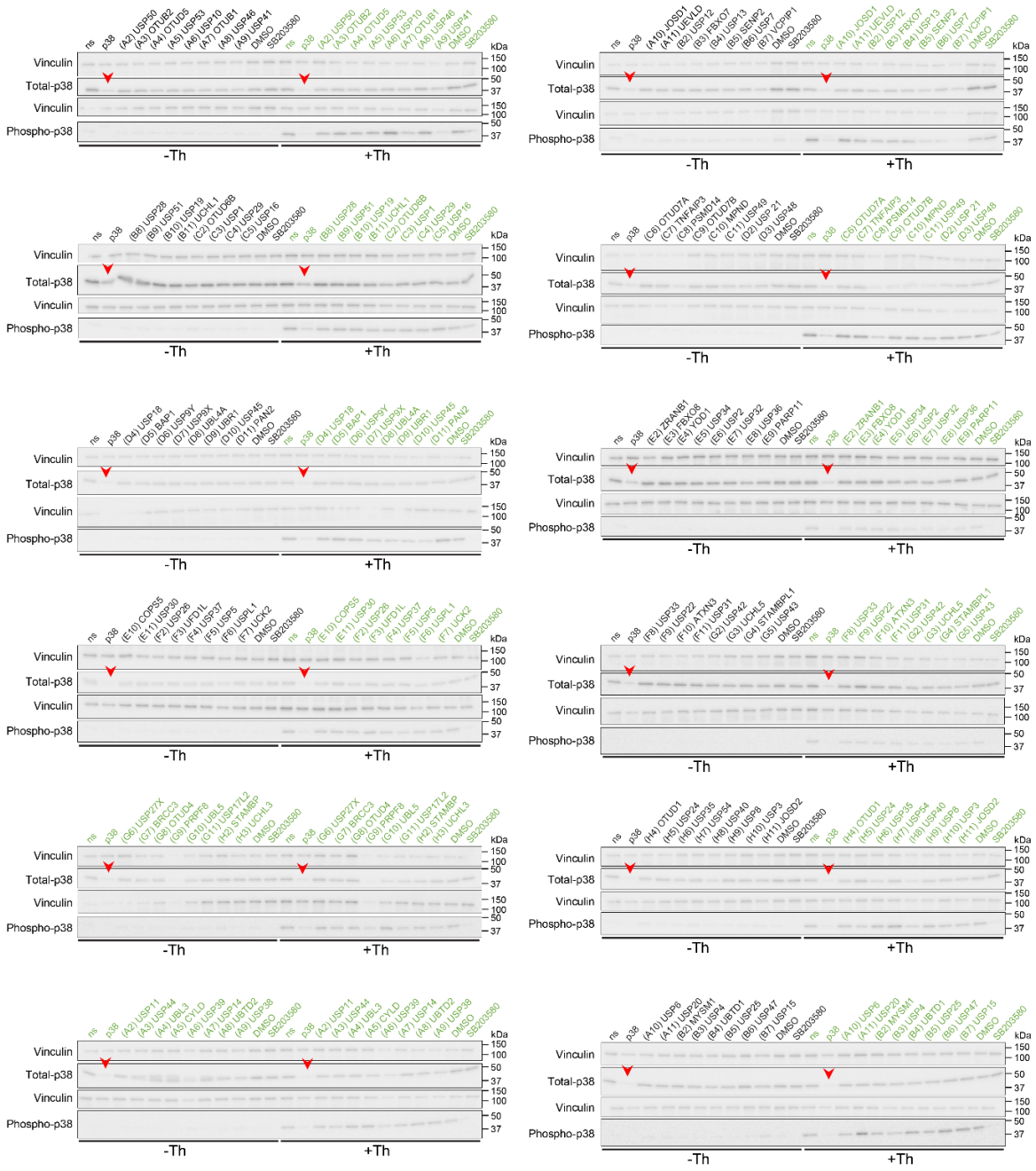
Data were analyzed using Prism 9.0 statistical software (GraphPad Software, La Jolla, CA) and Microsoft Excel. Statistical analysis methods are indicated in the figure legends.

Acknowledgements

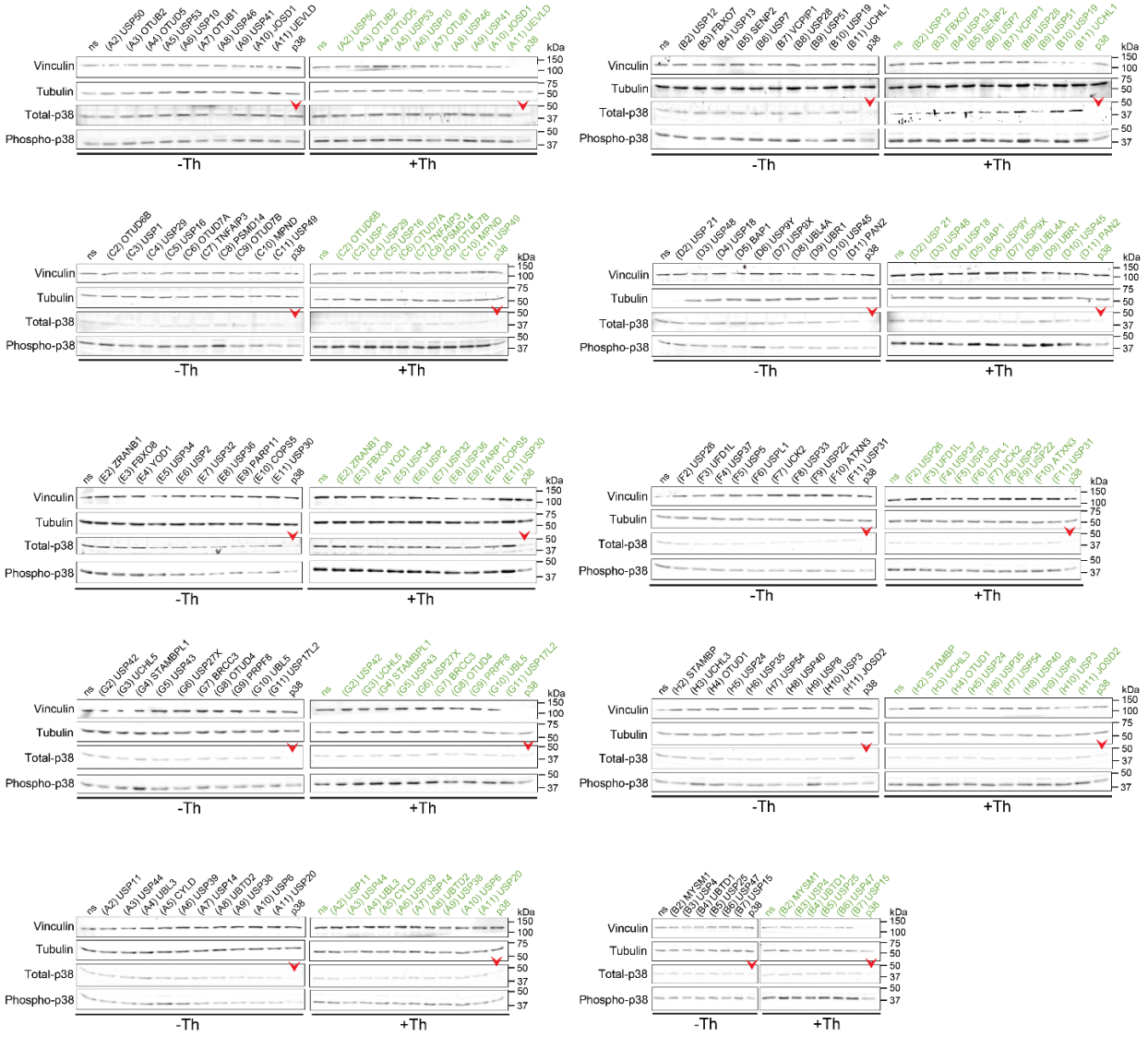
We thank members of the Trejo laboratory for helpful advice and discussions throughout this work, particularly Mika Caplan for editing and Anand Patwardhan for technical assistance.

Chapter 1, in full, is a reprint of the material as it appears in Journal of Biological Chemistry. Norton Cheng, JoAnn Trejo, Elsevier Inc, 2023. The dissertation author was the primary investigator and author of this paper.

Supplemental Information



Supplemental Figure 1-1. HeLa cell DUB siRNA library screen immunoblots of thrombin-stimulated p38 phosphorylation.



Supplemental Figure 1-2. Endothelial EA.hy926 cells DUB siRNA library screen immunoblots of thrombin-stimulated p38 phosphorylation.

Supplemental Table 1-1. ANOVA results

Figure 1-6					
Panel A: CYLD-KD					
p38	SS	DF	MS	F (DFn, DFd)	P value
Interaction	0.2894	4	0.07234	F (4, 27) = 1.895	P=0.1402
Time	5.666	2	2.833	F (2, 27) = 74.22	P<0.0001
siRNA	0.6852	2	0.3426	F (2, 27) = 8.975	P=0.0010
Residual	1.031	27	0.03817		
ERK1/2	SS	DF	MS	F (DFn, DFd)	P value
Interaction	0.03913	4	0.009782	F (4, 27) = 0.05178	P=0.9947
Time	3.224	2	1.612	F (2, 27) = 8.534	P=0.0013
siRNA	0.03437	2	0.01718	F (2, 27) = 0.09097	P=0.9133
Residual	5.101	27	0.1889		
Panel B: USP34-KD (siRNA #5)					
p38	SS	DF	MS	F (DFn, DFd)	P value
Interaction	0.5967	2	0.2983	F (2, 18) = 10.03	P=0.0012
Time	4.789	2	2.394	F (2, 18) = 80.53	P<0.0001
siRNA	1.844	1	1.844	F (1, 18) = 62.03	P<0.0001
Residual	0.5352	18	0.02973		
ERK1/2	SS	DF	MS	F (DFn, DFd)	P value
Interaction	0.2441	2	0.1220	F (2, 18) = 0.7813	P=0.4727
Time	3.118	2	1.559	F (2, 18) = 9.980	P=0.0012
siRNA	0.03792	1	0.03792	F (1, 18) = 0.2427	P=0.6282
Residual	2.812	18	0.1562		
Panel C: USP34-KD (siRNA #8)					
p38	SS	DF	MS	F (DFn, DFd)	P value
Interaction	0.03650	2	0.01825	F (2, 12) = 1.344	P=0.2974
Time	1.264	2	0.6318	F (2, 12) = 46.51	P<0.0001
siRNA	0.1572	1	0.1572	F (1, 12) = 11.57	P=0.0053
Residual	0.1630	12	0.01358		
ERK1/2	SS	DF	MS	F (DFn, DFd)	P value
Interaction	0.02243	2	0.01122	F (2, 12) = 0.01435	P=0.9858
Time	0.5278	2	0.2639	F (2, 12) = 0.3376	P=0.7201
siRNA	0.03009	1	0.03009	F (1, 12) = 0.03849	P=0.8477
Residual	9.382	12	0.7818		

(Continued)

Supplemental Table 1-1. ANOVA results (continue)

Figure 1-6					
Panel D: USP47-KD					
p38	SS	DF	MS	F (DFn, DFd)	P value
Interaction	0.3476	4	0.08689	F (4, 18) = 12.80	P<0.0001
Time	2.193	2	1.096	F (2, 18) = 161.6	P<0.0001
siRNA	0.4583	2	0.2291	F (2, 18) = 33.76	P<0.0001
Residual	0.1222	18	0.006787		
ERK1/2	SS	DF	MS	F (DFn, DFd)	P value
Interaction	0.5444	4	0.1361	F (4, 18) = 0.4202	P=0.7920
Time	5.591	2	2.795	F (2, 18) = 8.630	P=0.0024
siRNA	1.409	2	0.7044	F (2, 18) = 2.175	P=0.1426
Residual	5.830	18	0.3239		
Figure 1-8					
Panel B:					
ANOVA table	SS	DF	MS	F (DFn, DFd)	P value
Interaction	0.1051	4	0.02627	F (4, 18) = 0.5511	P=0.7007
Time	3.793	2	1.896	F (2, 18) = 39.78	P<0.0001
siRNA	8.622	2	4.311	F (2, 18) = 90.43	P<0.0001
Residual	0.8581	18	0.04767		

Chapter 2 USP34 REGULATES ENDOTHELIAL PAR1 MRNA TRANSCRIPT EXPRESSION AND CELLULAR SIGNALING

Abstract

G protein-coupled receptors (GPCR) controls various cellular signaling and are regulated by subcellular trafficking and interaction with other signaling pathway components – which are both involve posttranslational modifications (PTM) of the receptors and their interacting partners, such as phosphorylation and ubiquitination. While GPCRs have been characterized to be ubiquitinated, regulation of GPCR by ubiquitin is still an emerging field and its pharmacological relevance is unclear. In our previous studies, ubiquitination of a member of GPCR, protease-activated receptor 1 (PAR1), was found to control a pro-inflammatory signaling pathway in endothelial cells stimulated by thrombin. The polyubiquitinated PAR1 locally induces autoactivation of p38α mitogen-activated protein kinase (MAPK) in the endosomes and affects endothelial integrity. While the E3 ligase NEDD4-2 has been identified to be critical for endosomal PAR1-p38 MAPK signaling pathway, several deubiquitinases (DUB) have been proposed to regulate p38 phosphorylation and its downstream effect in endothelial cells. We further investigated how one of the proposed DUBs, ubiquitin specific peptidase 34 (USP34), regulates thrombin-induced, ubiquitin-driven PAR1-p38 signaling. Here, we show that USP34 regulates PAR1 total and surface expression via down-regulating *F2R* (PAR1) gene expression at the transcription level. Although the exact mechanism has yet to be determined, these results suggest that ubiquitin and DUBs may be involved in GPCR signaling at various stages.

Introduction

G protein-coupled receptors (GPCR) is a large protein family consists of more than 799 members (198). Many of them bind to specific ligands and are subsequently activated. Such

activation triggers a series of cellular signal transductions and regulates a plethora of cell behaviors, making them important for cells to interact with their environments. Due to their critical nature, many GPCRs are targets of FDA-approved drugs, designed to combat a wide range of human diseases by modulating GPCR activity. Canonically, an activated GPCR interacts with a specific combination of G protein subunits and regulates second messengers and several downstream effectors. Simultaneously, the activated GPCR is internalized and either recycled to cell surface, or further prepared to be degraded. Many aspects of these processes and the effectors are known to be controlled by protein phosphorylation, such as desensitization of GPCR, arrestin-mediated signaling, and downstream signaling pathways. Although other posttranslational modifications (PTM) such as ubiquitination, lipidation, and glycosylation, have been reported to be involved in GPCR regulation, our understanding is still rather limited (5).

Protein ubiquitination is an important PTM that mediates protein stability and protein-protein interactions (199). Ubiquitin is a small, conserved protein that can be covalently linked to another protein, including ubiquitin, majorly to their lysine (K) residue by a group of protein called E3 ligases. It is known that there are several types of chained poly-ubiquitin, including K63 and K48, can be attached to proteins. Attached ubiquitins can also be removed by a group of proteases called deubiquitinases (DUB). Both E3 ligases and DUBs can exhibit specific linkage activity (16,20) and are involved in many human diseases due to their roles in regulating protein abundance as well as interactions. However, our knowledge about protein ubiquitination/deubiquitination in the context of GPCR biology is still preliminary. Furthermore, while ubiquitination of GPCR and/or other components is thought to regulate receptor trafficking and cell signaling (5,34,121), the roles of DUB in this picture have been understudied. Several studies, which examined selected candidate DUBs, have shown that some DUBs regulate cell surface expression, lysosomal

trafficking, and stability of specific GPCRs (**Table 0.1**). This growing body of evidence suggests an unexplored area of GPCR regulation which is controlled by DUBs.

In our previous research, an irreversibly activated GPCR, protease-activated receptor 1 (PAR1) is found to be poly-ubiquitinated and plays a critical role in endothelial integrity. Ubiquitination of PAR1 by neural precursor cell expressed developmentally down-regulated 4-like (NEDD4L, as known as NEDD4-2) drives a pro-inflammatory signal from endosomes and activates p38α mitogen-activated protein kinase (MAPK) (11,12). To identify the DUB(s) that regulate PAR1-mediated p38 MAPK signaling, we deployed a comprehensive RNA interference (RNAi) screen in endothelial cells and HeLa cells, and showed that two DUBs, cylindromatosis (CYLD) and ubiquitin-specific peptidase 34 (USP34) regulate p38 phosphorylation and its downstream effect (200). Although both DUBs regulate PAR1-mediated endosomal p38 MAPK activation, they differentially regulate endothelial leakage and pro-inflammatory cytokine expression, suggesting distinct mechanisms by which these two DUBs are involved in PAR1 signaling.

While this previous screen and following validations revealed that USP34 regulates PAR1-induced p38 activation and plays a role in IL-6 mRNA expression, it is unknown how USP34 integrates into the endosomal signaling of PAR1. In this study, we characterized USP34 expression in endothelial cells, and examined whether USP34 plays a role in regulating PAR1 stability and trafficking, as well as the abundance and ubiquitination status of proteins that are key to PAR1-p38 signaling axis. Here we show that although USP34 may not deubiquitinate PAR1, USP34 expression plays a role in PAR1 abundance via regulating its transcription, indirectly down-regulating PAR1-mediated signaling including endosomal p38 activation.

Results

USP34 regulates thrombin-induced p38 and ERK1/2 signaling

We showed that USP34 expression is highly abundant in HUVEC-derived endothelial EA.hy926 cells and controls thrombin-induced p38 MAPK endosomal signaling (11,12,200). To determine whether USP34 regulates thrombin signaling globally, we examined ERK1/2 signaling, which occurs downstream of activated PAR1 coupling to plasma membrane localized heterotrimeric G proteins (201). Endothelial cells were transfected with a validated short interfering RNA (siRNA) targeting USP34 mRNA or non-specific (NS) control siRNA and stimulated with thrombin. USP34 siRNA transfected cells displayed a marked increase in p38 MAPK activation that peaked at 7.5 min following thrombin stimulation, compared to NS siRNA control transfected cells (Figure 2-1, A and B). The enhanced p38 MAPK phosphorylation induced by thrombin in USP34 depleted cells was blocked by vorapaxar, a PAR1 selective antagonist, and BIRB796, a p38 MAPK inhibitor (Figure 2-1, D-G), indicating a critical role for PAR1 and p38 autoactivation in thrombin-stimulated p38 MAPK signaling. Interestingly, knockdown of USP34 in endothelial cells also yielded a modest increase in thrombin induced ERK1/2 signaling after 7.5 min of thrombin incubation (Figure 2-1, A and C). We also examined the interaction between thrombin treatment time and siRNA transfection (NS siRNA versus USP34 siRNA) on p38 phosphorylation and ERK1/2 phosphorylation by two-way ANOVA analysis. Both interaction terms were significant (p38: $p < 0.0001$; ERK1/2: $p = 0.0332$; see **Supplemental Table 2-1**), meaning the effect of thrombin treatment depends on which siRNA the cells were transfected with. These data suggest that USP34 regulates both thrombin-activated PAR1-induced p38 MAPK endosomal signaling as well as ERK1/2 signaling, which proceeds from the plasma membrane.

Endogenous USP34 is localized in the nucleus and cytoplasm

To evaluate the subcellular localization of endogenous USP34 in endothelial cells, we utilized a biochemical cellular fractionation assay and immunofluorescence confocal microscopy and detected USP34 with antibodies. Endothelial cells were subjected to cellular fractionation, which yielded nuclear, cytoplasmic and membrane fractions that were verified by the detection of the p84 nuclear marker, Na^+/K^+ ATPase plasma membrane marker and GAPDH, a cytoplasmic marker (**Figure 2-2**, A). USP34 was detected predominantly in cytoplasmic and nuclear fractions with minimal detection in the membrane fraction of endothelial cells (**Figure 2-2**, B and C). In addition, there were no considerable changes in USP34 presence in the cellular fractions following thrombin treatment (**Figure 2-2**, B and C). The subcellular localization of endogenous USP34 detected by immunofluorescence microscopy also indicated that USP34 resides primarily in the nucleus and sparsely in cytoplasm with no apparent translocation to PAR1 following thrombin stimulation (**Figure 2-2**, E). To further substantiate endogenous USP34 subcellular localization, an HA-epitope tag was knocked into the USP34 gene using CRISPR-Cas9 in HeLa cells and verified by immunoblot (Figure 2, G). A similar pattern of USP34 expression was detected with anti-HA antibodies and showed USP34 localization primarily in the nucleus with less expression in the cytoplasm (**Figure 2-2**, F), whereas no signal was detected in parental cells lacking the HA-epitope. These findings suggest that USP34 is likely to function in the nucleus and cytoplasm.

USP34 does not modulate PAR1-p38 signaling pathway component expression or ubiquitination

Thrombin-activated PAR1 ubiquitination mediated by the E3 ligase NEDD4-2 promotes recruitment of TAB1 and TAB2 resulting in p38 MAPK endosomal signaling (11-13). Thus, we first determined if USP34 modulates the expression and/or the ubiquitination status of PAR1-stimulated p38 MAPK signaling pathway components. In endothelial cells, knockdown of USP34

expression by siRNA had no significant effect on the expression of NEDD4-2, TAB1 or TAB2 proteins compared to NS siRNA transfected control cells (**Figure 2-3**, A-D). Next, tandem ubiquitin-binding entities (TUBEs) beads that bind to and enrich polyubiquitinated proteins were used to assess the role of USP34 in regulating the ubiquitination status of PAR1-p38 signaling pathway components. Cells were transfected with NS- or USP34-specific siRNAs and stimulated with or without thrombin, and polyubiquitinated proteins were enriched from the whole cell lysates using TUBEs. Consistent with our previous report (12), thrombin induced a rapid increase in NEDD4-2 ubiquitination in NS siRNA control cells that was comparable in USP34-specific siRNA transfected cells (**Figure 2-3**, E and F). Whereas no change in TAB1, TAB2 or p38 ubiquitination status was observed in thrombin treated cells transfected with USP34 or NS siRNAs (**Figure 2-3**, E). These results suggest that USP34 regulates PAR1-p38 signaling without altering the expression or ubiquitination status of key p38 signaling pathway components downstream of PAR1.

PAR1 cell surface expression but not internalization is regulated by USP34

PAR1 displays both constitutive and agonist-induced internalization, which occurs through clathrin-mediated endocytosis (202-204). To define the function of USP34 in PAR1 trafficking, we examined cell surface expression of endogenous PAR1 in USP34-depleted endothelial cells treated with or without thrombin. After a 30 min incubation, ~40% of PAR1 internalized from the cell surface in control NS siRNA transfected cells, whereas knockdown of the μ2 subunit of the adaptor protein complex 2 (AP2), the major clathrin adaptor, significantly increased expression of PAR1 at the cell surface and inhibited constitutive internalization (**Figure 2-4**, B), as expected (202,203). Surprisingly, depletion of USP34 resulted in a significant increase in surface expression of PAR1, although the extent of PAR1 constitutive internalization was not significantly affected

(**Figure 2-4**, A). In cells treated with the PAR1-specific agonist peptide TFLLRNPNDK that rate of receptor internalization was similar in NS and USP34 siRNA-treated cells, although USP34 knockdown significantly increased PAR1 surface expression (**Figure 2-4**, C). Whereas depletion of the μ2 subunit of the AP2 complex, significantly reduced agonist triggered PAR1 internalization (**Figure 2-4**, D) as previously reported (205). These data indicate that USP34 controls expression of PAR1 at the cell surface through a mechanism that occurs independent of receptor internalization.

USP34 regulates PAR1 protein expression but does not alter PAR1 ubiquitination or protein stability

We showed previously that basal ubiquitination of PAR1 functions to retain the receptor at the cell surface by impeding AP2 interaction with the receptor and constitutive internalization (204). Thus, we next sought to determine if USP34 regulated PAR1 ubiquitination in endothelial cells using TUBEs followed by immunoblotting with anti-ubiquitin antibodies. Endothelial cells were transfected with NS or USP34 siRNA, stimulated with thrombin, lysed and ubiquitinated PAR1 was enriched using TUBEs that bind to polyubiquitinated proteins. Indeed, in USP34 knockdown cells the abundance of ubiquitinated PAR1 appeared greater than that detected in NS siRNA-transfected control cells (**Figure 2-5**, A). However, the total amount of PAR1 protein similarly increased in USP34 depleted cells (Figure 5, A and B) Therefore, after normalization, there was no significant difference in the thrombin-induced ubiquitination of PAR1 in NS versus USP34 siRNA-transfected cells (**Figure 2-5**, A and C). To verify these findings, endothelial cells transfected with NS- and USP34-specific siRNAs were treated with thrombin, lysed, immunoprecipitated with anti-PAR1 antibodies and ubiquitination detected using anti-ubiquitin antibodies. Like the TUBE assays, ubiquitination of immunoprecipitated PAR1 appeared to

increase in USP34 knockdown cells compared to control cells, however a greater abundance of total PAR1 protein was also detected in USP34 siRNA transfected cells (**Figure 2-5**, D and E). After normalization, thrombin induced PAR1 ubiquitination was similar in USP34 depleted cells compared to control cells (**Figure 2-5**, C and F). Thus, PAR1 ubiquitination is not directly regulated by USP34, but rather USP34 appears to control PAR1 protein expression, which is consistent with increased expression of the receptor at the cell surface.

In previous studies, we showed that PAR1 sorts through an atypical endosomal-lysosomal pathway independent of ubiquitination and ubiquitin-binding ESCRT components (206,207). Although PAR1 ubiquitination is not required to drive PAR1 lysosomal degradation, ubiquitination of ancillary adaptor proteins such as ALG-2-interacting protein X (ALIX) and α-arrestins are necessary to facilitate receptor lysosomal sorting (206-208). These studies raise the possibility that USP34 may function indirectly to control PAR1 degradation in lysosomes. To determine the role of USP34 in PAR1 lysosomal degradation, we measured the half-life of PAR1 protein turnover in endothelial cells depleted of USP34. The rate of PAR1 degradation was measured in endothelial cells transfected with NS and USP34 siRNAs treated with cycloheximide (CHX) to inhibit protein synthesis. While PAR1 expression was significantly increased in the USP34 knockdown cells (**Figure 2-6**, A and B), the rate of PAR1 degradation was com parable to that observed in NS siRNA cells treated with CHX (**Figure 2-6**, A and C). Taken together these results suggest that USP34 is unlikely to regulate PAR1 protein expression through processes like receptor ubiquitination, internalization or endosomal-lysosomal degradation.

USP34 regulates PAR1 mRNA expression

In addition to regulating protein trafficking and signaling, DUBs have been shown to control protein translation by modulating the ubiquitination status of ribosomes (16). In addition,

USP34 has been reported to regulate gene transcription and DNA repair (168,209). These suggest that USP34 may regulate USP34 expression at the gene transcriptional or translational level. To determine if USP34 regulates PAR1 mRNA expression, endothelial cells transfected with NS- or USP34-specific siRNA were treated with or without actinomycin D, a transcription inhibitor, and the abundance of the PAR1 encoding *F2R* gene mRNA transcripts were measured by qRT-PCR. In cells transfected with USP34-specific siRNA, a significantly higher abundance of *F2R* mRNA transcripts were detected compared to the NS siRNA treated control cells (**Figure 2-7**, A). However, USP34 depletion had no impact on the half-life of the long lived *F2R* mRNA transcript over the 6 h timeframe (**Figure 2-7**, A). Like PAR1, USP34 depletion also increased the PAR2 encoding *F2RL1* gene mRNA transcripts but failed to markedly impact the mRNA half-life compared to NS siRNA treated control cells (**Figure 2-7**, B). These findings are the first to demonstrate that a DUB can regulate GPCR gene expression resulting in increased cell surface expression and cellular signaling in endothelial cells.

Discussion

Several GPCRs have been demonstrated to regulate endothelial functions, either through the canonical, G protein-mediated RhoA/MLC and MAPK cascade signaling pathways, or the endosomal, TAB adaptor proteins-dependent p38 MAPK activation (11-13). It is established that PAR1, a thrombin receptor, is ubiquitinated by activated NEDD4-2 hence mediating an endosomal activation of p38 MAPK. While such K63 polyubiquitination has been shown to be required for TAB protein and p38 MAPK recruitment, our understanding is limited as to how this signaling complex is regulated. We hypothesized that a de-ubiquitination event facilitated by DUB(s) may play a role to down-regulated this ubiquitin-driven PAR1-p38 MAPK signaling pathway. In the previous chapter, we deployed a genome-wide RNAi screen to identify DUB(s) which regulates

thrombin-mediated p38 MAPK autophosphorylation and downstream effects such as endothelial barrier function and pro-inflammatory cytokine expression (200). USP34, as a DUB that has been shown to regulate p38 autophosphorylation in HeLa cells and *IL6* expression in EA.hy926 cell lines, is hypothesized to regulate PAR1 in endothelial cells through an unknown mechanism. Here, we assessed USP34's potential roles in PAR1 life cycle, including trafficking, stability, ubiquitination status, and expression level. This study shows that *F2R* (PAR1) mRNA expression is down-regulated by USP34, which subsequently limited surface receptor abundance thus further affecting thrombin-induced MAPK signaling.

We first tested whether USP34 specifically regulates thrombin-induced p38 MAPK phosphorylation in endothelial cells. Similar to our previous report (200), depletion of USP34 did up-regulated thrombin-induced p38 phosphorylation in EA.hy926 cells. But, unlike the previous observations, depletion of USP34 has an ambiguous effect on thrombin-induced ERK1/2 phosphorylation. It was later revealed that USP34 regulates PAR1 surface expression, upstream of both p38 and ERK1/2 MAPK activation. Also, ERK1/2 phosphorylation generally was observed to peak within 2.5 minutes (11), which together may explain this discrepancy.

Since DUBs may play diverse roles in regulating a signaling pathway, we took a comprehensive approach to examine whether USP34 is involved in p38 MAPK endosomal activation and/or any key PAR1 regulation mechanism. First, we examined whether the key components of PAR1-p38 signaling complex were potential USP34 substrates, which was shown to be unlikely. Second, we tested our hypothesis that USP34 down-regulates PAR1 ubiquitination thus affecting p38 autophosphorylation. Despite USP34 having been shown to exhibit protease activity towards K63 polyubiquitination (210), the result showed that the presence of this DUB is not linked to PAR1 ubiquitination status, while it may play a role in PAR1 protein expression.

Third, we examined whether USP34 regulate PAR1 trafficking and lysosomal degradation, which are associated with PAR1 putative ubiquitination site at its C-tail and ubiquitination of ALIX, respectively (204,206). Surprisingly, we failed to show that USP34 regulates PAR1 stability or trafficking, whereas many other DUBs have been reported to regulate intracellular trafficking and degradation of other GPCR (see **Table 0.1**). Instead, USP34 is shown to be involved in PAR1 expression at the transcription level, since its mRNA expression was increased when USP34 is depleted in EA.hy926 cells. Similarly, a mutation in USP8 has been recently reported to change vasopressin receptor 1B (V_{1B} receptor) expression by increasing *Avpr1b* promoter activity (134). These results mark the diverse role of DUBs in GPCR regulation.

We also showed that USP34 is localized to nucleus and cytoplasm in EA.hy926 cells by both cellular fractionation and microscopy, while USP34 contains two nuclear export signal (NES) regions (211). In HeLa cells, Sy *et al.* and our previous study reported that USP34 is found in nucleus and cytoplasm (168,200). In addition, while USP34 depletion enhanced p38 MAPK phosphorylation, it also suppressed *IL6* expression (200), which contradicts with the common model that p38 activation leads to *IL6* expression. These led us to hypothesize that the substrate of USP34 which regulates PAR1 expression might be a nuclear protein or one that translocate between nucleus and cytoplasm. Dai *et al.* previously demonstrated that overexpressed, truncated USP34 in laryngeal squamous cell carcinoma cell lines can interact and stabilize transcription factor SOX-2, suggesting USP34 may regulate other genes through similar mechanisms, including *F2R*. Alternatively, USP34 may regulate chromatin remodeling by regulating histone ubiquitination, thus exhibiting a more global change to an array of genes. In order to assess how USP34 distinctively regulates *F2R* and *IL6* mRNA expression, further research would require genomic and transcriptomic approaches to identify USP34 substrate transcription factor and

chromatin accessibility of those genes.

Figures

Figure 2-1. Knockdown of USP34 increases thrombin-induced p38 phosphorylation.

A, Immunoblots of cell lysates of endothelial EA.hy926 cells that were seeded, transfected with non-specific (NS) and USP34-specific siRNA, and stimulated with 10 nM α-thrombin for up to 10 minutes. Immunoblotted USP34 is indicated by > symbol.

B, Thrombin-induced p38 phosphorylation shown in panel (A). The integrated intensity of phosphorylated p38 species is divided by the integrated intensity of total p38. These ratios are normalized to the average of each replicate, then expressed as fractions over the average of NS-siRNA, 7.5 min control group. (N = 4)

C, Thrombin-induced ERK1/2 phosphorylation shown in panel (A). The integrated intensity of phosphorylated ERK1/2 species is divided by the integrated intensity of total ERK1/2. These ratios are normalized to the average of each replicate, then expressed as fractions over the average of NS-siRNA, 7.5 min control group. (N = 4)

D, Immunoblots of cell lysates of HeLa-PAR1 cells that were seeded, transfected with non-specific (NS) and USP34-specific siRNA. These cells are treated with either DMSO (vehicle) or vorapaxar during starvation and stimulated with 10 nM α-thrombin (+ DMSO or vorapaxar) for up to 10 minutes.

E, Immunoblots of cell lysates of HeLa-PAR1 cells that were seeded, transfected with non-specific (NS) and USP34-specific siRNA. These cells are treated with either DMSO (vehicle) or BIRB 796 during starvation and stimulated with 10 nM α-thrombin (+ DMSO or BIRB 796) for up to 10 minutes.

F, Thrombin-induced p38 phosphorylation shown in panel (D). The integrated intensity of phosphorylated p38 species is divided by the integrated intensity of total p38. These ratios are normalized to the average of each replicate, then expressed as fractions over the average of NS-siRNA, 0 min control group. (N = 3)

G, Thrombin-induced p38 phosphorylation shown in panel (E). The integrated intensity of phosphorylated p38 species is divided by the integrated intensity of total p38. These ratios are normalized to the average of each replicate, then expressed as fractions over the average of NS-siRNA, 0 min control group. (N = 3)

Error bar = standard deviation. Data were analyzed by two-way ANOVA, followed by Šídák's post hoc test. * $p < 0.05$, **** $p < 0.0001$; ns, not significant.

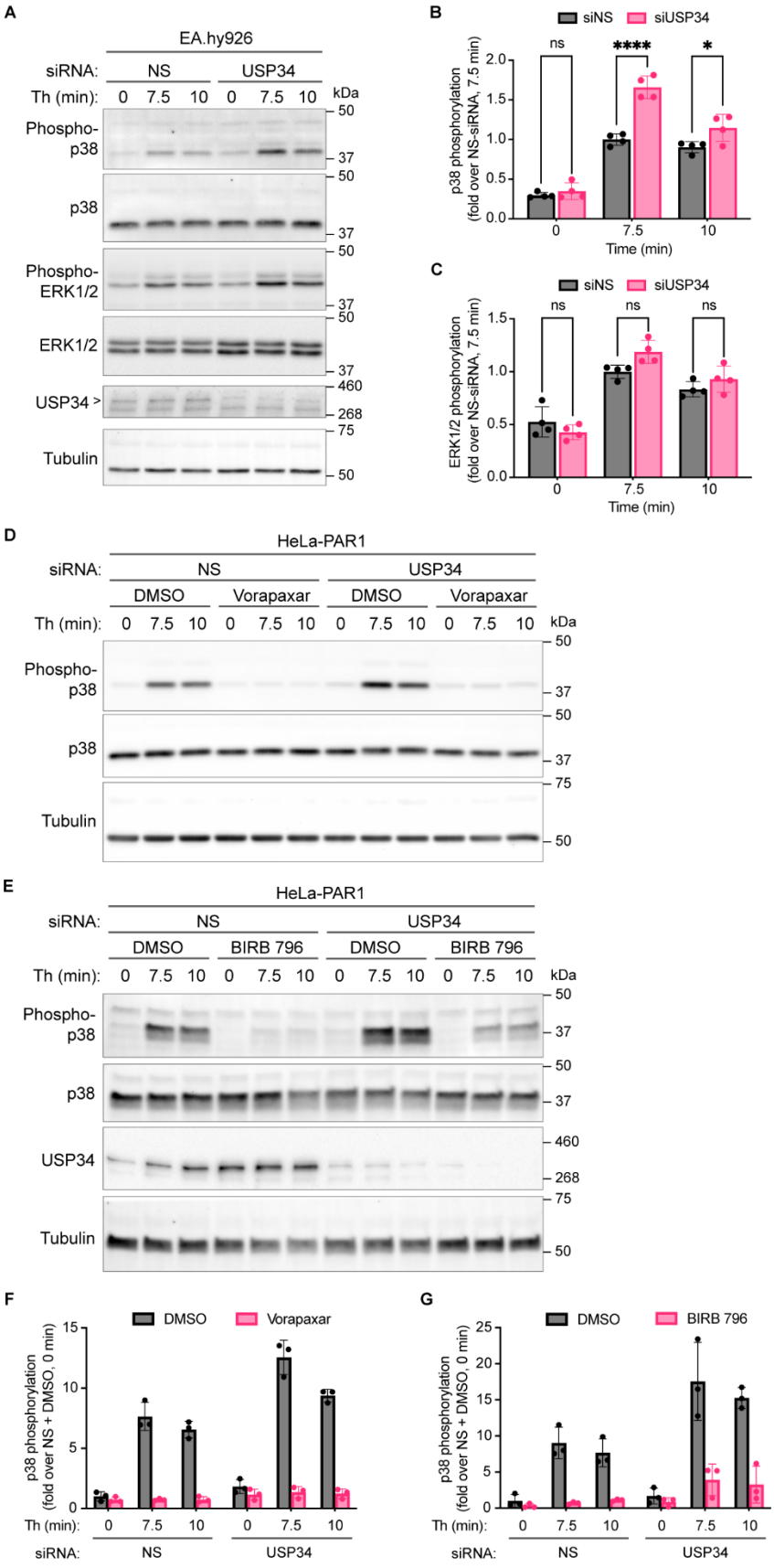

A
EA.hy926
siRNA:
NS
USP34
Th (min):
0 7.5 10 0 7.5 10
kDa
Phospho-p38
p38
Phospho-ERK1/2
ERK1/2
USP34
Tubulin
50
37
460
268
75
B
siNS
siUSP34
ns
****
*
p38 phosphorylation (fold over NS-siRNA, 7.5 min)
Time (min)
C
ERK1/2 phosphorylation (fold over NS-siRNA, 7.5 min)
D
HeLa-PAR1
DMSO
Vorapaxar
E
BIRB 796
F
G

Figure 2-2. USP34 is a nucleus- and cytoplasm-residing protein in endothelial EA.hy926 cells.

A, Cell fractions obtained from EA.hy926 were immunoblotted for USP34 (indicated by > symbol), p84 (nuclear fraction marker), GAPDH (cytoplasmic fraction marker), and sodium/potassium-transporting ATPase subunit alpha-1 (membrane fraction marker).

B, USP34 expression in nuclear fraction. The integrated intensity of USP34 is expressed as a fraction over the average of 0 min control group. (N = 3) Error bar = standard deviation.

C, USP34 expression in cytoplasmic fraction. The integrated intensity of USP34 is expressed as a fraction over the average of 0-min control group. (N = 3) Error bar = standard deviation.

D, Schematic diagram of cell fractionation experiment workflow.

E, Immunofluorescence of USP34 and PAR1 in EA.hy926 cells. Cells were seeded and grown overnight, and stimulated with 100 μM SFLLRN agonist peptide for up to 10 minutes. After fixation, primary and secondary antibodies are used to probe localization of USP34 and PAR1. Scale bar = 20 μm.

F, Immunofluorescence of HA-tagged USP34 in HeLa-PAR1$^{HA\text{-}USP34}$ cells. Scale bar = 20 μm.

G, Immunoblots of HA-tagged USP34 in HeLa-PAR1$^{HA\text{-}USP34}$ and its parental cells.

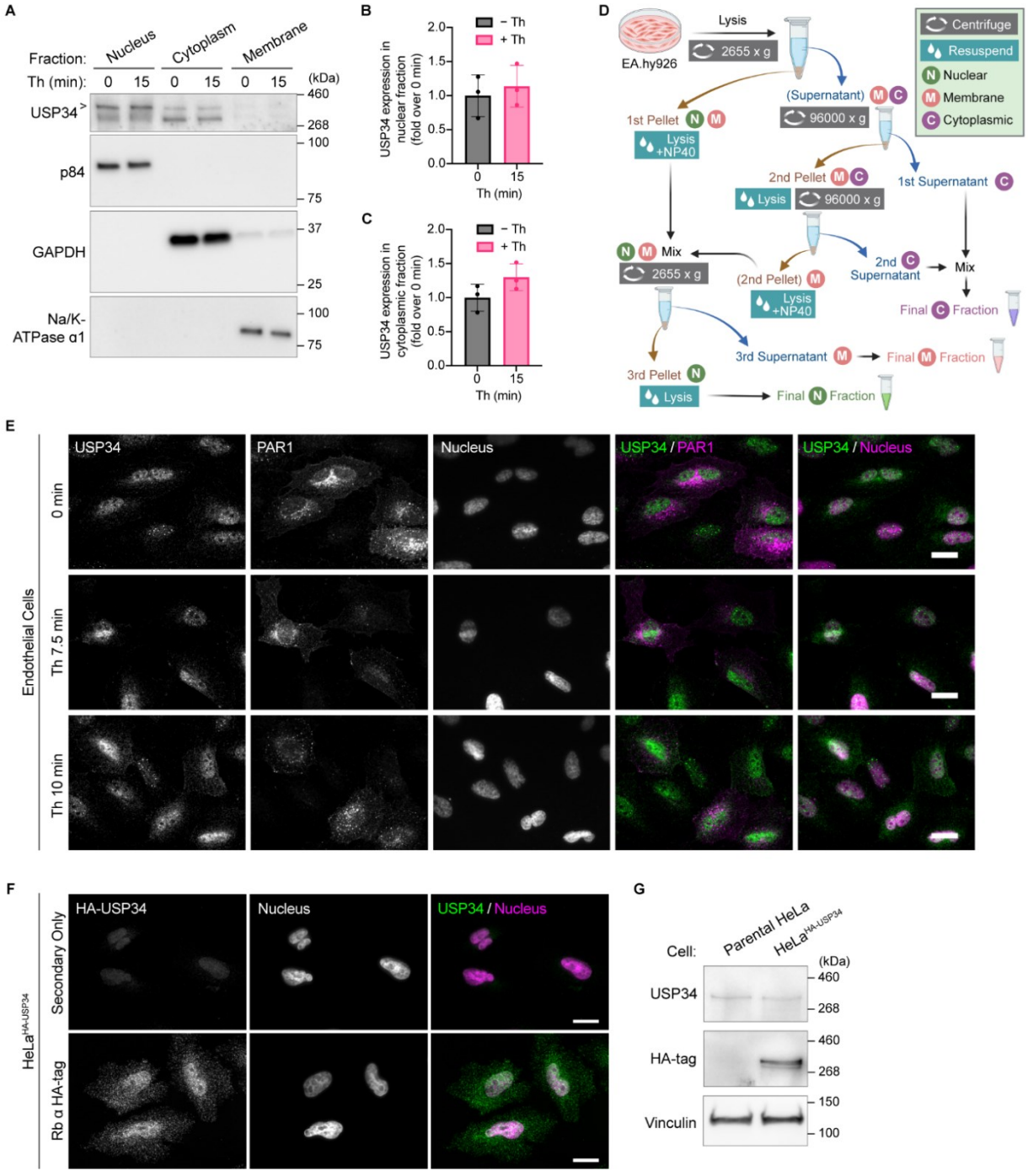

A
Fraction: Nucleus Cytoplasm Membrane
Th (min): 0 15 0 15 0 15 (kDa)
USP34
p84
GAPDH
Na/K-ATPase α1
460
268
100
75
37
25
100
75
B
USP34 expression in nuclear fraction (fold over 0 min)
− Th
+ Th
2.0
1.5
1.0
0.5
0.0
0
15
Th (min)
C
USP34 expression in cytoplasmic fraction (fold over 0 min)
− Th
+ Th
2.0
1.5
1.0
0.5
0.0
0
15
Th (min)
D
EA.hy926
Lysis
2655 x g
(Supernatant) M C
96000 x g
1st Pellet N M
Lysis +NP40
2nd Pellet M C
Lysis
96000 x g
1st Supernatant C
N M Mix
2655 x g
(2nd Pellet) M
Lysis +NP40
2nd C Supernatant
Mix
Final C Fraction
3rd Supernatant M
Final M Fraction
3rd Pellet N
Lysis
Final N Fraction
Centrifuge
Resuspend
N Nuclear
M Membrane
C Cytoplasmic
E
Endothelial Cells
0 min
Th 7.5 min
Th 10 min
USP34
PAR1
Nucleus
USP34 / PAR1
USP34 / Nucleus
F
HeLa HA-USP34
Secondary Only
Rb α HA-tag
HA-USP34
Nucleus
USP34 / Nucleus
G
Cell: Parental HeLa HeLa HA-USP34
(kDa)
USP34
HA-tag
Vinculin
460
268
460
268
150
100

Figure 2-3. Loss of USP34 does not alter expression and ubiquitination of the key components mediating PAR1-p38 signaling.

A, Immunoblots of cell lysates of EA.hy926 cells that were seeded, transfected with non-specific (NS) and USP34-specific siRNA, and stimulated with 10 nM α-thrombin for up to 10 minutes.

B, NEDD4-2 expression shown in panel (A). The integrated intensity of NEDD4-2 is normalized to the average of each replicate, then expressed as a fraction over the average of NS-siRNA, 0-min control group. (N = 4)

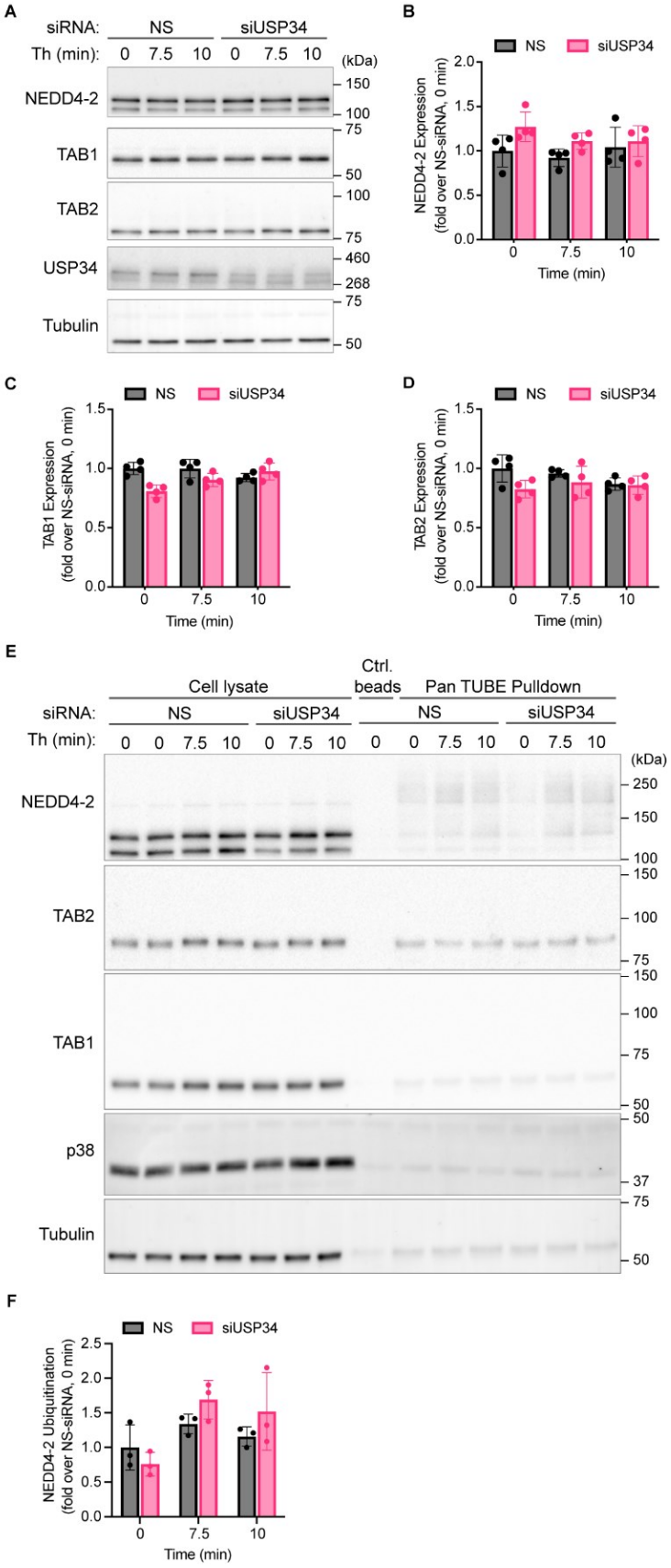
C, TAB1 expression shown in panel (A). The integrated intensity of TAB1 is normalized to the average of each replicate, then expressed as a fraction over the average of NS-siRNA, 0-min control group. (N = 4)

D, TAB2 expression shown in panel (A). The integrated intensity of TAB2 is normalized to the average of each replicate, then expressed as a fraction over the average of NS-siRNA, 0-min control group. (N = 4)

E, Immunoblots of enriched ubiquitinated proteins from EA.hy926 cell lysates using pan TUBE1 beads and input lysates. These cells were seeded, transfected with non-specific (NS) and USP34-specific siRNA, and stimulated with 10 nM α-thrombin for up to 10 minutes.

F, NEDD4-2 ubiquitination shown in panel (A). The integrated intensity of ubiquitinated NEDD4-2 (> 150 kDa in the lanes of Pan TUBE Pulldown) is divided by total NEDD4-2 expression (in the lanes of Cell lysate). These ratios are then normalized to the average of each replicate, then expressed as a fraction over the average of NS-siRNA, 0-min control group. (N = 3)

Error bar = standard deviation.


A
siRNA:
NS
siUSP34
Th (min):
0 7.5 10 0 7.5 10
(kDa)
NEDD4-2
150
100
TAB1
75
50
TAB2
100
75
USP34
460
268
Tubulin
75
50
B
NS
siUSP34
NEDD4-2 Expression (fold over NS-siRNA, 0 min)
Time (min)
C
TAB1 Expression (fold over NS-siRNA, 0 min)
Time (min)
D
TAB2 Expression (fold over NS-siRNA, 0 min)
Time (min)
E
Cell lysate
Ctrl. beads
Pan TUBE Pulldown
siRNA:
NS
siUSP34
Th (min):
0 0 7.5 10 0 7.5 10 0 0 7.5 10 0 7.5 10
(kDa)
NEDD4-2
250
150
100
TAB2
150
100
75
TAB1
150
100
75
50
p38
50
37
Tubulin
75
50
F
NS
siUSP34
NEDD4-2 Ubiquitination (fold over NS-siRNA, 0 min)
Time (min)

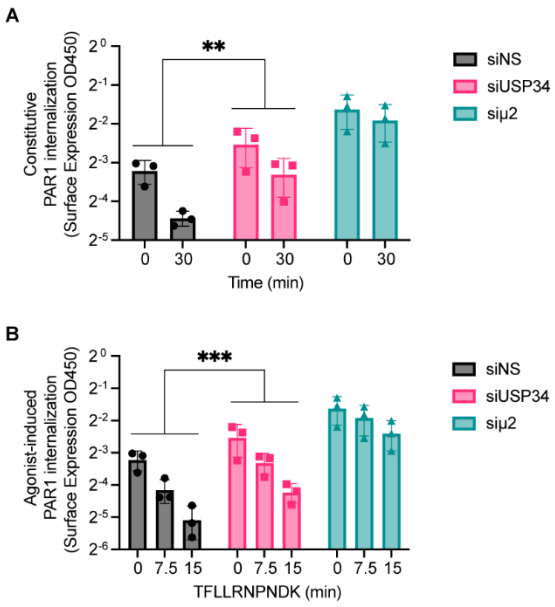


Figure 2-4. Knockdown of USP34 significantly increases PAR1 cell surface expression but does not affect PAR1 constitutive internalization or agonist-induced endocytosis rate.

A, Remaining PAR1 expression at the surface after constitutive internalization, measured by loss-of-surface-receptor assay. EA.hy926 cells were seeded and transfected with non-specific (NS), USP34-, or μ2-specific siRNA. The cells are labeled with mouse anti-PAR1 antibody (WEDE15) on ice, and either left on ice or incubated at 37°C for 30 minutes. The remaining PAR1 at cell surface is then measured by loss-of-receptor assay at 450 nm. The background OD450 (secondary antibody-only) values were averaged and subtracted from all raw OD450 readout values. Error bar = standard deviation. Multiple linear regression analysis was used to estimate the main effects of incubation duration, USP34-knockdown, biological replicates (date), and interaction term (incubation duration×USP34-knockdown), upon log(OD450) (see **Supplemental Table 2-2**). ** $p < 0.01$. (N = 3)

B, Remaining PAR1 expression at the surface after agonist-induced internalization, measured by loss-of-surface-receptor assay. EA.hy926 cells were seeded and transfected with non-specific (NS), USP34-, or μ2-specific siRNA. The cells are labeled with mouse anti-PAR1 antibody (WEDE15) on ice, and either left on ice or treated with TFLLRNPNDK agonist-peptide incubated at 37°C for up to 15 minutes. The remaining PAR1 at cell surface is then measured by loss-of-receptor assay at 450 nm. The background OD450 (secondary antibody-only) values were averaged and subtracted from all raw OD450 readout values. Error bar = standard deviation. Multiple linear regression analysis was used to estimate the main effects of agonist treatment duration, USP34-knockdown, biological replicates (date), and interaction term (agonist treatment duration×USP34-knockdown), upon log(OD450) (see **Supplemental Table 2-2**). *** $p < 0.001$. (N = 3)

Figure 2-5. Knockdown of USP34 upregulates PAR1 protein expression but does not alter PAR1 ubiquitination.

A, Immunoblots of enriched ubiquitinated proteins from EA.hy926 cell lysates using pan TUBE1 beads, immunoprecipitated PAR1 using anti-PAR1 (WEDE15) antibody and protein A beads, and input lysates. These cells were seeded, transfected with non-specific (NS) and USP34-specific siRNA, and stimulated with 10 nM α-thrombin for up to 10 minutes.

B, PAR1 expression shown in panel (A). The integrated intensity of PAR1 (> 55kDa in Cell lysates) is normalized to the average of each replicate, then expressed as a fraction over the average of NS-siRNA, 0-min control group. (N = 3)

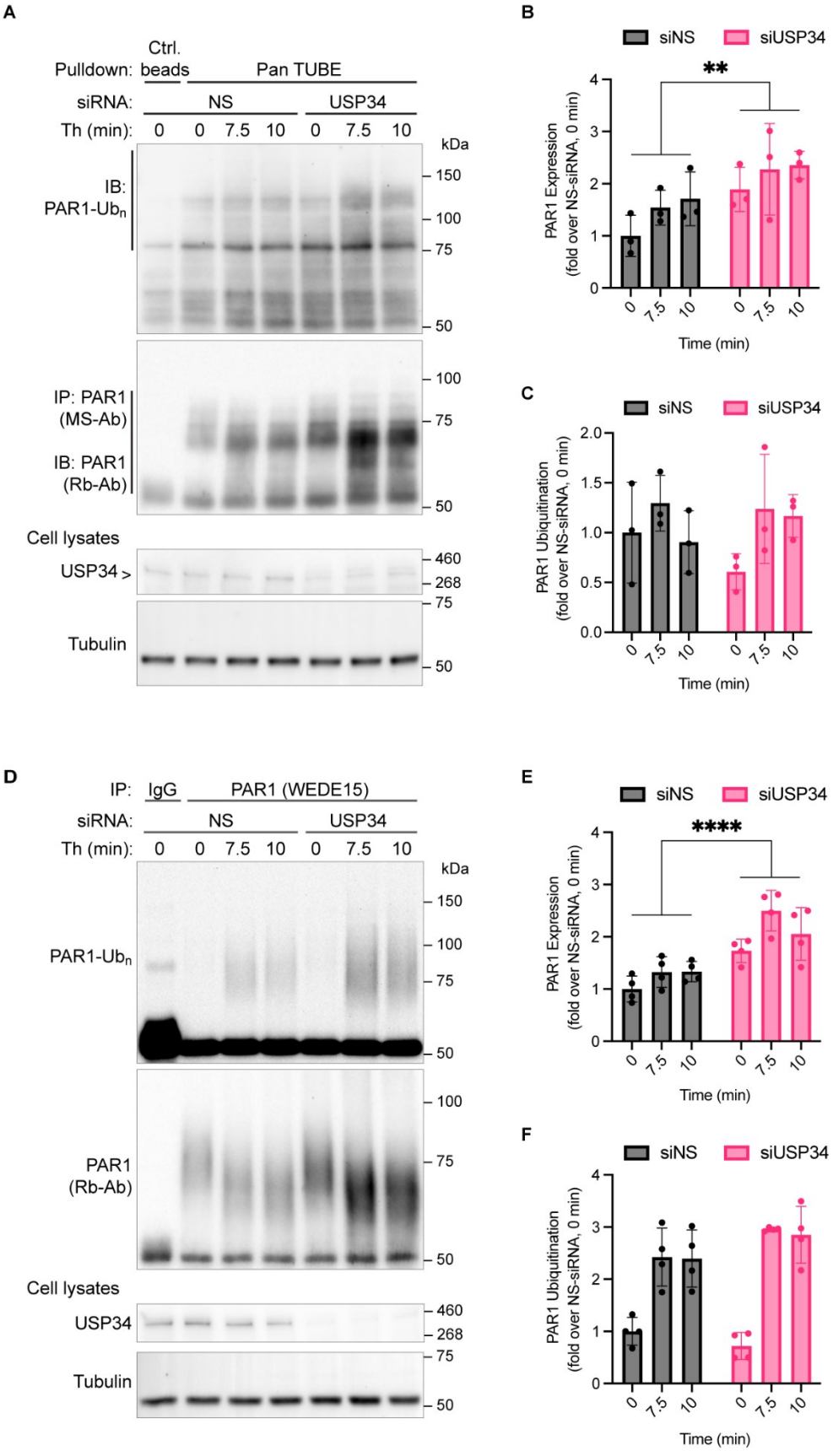
C, PAR1 ubiquitination shown in panel (A). The integrated intensity of ubiquitinated PAR1 (> 75 kDa in Pan TUBE) is divided by total PAR1 expression (> 55kDa in Cell lysates). These ratios are then normalized to the average of each replicate, then expressed as a fraction over the average of NS-siRNA, 0-min control group. (N = 3)

D, Immunoblots of immunoprecipitated PAR1 using anti-PAR1 (WEDE15) antibody and protein A beads, and input lysates from EA.hy926 cells. These cells were seeded, transfected with non-specific (NS) and USP34-specific siRNA, and stimulated with 10 nM α-thrombin for up to 10 minutes.

E, PAR1 expression shown in panel (A). The integrated intensity of PAR1 (> 55kDa in IP lysates) is normalized to the average of each replicate, then expressed as a fraction over the average of NS-siRNA, 0-min control group. (N = 3)

F, PAR1 ubiquitination shown in panel (A). The integrated intensity of ubiquitinated PAR1 (> 55 kDa in Ubiquitin blot) is divided by total PAR1 expression (> 55kDa in PAR1 blot). These ratios are then normalized to the average of each replicate, then expressed as a fraction over the average of NS-siRNA, 0-min control group. (N = 3)

Error bar = standard deviation. Data were analyzed by two-way ANOVA. ** $p < 0.01$, **** $p < 0.0001$.


A
Ctrl.
Pulldown: beads
Pan TUBE
siRNA:
NS
USP34
Th (min): 0 0 7.5 10 0 7.5 10
kDa
IB: PAR1-Ubn
150
100
75
50
IP: PAR1 (MS-Ab)
IB: PAR1 (Rb-Ab)
100
75
50
Cell lysates
USP34
460
268
Tubulin
75
50
B
siNS
siUSP34
**
PAR1 Expression (fold over NS-siRNA, 0 min)
Time (min)
C
PAR1 Ubiquitination (fold over NS-siRNA, 0 min)
D
IP: IgG
PAR1 (WEDE15)
PAR1-Ubn
PAR1 (Rb-Ab)
E
****
F

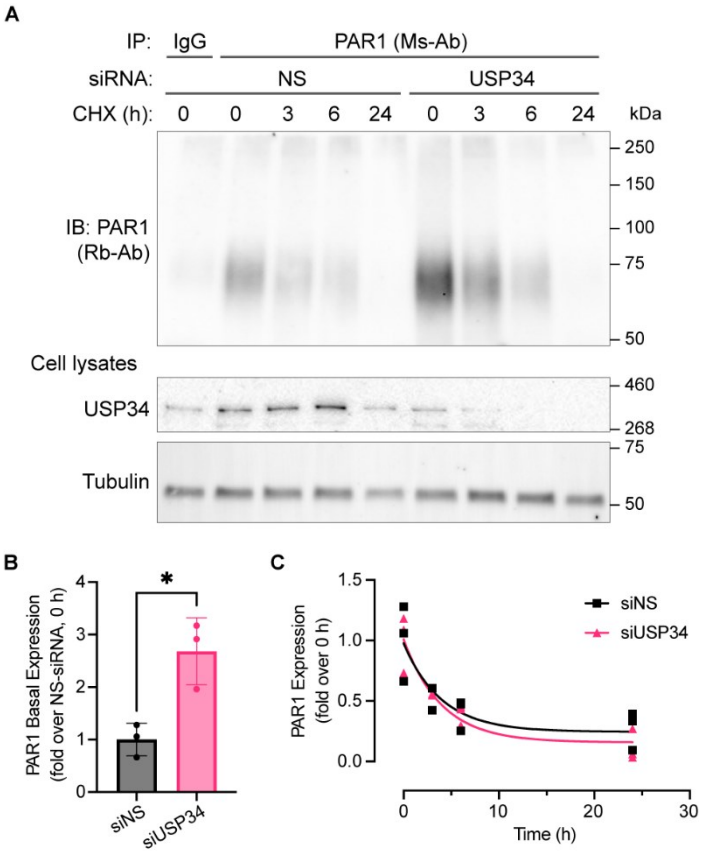


Figure 2-6. Loss of USP34 does not affect PAR1 basal degradation.

A, Immunoblots of immunoprecipitated PAR1 using anti-PAR1 (WEDE15) antibody and protein A beads, and input lysates from EA.hy926 cells. These cells were seeded, transfected with non-specific (NS) and USP34-specific siRNA, and treated with cycloheximide (CHX) for up to 24 hours.

B, PAR1 basal expression shown in panel *A*. The integrated intensity of PAR1 is normalized to the average of each replicate, then expressed as a fraction over the average of NS-siRNA, 0-h control group. Error bar = standard deviation. Data were analyzed by two-tailed unpaired Student's *t* test. * $p < 0.05$. (N = 3)

C, PAR1 basal degradation shown in panel *A*. The integrated intensity of PAR1 is normalized to the average of each replicate, then expressed as a fraction over the average of respective 0-h control group. Non-linear curve fitting was performed by modeling one-phase decay, least squares fit. (N = 3)

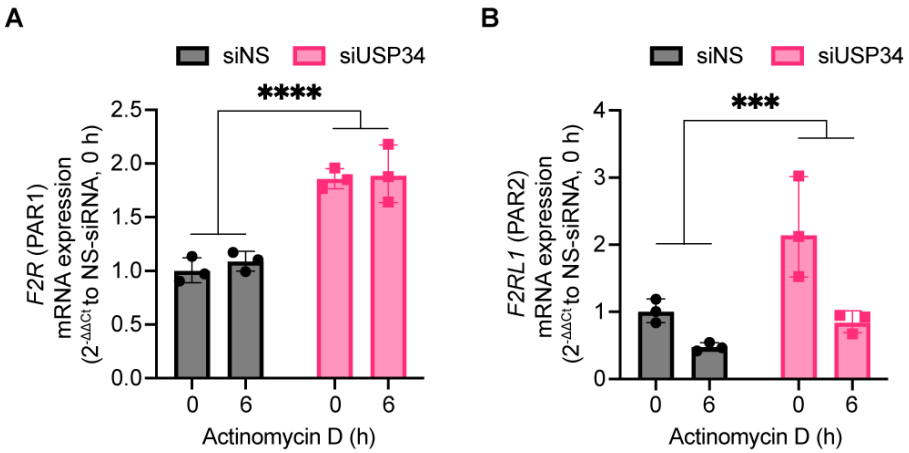


Figure 2-7. Loss of USP34 significantly upregulates PAR1 mRNA expression.

A, *F2R* (PAR1) mRNA expression in EA.hy926 cells that were transfected with non-specific (NS) and USP34-specific siRNA, and treated with 10 µg/mL actinomycin D for up to 6 hours. (N = 3)

B, *F2RL1* (PAR2) mRNA expression in EA.hy926 cells that were transfected with non-specific (NS) and USP34-specific siRNA, and treated with 10 µg/mL actinomycin D for up to 6 hours. (N = 3)

Error bar = standard deviation. Data were analyzed by two-way ANOVA. *** $p < 0.001$, **** $p < 0.0001$.

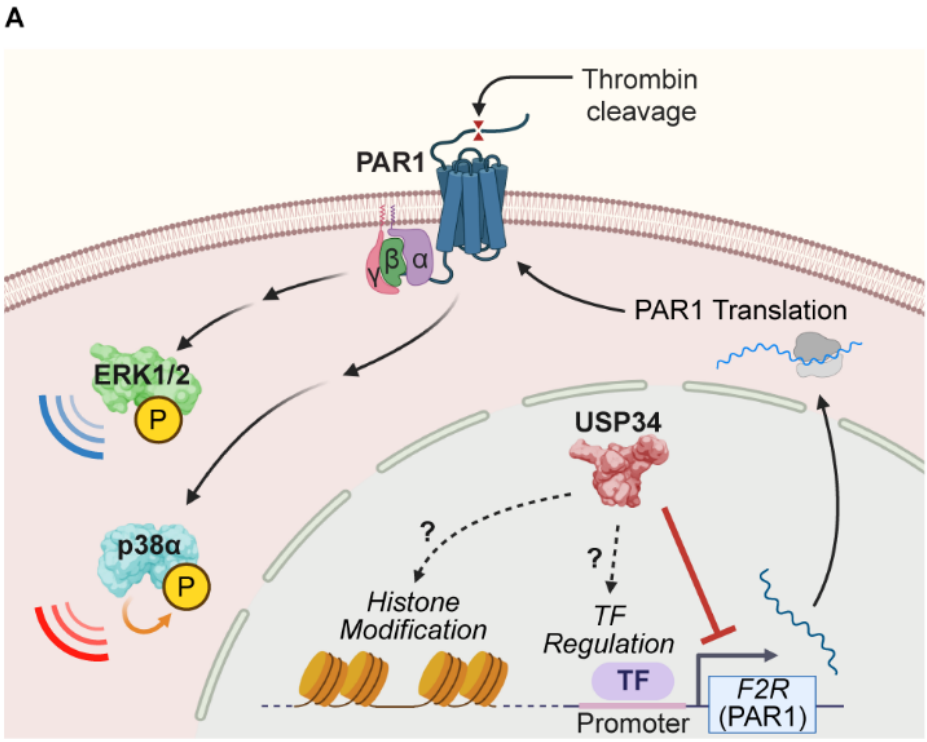


Figure 2-8. Hypothesized model describing regulation of PAR1 signaling by USP34.

Material and Methods

Reagents and Antibodies

Human α-Thrombin was obtained from Enzyme Research Laboratories (catalog no. HT1002a, South Bend, IN). PAR1-specific agonist peptide, TFLLRNPNDK peptide agonist was synthesized at the Tufts University Core Facility (Boston, MA). Vorapaxar (SCH 530348, catalog no. 1755) was obtained from Axon MedChem (Groningen, Netherlands). The following antibodies were obtained from Cell Signaling Technology (Danvers, MA): p38 MAPK (catalog no. 9212), phospho-p38 MAPK (catalog no. 4511), p44/42 MAPK ERK1/2 (catalog no. 9102), phospho-p44/42 MAPK ERK1/2 (catalog no. 9106), HA-Tag (catalog no. 3724), TAB1(catalog no. 3226), TAB2 (catalog no. 3745), NEDD4L (catalog no. 4013), and Na/K-ATPase α1 (catalog no. 3010). USP34 (catalog no. A300-824A) was purchased from Fortis Life Sciences (Waltham, MA). GAPDH antibody (catalog no. GTX627408) and nuclear matrix protein p84 antibody (catalog no. GTX70220) were obtained from GeneTex (Irvine, CA). Horseradish peroxidase (HRP)-conjugated goat-anti rabbit (catalog no. 1706515), HRP-conjugated goat-anti mouse (catalog no. 1706516), StarBright Blue 520 goat anti-mouse (catalog no. 12005867), StarBright Blue 700 goat anti-rabbit (catalog no. 12004162), and hFAB Rhodamine Tubulin (catalog no. 12004166) were from BioRad (Hercules, CA). Vinculin antibody (catalog no. V9131), bovine serum albumin (BSA, catalog no. 9647), fibronectin (catalog no. F1141), and BIRB 796 (catalog no. 506172) were from Sigma-Aldrich (Irvine, CA). AllStars negative control non-specific siRNA (catalog no. 1027281) was purchased from Qiagen (Hilden, Germany). USP34-specific siRNA (catalog no. J-006082-05; 5'-GCA GGG AAG UUC UGA CGA A-3') was purchased from Horizon Discovery (Waterbeach, UK).

Cell Culture

Human umbilical vein endothelial cell (HUVEC)-derived EA.hy926 cells were obtained from American Type Culture Collection (ATCC) (Manassas, VA), grown, propagated, and used between P2 and P10 according to ATCC instructions. These cells were maintained in Dulbecco's Modified Eagle's Medium (DMEM) (catalog no. 10-013-CV, Corning, Corning, NY) added with 10% fetal bovine serum (FBS) (catalog no. FB-01, Omega Scientific, Vista, CA), at 37°C with 8% CO_2. HUVEC-derived EA.hy926 cells are authenticated by short tandem repeat (STR) profiling as noted by ATCC and are routinely monitored for mycoplasma using Venor™ GeM Mycoplasma detection kit (catalog no. MP0025-1KT, Sigma-Aldrich, Irvine, CA) per the manufacturer's instructions.

Signaling Assays and Immunoblotting

EA.hy926 cells were seeded at 4.8×10^4 cells per well in a 48-well plate, transfected with siRNAs at 28 nM using TransIT-X2 Dynamic Delivery System (catalog no. MIR 6004, Mirus Bio, Madison, WI), and incubated with DMEM + 10% FBS at 37°C with 8% CO_2 for 2 days and serum-starved overnight with DMEM + 0.4% FBS. For HeLa cells, they were seeded at 1.4×10^4 cells per well in a 48-well plate, transfected with siRNAs at 50 nM using Oligofectamine Transfection Reagent (Thermo Fisher Scientific, Waltham, MA). Cells were then serum-starved for 60 min at 37°C, followed by stimulation with 10 nM α-thrombin for various times. Cells were lysed directly in 2X Laemmli Sample Buffer + DTT and boiled for 5 min at 95°C. Equivalent amounts of cell lysates were resolved by SDS-PAGE, transferred to PVDF membranes, and immunoblotted with antibodies as indicated. Membranes were developed by chemiluminescence or fluorescence detection using the ChemiDoc Imaging System (BioRad, Hercules, CA), quantified, and analyzed by densitometry using NIH ImageJ software or Image Lab 6.1 (BioRad, Hercules, CA).

Cellular Fractionation

EA.hy926 cells were seeded at 1.9×10^6 cell/dish in 60-mm petri dishes and incubated for 2 days. These cells were washed twice and collected with ice cold 1X PBS. The cell suspensions were centrifuged for 3 min at 105 × g at 4°C and resuspended in 250 µL of 1X hypotonic lysis buffer (20 mM Tris pH 7.4, 10 mM NaCl, 3 mM $MgCl_2$, 1X Roche complete EDTA-free Protease Inhibitor Cocktail, 1 mM PMSF). The lysates were further incubated for 30 min and vortex-mixed for 10 seconds for complete lysis. Cell lysates were sheared by passing through a 27-gauge needle 10 times. Protein concentrations were equalized with 1X hypotonic lysis buffer using a BCA protein assay (Thermo Fisher Scientific, Waltham, MA). 250 µL of each equalized cell lysate were centrifuged at 2655 × g for 10 min at 4°C to isolate nuclear fraction as the first pellet. If needed, after transferring the supernatant to a new tube, the pellet can be resuspended with the residual supernatant and be centrifuged again. The supernatant was ultracentrifuged at 96000 × g at 4°C for 1 hour to separate cytoplasmic fraction (the first supernatant) from membrane fraction (second pellet). The second pellet was resuspended in 250 µL of 1X hypotonic lysis buffer using 27-gauge needle and ultracentrifuged again at 96000 × g at 4°C for 1 hour. The resulted second supernatant was added to the first supernatant (500 µL total) as the final cytoplasmic fraction.

The second pellet (membrane fraction) was washed with 1X hypotonic lysis buffer three times and resuspended in 250 µL of 1X hypotonic lysis buffer. The first pellet (nuclear fraction) was also resuspended in 250 µL of 1X hypotonic lysis buffer. These were combined and solubilized by adding 25 µL NP-40, vortex-mixing for 10 seconds, and incubating on ice for 30 min. The mixture was centrifuged at 2655 × g for 10 min at 4°C to isolate the third supernatant as the final membrane fraction. Similarly, afterwards the pellet can be resuspended with the residual supernatant and be centrifuged again. The resulted third pellet was then washed three times with

250 µL of 1X hypotonic lysis buffer (2655 × g for 10 min at 4°C between each wash) and eventually resuspended in 250 µL of 1X hypotonic lysis buffer as the final nuclear fraction. The membrane and nuclear fractions were sonicated to maximize solubilization.

All fraction samples were mixed with 2X Laemmli Sample Buffer + DTT and boiled for 15 min at 65ºC.

Generation of HeLa$^{HA\text{-}USP34}$ using CRISPR/Cas9

The knock-in tagging of endogenous *USP34* gene in HeLa-PAR1 cells was performed using TrueTag Donor DNA Kit, HA (catalog no. A53809, Thermo Fisher Scientific, Waltham, MA), which contains 2X Phusion Flash High Fidelity PCR Master Mix (catalog no. F548S) and TrueTag donor DNA templates. These templates carry cassettes of puromycin- or blasticidin-resistance gene and HA epitope tag sequence, which can be recombined to the upstream (N-terminus) or downstream (C-terminus) of target coding sequence. The N-HA-blast donor template was amplified and extended by polymerase chain reaction (PCR) with customized DNA primers (forward: 5'- TCC GAA GCG GGG GAG GGG GGG GGC GGC GGC CGA ACG ATG GGA GGT AAG CCC TTG CAT TCG-3' and reverse: 5'-TTT AAC ACC TCC ACC AGG TCT GCG CAG TTC TCG CAA CCG CTT CCA CTA CCT GAA CC-3') and purified with DNA-binding column provided and subsequent elution.

HeLa cells overexpressing PAR1 were seeded at 1.75×10^5 cells per well in a 6-well plate. The media in the seeded wells was replaced by Opti-MEM + 30% FBS on the day of transfection. TrueCut Cas9 Protein v2 (catalog no. A36498), USP34-targeting single guide RNA (target sequence: 5'-CGC AGT TCT CGC ACA TCG TT-3', spanning the start codon of *USP34* gene), and 2.5 µg donor DNA were mixed in Opti-MEM I Reduced Serum Medium (catalog no. 31985070). Lipofectamine CRISPRMAX Cas9 Transfection Reagent (catalog no. CMAX00001)

was separately diluted in Opti-MEM. Both mixtures were incubated at room temperature for 1 minute then were combined and further incubated for 10 minutes. The complete transfection mixture was then added to the cells drop-wise. The transfected cells were grown for 48 hours and subcultured into larger vessels. 10 μg/mL blasticidin (catalog no. A1113903) was used to select for cells that carry recombined genome. Cell lysates were run with immunoblotting to validate the incorporation of HA epitope tag to endogenous USP34.

Immunofluorescence Confocal Microscopy

EA.hy926 cells were seeded at 3×10^4 cells per well in a 24-well plate and grown on fibronectin-coated coverslips (catalog no. 1943-10012A, Bellco Glass, Vineland, NJ) for 24 h. Cells were fixed with 4% (w/v) paraformaldehyde for 10 minutes and subsequently permeabilized with 0.2% (v/v) Triton X-100 at room temperature (20-22˚C) for 10 minutes, and blocked with 3% BSA/PBS for 60 min at room temperature (20-22˚C). Primary antibodies rabbit anti-USP34 (catalog no. A300-824A) at 1:200 dilution and mouse anti-PAR1 (WEDE15) at 1:500 dilution were used for staining. Secondary antibodies goat anti-Rabbit IgG (H+L) conjugated to Alexa Fluor 594 (catalog no. A-11012, Thermo Scientific) and goat anti-Mouse IgG (H+L) conjugated to Alexa Fluor 647 (catalog no. A-21235, Thermo Scientific) at 1:500 dilution was used. All antibodies were prepared in the blocking buffer and incubated with coverslips for 60 minutes. Nuclei were stained with Hoechst 33342 solution (catalog no. 62249, Thermo Scientific) prepared in blocking buffer at 1:2000 dilution. Coverslips were mounted with ProLong Gold Antifade Mountant (catalog no. P36934, Thermo Fisher Scientific, Waltham, MA).

Confocal microscopy image acquisition was performed using Olympus IX81 spinning-disk Microscope (Tokyo, Japan), equipped with a CoolSNAP HQ2 CCD Camera (Andor, Belfast, UK), a 60× 1.40 NA oil PlanApo objective lens (Olympus), and appropriate filters. At least three random

fields of view for each coverslip were acquired using MetaMorph software (MDS Analytical Technologies, Sunnyvale, CA) with multiple focal positions. Image stacks were processed to generate Z-projection (maximum-intensity method) images using NIH Fiji software.

Tandem Ubiquitin-Binding Entities (TUBEs) Pulldown of Cell Lysate

EA.hy926 cells were seeded at 1.0×10^6 cells per dish in 100-mm petri dishes, transfected, starved, and stimulated with 10 nM thrombin as described above. Cells were then collected into NP-40-based lysis buffer supplemented with protease, phosphatase, and deubiquitinase inhibitors (50 mM Tris pH 7.5, 150 mM NaCl, 1% [v/v] NP-40, 10 mM β-Glycerophosphate, 1X Roche complete EDTA-free Protease Inhibitor Cocktail, 1 mM $NaVO_4$, 10 mM NaF, 2 mM NaPP, 50 μM PR619, 20 mM NEM) on ice. The cell suspensions were briefly sonicated and clarified by centrifugation. Protein concentrations were determined using a bicinchoninic acid (BCA) protein assay (Thermo Fisher Scientific, Waltham, MA) and equalized with lysis buffer. Two-thirds of each lysate was used for TUBE pulldown, while one-third of each clear lysate was used for PAR1 immunoprecipitation to measure total expression.

To reduce non-specific protein immobilization onto the beads, magnetic control beads (catalog no. UM400M, LifeSensors, Malvern, PA) were mixed and incubated with cell lysates for 30 min at 4°C. Following control bead removal, magnetic TUBE1 beads (catalog no. UM401M, LifeSensors, Malvern, PA) were mixed and incubated with pre-cleared cell lysates overnight to capture ubiquitinated proteins. Beads were washed and resuspended in 2X Laemmli Sample Buffer + DTT and boiled for 5 min at 95°C.

For PAR1 immunoprecipitation, anti-PAR1 (WEDE15) antibody, mouse-IgG control antibody, and BSA-blocked protein A-sepharose CL-4B beads (Cytiva, Marlborough, MA) were incubated with the lysates overnight. Beads were washed and proteins were eluted with 2X

Laemmli Sample Buffer + DTT and boiled for 5 min at 95ºC. All samples were then immunoblotted as described above.

Loss-of-surface-receptor Assay

EA.hy926 cells were seeded at 9.0×10^4 cells per well in a 24-well plate, transfected, starved as described above in 4 separate plates. Each plate was incubated with diluted (1:500) mouse anti-PAR1 (WEDE15) antibody (except the secondary-only wells) to label the surface cohort of receptor for 1 hour and washed with starvation buffer. While one plate was kept on ice, one plate was moved to 37ºC and incubated for 30 min, and two plates were treated with 100 mM PAR1-specific agonist peptide, TFLLRNPNDK, for 7.5 min and 15 min. The cells were fixed with cold 4% (w/v) paraformaldehyde for 5 min and further incubated with HRP-conjugated goat anti-mouse IgG secondary antibody (diluted at 1:1000) for 1 hour at room temperature. Cells were gently washed and TMB substrate solution (catalog no. 34022, Thermo Scientific, Waltham, MA) was added to each well and developed for 10-30 minutes. Equal amount of TMB solutions from each well were replaced to another plate to be mixed with 1 N HCl to stop the reaction. Optical density of each well was determined with a microplate spectrophotometer at OD 450 nm.

Detection of PAR1 Ubiquitination and Measurement of PAR1 Basal Degradation

EA.hy926 cells were seeded at 1.0×10^6 cells per dish in 100-mm petri dishes, transfected, and starved as described above. For detecting PAR1 ubiquitination, cells were treated with 10 nM thrombin. For measuring PAR1 basal degradation, cells were treated with 2 µg/mL cycloheximide. Cells were collected into lysis buffer supplemented with protease and deubiquitinase inhibitors (50 mM Tris pH 8.0, 150 mM NaCl, 1% [v/v] NP-40, 5 mM EDTA, 0.5% [w/v] sodium deoxycholate, 0.1% [w/v] SDS, 1 µg/mL leupeptin, 1 µg/mL aprotinin, 1 µg/mL pepstatin, 10 µg/mL benzamidine, 1 µg/mL PMSF, 1 µg/mL TPI, 50 µM PR619, 20 mM NEM, 3 mM *o*-

phenanthroline) on ice. Cell lysates were sheared by passing through 22-gauge needle 10 times and then clarified by centrifugation at 14,000 rpm for 20 min at 4°C. Protein concentrations were equalized with lysis buffer using a BCA protein assay (Thermo Fisher Scientific, Waltham, MA). Mouse monoclonal anti-PAR1 WEDE15 was purified from hybridoma as previously described (212) and antibody and mouse-IgG control antibody were separately mixed and incubated with lysates for 1 hour. BSA-blocked protein A-sepharose CL-4B beads (Cytiva, Marlborough, MA) were added and incubated for 2 hours. Beads were washed and proteins were eluted in 2X Laemmli Sample Buffer + DTT and boiled for 5 min at 95ºC. Samples were then immunoblotted as described above, with rabbit polyclonal anti-PAR1 (C5433) Rabbit polyclonal C5433 anti-PAR1 antibody was described previously (202). at 1:3000 and mouse anti-ubiquitin (P4D1, Santa Cruz Biotechnology, Dallas, TX) at 1:1000.

Real-time Quantitative Polymerase Chain Reaction (RT-qPCR)

RNA was isolated from endothelial EA.hy926 cells seeded at 3.2×10^5 cells per well in a 6-well plate grown overnight and treated with actinomycin D (catalog no. A9415, Sigma-Aldrich, Irvine, CA) using Direct-zol RNA Miniprep Plus Kit (catalog no. R2072, Zymo Research, Irvine, CA). Total RNA was quantified and 0.5 µg total RNA was used for cDNA synthesis reaction with the SuperScript IV VILO Master Mix with ezDNase enzyme kit (catalog no. 111766050, Thermo Fisher Scientific, Waltham, MA). Quantitative RT-PCR was performed with TaqMan Fast Advanced Master Mix (catalog no. 4444964, Thermo Fisher Scientific, Waltham, MA) and TaqMan Gene Expression Probes USP34 (catalog no. Hs00611330_m1), F2R (catalog no. Hs05045041_s1), F2RL1 (catalog no. Hs00608346_m1) and 18S (catalog no. Hs03003631_g1, primer-limited) using a QuantStudio™ 3 Real-Time PCR System (Thermo Fisher Scientific, Waltham, MA). Messenger RNA transcript levels were analyzed using the comparative CT

(threshold cycle) method, and normalized to 18S ribosomal RNA expression. Briefly, the number of cycles until threshold (Ct) was determined for each target, and the Ct value for 18S was subtracted from the Ct value for each target, the differences in expression was then determined using the $2^{-\Delta\Delta Ct}$ method.

Statistical Analysis

Data were analyzed using Prism 10.2 statistical software (GraphPad Software, La Jolla, CA) and Microsoft Excel. Statistical analysis methods are indicated in the figure legends. Detailed statistical analysis results are included in Supplemental Information.

Acknowledgements

We thank all members of the Trejo laboratory for comments and advice. We especially thank Mika Caplan for constructive discussions and advice in manuscript preparation.

Chapter 2, in part, is currently being prepared for submission for publication of the material. Norton Cheng, Monica L. Gonzalez Ramirez, Chloe Edwards and JoAnn Trejo. The dissertation author was the primary investigator and author of this paper.

Supplemental Information

Supplemental Table 2-1. ANOVA results for Figure 2-1

Panel B: p38 phosphorylation

- Two-way ANOVA

Source of variation	SS	DF	MS	F (DFn, DFd)	P value
Interaction	0.3862	2	0.1931	F (2, 18) = 16.14	<0.0001
Time	4.262	2	2.131	F (2, 18) = 178.2	<0.0001
siRNA	0.6064	1	0.6064	F (1, 18) = 50.70	<0.0001
Residual	0.2153	18	0.01196		

- Post hoc multiple comparisons

Time	Mean 1	Mean 2	Mean Diff.	SE of diff.	N1	N2	t	DF	Adjusted P Value
siUSP34 - NS									
0	0.3490	0.2975	0.05150	0.07733	4	4	0.6660	18.00	0.8851
7.5	1.659	1.000	0.6593	0.07733	4	4	8.525	18.00	<0.0001
10	1.147	0.9038	0.2430	0.07733	4	4	3.142	18.00	0.0168

Panel C: ERK1/2 phosphorylation

- Two-way ANOVA

Source of variation	SS	DF	MS	F (DFn, DFd)	P value
Interaction	0.08555	2	0.04278	F (2, 18) = 4.139	0.0332
Time	1.576	2	0.7881	F (2, 18) = 76.25	<0.0001
siRNA	0.02325	1	0.02325	F (1, 18) = 2.250	0.1510
Residual	0.1860	18	0.01033		

- Post hoc multiple comparisons

Time	Mean 1	Mean 2	Mean Diff.	SE of diff.	N1	N2	t	DF	Adjusted P Value
siUSP34 - NS									
0	0.4273	0.5253	-0.09800	0.07189	4	4	1.363	18.00	0.4678
7.5	1.188	0.9998	0.1885	0.07189	4	4	2.622	18.00	0.0509
10	0.9298	0.8335	0.09625	0.07189	4	4	1.339	18.00	0.4827

Supplemental Table 2-2. Multiple linear regression models for Figure 2-4

Panel A: Constitutive internalization of PAR1

- Multiple linear regression
- Log-transformed OD450 value (based on the assumption that the relationship between incubation duration and PAR1 surface expression is multiplicative)
- log_OD450 ~ Intercept + siRNA + Duration + Replicate + siRNA : Duration

NS versus siUSP34

Independent variable	Estimate	Standard error	|t|	P value
Intercept	-1.114	0.04421	25.2	<0.0001
siRNA[siUSP34]	0.1927	0.05105	3.776	0.0092
Duration	-0.01205	0.001702	7.08	0.0004
Replicate[2]	0.204	0.04421	4.614	0.0036
Replicate[3]	0.2083	0.04421	4.711	0.0033
siRNA[siUSP34] : Duration	0.004326	0.002406	1.798	0.1224

$R^2 = 0.9617$

F (DFn, DFd) = 30.13

NS versus siμ2

Independent variable	Estimate	Standard error	|t|	P value
Intercept	-1.098	0.04011	25.2	<0.0001
siRNA[siUSP34]	0.4708	0.04631	3.776	0.0092
Duration	-0.01205	0.001544	7.08	0.0004
Replicate[2]	0.1653	0.04011	4.614	0.0036
Replicate[3]	0.1991	0.04011	4.711	0.0033
siRNA[siUSP34] : Duration	0.009187	0.002183	1.798	0.1224

$R^2 = 0.9865$

F (DFn, DFd) = 87.58

Panel B: Agonist-induced internalization of PAR1

- Multiple linear regression
- Log-transformed OD450 value (based on the assumption that the relationship between treatment duration and PAR1 surface expression is multiplicative)
- log_OD450 ~ Intercept + siRNA + Duration + Replicate + siRNA : Duration

NS versus siUSP34

Independent variable	Estimate	Standard error	|t|	P value
Intercept	-1.098	0.03839	28.59	<0.0001
siRNA[siUSP34]	0.2004	0.04588	4.368	0.0009
Duration	-0.03826	0.003351	11.42	<0.0001
Replicate[2]	0.2022	0.03554	5.689	0.0001
Replicate[3]	0.1649	0.03554	4.640	0.0006
siRNA[siUSP34] : Duration	0.005016	0.004739	1.059	0.3106

$R^2 = 0.9652$

F (DFn, DFd) = 66.55

(continued)

Supplemental Table 2-2. Multiple linear regression models for Figure 2-4 (continue)

NS versus siμ2				
Independent variable	Estimate	Standard error	|t|	P value
Intercept	-1.107	0.04281	25.85	<0.0001
siRNA[siUSP34]	0.4783	0.05117	9.347	<0.0001
Duration	-0.03826	0.003737	10.24	<0.0001
Replicate[2]	0.2013	0.03964	5.078	0.0003
Replicate[3]	0.1924	0.03964	4.854	0.0004
siRNA[siUSP34] : Duration	0.02280	0.005285	4.313	0.0010
$R^2 = 0.9789$ F (DFn, DFd) = 111.5				

Supplemental Table 2-3. ANOVA results for Figure 2-5

Panel B: expression of PAR1 - Two-way ANOVA					
Source of variation	SS	DF	MS	F (DFn, DFd)	P value
Interaction	0.04654	2	0.02327	F (2, 12) = 0.08993	0.9146
Time	1.149	2	0.5743	F (2, 12) = 2.219	0.1514
siRNA	2.585	1	2.585	F (1, 12) = 9.989	0.0082
Residual	3.106	12	0.2588		
Panel E: expression of PAR1 - Two-way ANOVA					
Source of variation	SS	DF	MS	F (DFn, DFd)	P value
Interaction	0.2671	2	0.1336	F (2, 18) = 1.250	0.3101
Time	1.215	2	0.6075	F (2, 18) = 5.687	0.0122
siRNA	4.593	1	4.593	F (1, 18) = 42.99	<0.0001
Residual	1.923	18	0.1068		

Supplemental Table 2-4. Student's t test result and multiple linear regression model for Figure 2-6

Panel B: expression of PAR1

- two-tailed unpaired Student's t test

Mean [NS] = 1.000
Mean [siUSP34] = 2.683
t = 4.103
Degree of freedom = 4
P value = 0.0148

Panel B & C [alternative]: degradation of PAR1

- Multiple linear regression
- Log-transformed integrated intensity value (based on the assumption that the relationship between time and PAR1 expression is multiplicative)

NS versus siUSP34

Independent variable	Estimate	Standard error	|t|	P value
Intercept	7.715	0.1216	63.43	<0.0001
siRNA[siUSP34]	0.4961	0.1281	3.873	0.0013
Duration	-0.02250	0.006988	3.219	0.0054
Replicate[2]	0.1037	0.1204	0.8612	0.4018
Replicate[3]	-0.1414	0.1204	1.175	0.2573
siRNA[siUSP34] : Duration	-0.02058	0.009866	2.086	0.0534

R^2 = 0.8009
F (DFn, DFd) = 12.87

Supplemental Table 2-5. ANOVA results for Figure 2-7

Panel A: mRNA expression of *F2R* (PAR1) - Two-way ANOVA - ΔCt					
Source of variation	SS	DF	MS	F (DFn, DFd)	P value
Interaction	0.006929	1	0.006929	F (1, 8) = 0.3087	0.5937
Time	0.01522	1	0.01522	F (1, 8) = 0.6781	0.4341
siRNA	2.139	1	2.139	F (1, 8) = 95.31	<0.0001
Residual	0.1795	8	0.02244		
Panel B: mRNA expression of *F2RL1* (PAR2) - Two-way ANOVA - ΔCt					
Source of variation	SS	DF	MS	F (DFn, DFd)	P value
Interaction	0.05616	1	0.05616	F (1, 8) = 0.5321	0.4865
Time	4.428	1	4.428	F (1, 8) = 41.95	0.0002
siRNA	2.770	1	2.770	F (1, 8) = 26.24	0.0009
Residual	0.8444	8	0.1056		

Chapter 3 CYLD DEUBIQUITINASE REGULATES ENDOTHELIAL PAR1 UBIQUITINATION AND SIGNALING

Introduction

Signaling pathways mediated by G protein-coupled receptors (GPCR) play crucial roles in human cell physiology and pathology (198,213). GPCR signaling transduction systems has been shown to involve many modes of regulation and complex signaling network and to help cells maintain homeostasis and interact with their ever-dynamic environments. In the classical view, a GPCR is activated when bound to certain molecules, thus inducing interactions with heterotrimeric G proteins and signaling through second messengers and tiered kinase cascade. Meanwhile, the activated GPCR itself is also desensitized by internalization and subsequent sorting or degradation. These processes have been characterized to be governed by post-translational modifications (PTM), such as phosphorylation and ubiquitination (5). Other types of PTM of GPCR have also been identified, whereas our understanding about the functions and regulatory mechanisms of those PTMs are limited.

Ubiquitin is an evolutionarily conserved small protein which can be linked to itself or other proteins by E3 ligases. Besides mono-ubiquitination, a chain of repeated ubiquitin linked to different lysine (K) residues of itself can also be attached to another protein. These polyubiquitin chains can be categorized based on the lysine residue that forms the inter-ubiquitin linkages, such as K11, K48 and K63. On the contrary, deubiquitinases (DUB) remove ubiquitin from their substrate proteins. Both E3 ligases and DUBs can be selective towards a number of linkage types and their activities are regulated by many factors such as protein-protein interactions and subcellular localizations (16,20). Despite that many GPCR are known to be ubiquitinated, GPCR ubiquitination was an under-appreciated type of PTM which was believed to mainly regulate

trafficking and degradation of the receptor, but recent studies has start to demonstrate that GPCR ubiquitination has direct impact to their signaling (11,14,15,121).

In our previous studies, protease-activated receptor 1 (PAR1) was found to be a member of GPCR that is ubiquitinated and mediates inflammatory signaling in endothelial cells. Thrombin, an endogenous PAR1 agonist, cleaves PAR1 and activates the receptor, and stimulates NEDD4-2 E3 ligase to poly-ubiquitinate the activated PAR1 (12). This poly-ubiquitin chain is recognized and bound by adaptor TAB proteins and recruit p38α mitogen-activated protein kinase (MAPK) at endosomes (11). Such non-canonical, ubiquitin-driven signaling has been shown to be critical for endothelial inflammation and affects endothelial dysfunction and cytokine expression. With a comprehensive RNA interference (RNAi) screen in endothelial cells and HeLa cells to identify DUBs that regulates thrombin-induced p38 signaling, we recently found that cylindromatosis (CYLD) and ubiquitin-specific peptidase 34 (USP34) may play important roles in p38 signaling and cytokine expression. Additionally, we found that CYLD depletion affects thrombin-stimulated barrier disruption (200). These evidence suggests that PAR1 ubiquitination may be regulated by these DUBs.

While USP34 has been shown to regulate PAR1 mRNA and protein expression, rather that PAR1 ubiquitination (Chapter 2), it was still unclear whether CYLD is responsible for regulating PAR1 ubiquitination. Here, we show that CYLD interacts with PAR1 and regulates PAR1 ubiquitination status. However, the detailed mechanisms and spatial-temporal regulation of thrombin-induced p38 activity still need to be further investigated.

Results

CYLD regulates thrombin-induced, PAR1-stimulated p38 signaling

We first confirmed that CYLD depletion affects thrombin-induced PAR1 signaling by

transfecting non-specific (siNS) and CYLD-specific siRNAs (siCYLD #7 and #8, individually) to HUVEC-derived EA.hy926 endothelial cells. In accordance with our previous results, there were significant increases in thrombin-induced p38 MAPK phosphorylation around 7.5 minutes (**Figure 3-1**, A-F). Although not significant when tested with post hoc multiple comparisons, we observed consistent increases in basal p38 phosphorylation when either CYLD-targeting siRNA was introduced. Due to the non-linear change of thrombin-induced p38 phosphorylation, we may not be able to discover a significant interaction term between CYLD-depletion and thrombin treatment time using two-way ANOVA, without truncating timepoints thus sacrificing statistical power. However, the two-way ANOVA result suggests that CYLD-depletion caused a significant overall increase in p38 phosphorylation (**Supplemental Table 3-1**). Surprisingly, it was also observed that CYLD depletion also has an effect on ERK1/2 phosphorylation, while the post hoc multiple comparisons only revealed one significant increase in cells transfected with CYLD siRNA #8. These results suggest that CYLD is involved in PAR1-mediated signaling pathways.

We then aimed to examine whether PAR1 activation is required for such up-regulations in both p38 MAPK and ERK1/2 phosphorylation, by adding vorapaxar, a PAR1 inhibitor, to the cell culture before and during the thrombin treatment. The vorapaxar treatment greatly decreased thrombin-induced p38 MAPK phosphorylation in both NS and CYLD siRNA-transfected cells almost to the baseline (**Figure 3-1**, G and H), suggesting that CYLD is unlikely to affect another signaling pathway triggered by thrombin hence increasing p38 phosphorylation. The three-way ANOVA result found not only that the effect of thrombin on p38 MAPK phosphorylation depends on the presence of CYLD (Thombin × siRNA), but also that the inhibitory effect of vorapaxar on the thrombin-induced p38 phosphorylation depends on the presence of CYLD (Thombin × siRNA × Vorapaxar) (**Supplemental Table 3-1**). Together, these data show that PAR1 activation is

required for the up-regulated thrombin-induced p38 phosphorylation caused by CYLD depletion.

It is shown that the auto-phosphorylation activity of p38α is responsible for thrombin-induced p38 activation (11), thus we hypothesize that the auto-phosphorylation activity of p38α is also regulated by CYLD. To test this, we used a p38 inhibitor, BIRB 796, to block thrombin-induced p38 auto-phosphorylation in endothelial cells. As expected, BIRB 796 treatment inhibited thrombin-induced p38 phosphorylation in both siRNA groups at 7.5 min, but there was residual activity observed as the BIRB 796 treatment did not completely block p38 auto-phosphorylation (**Figure 3-1**, I and J). The three-way ANOVA result confirmed that the effect of thrombin on p38 phosphorylation depends on whether CYLD was depleted (Thombin × siRNA), as expected. However, we failed to detect a significant interaction between p38 inhibition and the combined effect of thrombin and CYLD depletion (Thombin × siRNA × BIRB 796) (**Supplemental Table 3-1**). This may be due to the insufficient inhibition of p38 activity, therefore it is inconclusive whether CYLD regulates p38 phosphorylation by inhibiting p38 auto-phosphorylating activity.

CYLD does not regulate PAR1 surface expression or internalization

Since it was suggested that CYLD may regulate both p38 and ERK1/2 signaling pathway mediated by PAR1, we aimed to test the hypothesis that CYLD, similar to USP34, may regulate PAR1 surface expression or internalization. Here, we utilized ELISA-based assays to measure constitutive PAR1 internalization and agonist-induced receptor endocytosis in endothelial cells by depleting CYLD with siRNA transfection. As a control, we also include a group of cells which were transfected with siRNA targeting clathrin adaptor AP-2 μ2 subunit. Expectedly, depletion of AP-2 μ2 subunit significantly increased surface PAR1 expression across all time points and inhibited PAR1 internalization regardless of agonist stimulation. (**Figure 3-2**, A and B). Unlike USP34-knockdown, inhibiting CYLD expression did not cause significant change to surface

expression of PAR1 in endothelial cells (**Supplemental Table 3-2**). Furthermore, CYLD depletion was not found to affect PAR1 constitutive and agonist-induced internalization. Therefore, we conclude that CYLD does not regulate cell surface expression of PAR1 nor does it regulate the internalization of the receptor.

CYLD does not regulate PAR1-stimulated p38 pathway components expression, but may modulate post-translational modifications of TAB1

It has been shown that thrombin-induced, noncanonical p38 activation requires an E3 ligase NEDD4-2, which is activated upon PAR1 activation and is responsible for PAR1 poly-ubiquitination (12). Additionally, adaptor TAB proteins, such as TAB1 and TAB2, are critical for mediating the endosomal p38 phosphorylation (11,13). Therefore, we hypothesize that CYLD may play a role in regulating the abundance of these key components of the PAR1-p38 signaling pathway. By depleting CYLD in the endothelial cells, we observed upregulation of NEDD4-2 in the CYLD siRNA #7-transfected cells, while no change was found in the siRNA #8-transfected group, suggesting that it may be an off-target effect (**Figure 3-3**, A, B, E, and F). As previously described (11), TAB1 expression was increased after thrombin treatment, which was not affected by CYLD depletion. TAB2 expression was also not affected (**Figure 3-3**, A, C, D, E, G, and H).

Interestingly, despite the observation that CYLD depletion did not lead to considerable changes on the abundance of the key pathway components, the presence of CYLD was found to modulate an unidentified TAB1 cohort with a slightly larger molecular weight (approximately +2 kDa) by immunoblot (**Figure 3-3**, A and E). Because TAB1 plays an important role in triggering p38α auto-phosphorylation (129), we suspect that this extra band might be the phosphorylated form of TAB1 due to its presumed proximity to p38 MAPK, or another type of post-translationally modified cohort. We first tested whether enhanced p38 activity was responsible for the increased,

putative TAB1 phosphorylation. Even though the cells were treated with the p38 inhibitor, BIRB 796, we still detected the extra band above the major TAB1 cohort (**Figure 3-3**, I). To further confirm whether the TAB1 is phosphorylated, we immunoprecipitated TAB1 along with modified cohort, and used lambda protein phosphatase (λPP) to remove phosphate groups from any phosphorylate residue of TAB protein. Surprisingly, the presumably post-translationally modified TAB1 was still detectable (**Supplemental Figure 3-1**, A), suggesting such modification may not be phosphorylation. We also tested whether it is mono-ubiquitination of TAB1, but we were not able to detect ubiquitin-conjugated TAB1 by immunoprecipitation and subsequent immunoblot (**Supplemental Figure 3-1**, B). Therefore, it is still unclear which type of modification to TAB1 is modulated by the CYLD depletion, and the biological relevance of this particular TAB1 PTM remains to be explored.

CYLD regulates thrombin-induced PAR1 ubiquitination without modulating PAR1 protein abundance

We have previously reported PAR1 is poly-ubiquitinated when activated by thrombin and that ubiquitination of PAR1 is required for the p38 MAPK auto-phosphorylation (11). Therefore, we hypothesized that CYLD might negatively regulates PAR1 ubiquitination and subsequent p38 MAPK activation. We tested this hypothesis by enriching endogenous PAR1 from cells that are transfected with NS or CYLD-depleting siRNA, and used ubiquitin-specific antibody to perform immunoblotting and detect PAR1 ubiquitination induced by thrombin treatment. Strikingly, we observed a significant increase in PAR1 ubiquitination in endothelial cells (**Figure 3-4**, A and C). Additionally, the CYLD-depletion did not affect the protein expression of PAR1 in endothelial cells, despite the increased ubiquitination (**Figure 3-4**, A and B). In parallel, we confirmed that CYLD does not regulate PAR1 (*F2R*) gene expression by using quantitative real-time PCR to

measure mRNA transcript expression in endothelial cells transfected with CYLD- versus non-specific siRNA (**Figure 3-4**, D). These results suggest that PAR1 is a substrate of, while CYLD does not regulate PAR1 protein expression.

CYLD is localized to cytoplasm in endothelial cells and may interact with PAR1

Since we observed that CYLD regulates PAR1 ubiquitination, it is to be evaluated whether CYLD directly interacts with PAR1. First, we overexpressed HA-tagged CYLD in endothelial cells and probe the recombinant proteins by performing immunofluorescence with HA-tag-specific antibody. We found that HA-tagged CYLD is localized to cytoplasm in endothelial cells in a diffused manner (**Figure 3-5**, A).

We then performed reciprocal co-immunoprecipitation experiments with PAR1-overexpressing HeLa cells and endothelial cells. We found that PAR1 and endogenous CYLD co-associate regardless of thrombin treatment in both cell lines (**Figure 3-5**, B and C). Together, these data suggest that CYLD may form a complex with PAR1 basally, while it is unclear whether such interaction is indirect thus requiring adaptor proteins.

Thrombin induced phosphorylation of p38 kinase activity biosensors at endosomes and nuclei

Upon thrombin cleavage, activated PAR1 promotes NEDD4-2 E3 ligase activity via G protein and c-Src signaling at plasma membrane. Stimulated NEDD4-2 is shown to ubiquitinates PAR1 and promotes p38 phosphorylation, even when the receptors are trapped at cell surface by blocking endocytosis (12). This work suggested that PAR1 and p38 may form a signaling complex as soon as PAR1 is ubiquitinated and recruits the adaptor TAB proteins thus triggering p38 auto-activation. Since CYLD co-associates with PAR1 basally, we aim to understand whether CYLD plays a role in fine-tuning p38 auto-activation constitutively, or if CYLD has differential effect upon p38 signaling at various subcellular localizations. To monitor p38 kinase activity specifically

at different subcellular localizations, we modified a FRET-based p38 kinase activity biosensor (PerKy) (214) and added signal peptides or truncated protein domains to direct the recombinant biosensors to specific organelles or structures. The improved PerKy-EV FRET biosensor and the S/A mutant variant (a serine-to-alanine substitution at the kinase substrate region thus it will not be phosphorylated) were validated by over-expression in HeLa cells. We used GFP-Trap beads, which recognize YPet within the biosensors, to immunoprecipitate the biosensor variants and detect biosensor phosphorylation with phosphor-c-Jun antibody that recognizes the kinase substrate region. We observed a steady increase in phosphorylation of the untargeted PerKy-EV biosensor over time after the cells were stimulated with thrombin, while the mutant variant was not phosphorylated despite the thrombin-induced p38 activation was presented in the cells (**Supplemental Figure 3-2**).

We then overexpressed all 6 variants of p38 FRET biosensors in HeLa cells to validate their localization using immunofluorescence (**Figure 3-6**, A and B). The untargeted PerKy-EV and the S/A-mutant biosensors were diffusely expressed in cytoplasm. The PerKy-EV-2xFYVE variant contains a phosphatidylinositol 3-phosphate-binding FYVE domain and was sorted to early endosomes, which was marked with early endosome antigen 1 (EEA1) staining. The PerKy-EV-CAAX variant contains a CAAX motif, which is presumably prenylated and anchored to plasma membrane, delineated by the CellMask stain. The lysosomal LAMP1-PerKy-EV is constructed with a truncated LAMP1 protein fused to the biosensor to localize it to lysosomes, which was also confirmed by co-staining the cells with LysoTracker. And finally, the nuclear variant PerKy-EV-NLS is generated by inserting a nuclear localization signal (NLS) peptide to the base PerKy-EV, which was exclusively expressed in the nuclei that was visualized by the nuclear stain. To validated that the added parts in the location-targeted recombinant biosensor does not interfere with their

interaction with p38 MAPK, we stimulated the cells expressing the biosensors with anisomysin and observed phosphorylation of these biosensors (**Figure 3-6**, D).

To assess thrombin-induced p38 kinase activity at these subcellular locations using epifluorescent FRET imaging, flag-tagged-PAR1 and each of the four targeted PerKy-EV variants were co-expressed in HeLa cells. We observed an initial decrease and recovery of FRET ratio (YFP_{FRET}/CFP) during the first 10 minutes after thrombin treatment, followed by gradual increase of FRET ratio up to 35 minutes post-stimulation. However, there was no FRET ratio increase above the baseline when the cells were transfected with the S/A mutant variant (**Figure 3-6**, E). In case of the endosomal (2xFYVE), we observed inconsistent initial decline and recovery, followed by FRET ratio increase started around 5-10 minutes post-stimulation (**Figure 3-6**, F). The nuclear (NLS) variant also exhibits response to thrombin stimulation, with FRET ratio increase started at 5-15 minutes post-stimulation (**Figure 3-6**, G). For the plasma membrane (CAAX), we also observed the rapid drop and rebound of FRET ratio, but it did not exhibited FRET ratio increase beyond the baseline (**Figure 3-6**, H).

We also examined the biosensor phosphorylation using complementary immunoblotting. The four localization-specific variants of p38 biosensor were co-expressed with flag-tagged PAR1 in HeLa cells. In accord with the FRET imaging results, we observed thrombin-induced phosphorylation of the endosomal (2xFYVE) and nuclear (NLS) biosensors, while the plasma membrane (CAAX) and lysosomal (LAMP1) variants were agnostic to thrombin treatment (**Figure 3-6**, C). Together, these results suggest that thrombin-induced p38 kinase activity is largely present at endosomes and it may translocate to nucleus and affect its downstream effectors in the signaling pathway.

To investigate whether CYLD regulates thrombin-stimulated p38 activity kinetics at

endosomes specifically in endothelial cells, we attempted to over-express the endosomal (2xFYVE) PerKy-EV biosensor in EA.hy926 cells and inhibited the CYLD protease activity with subquinocin. The preliminary result suggests that inhibition of CYLD might increase thrombin-stimulated p38 kinase activity at endosomes (**Supplemental Figure 3-3**).

Discussion

While it has been established that many GPCRs are found ubiquitinated during their life cycle (5), our understanding of the important players in the regulation of GPCR ubiquitination is still limited. Furthermore, most of our current knowledge surrounding GPCR ubiquitination and how deubiquitinases are involved are largely focused on the degradation of GPCR (215,216). There have been several studies pointed out that GPCR ubiquitination are involved in more than just receptor stability, such as biased signaling, recycling, and endosomal signaling (11,14,15,217). In our previous reports, we have characterized a non-canonical, ubiquitin-driven signaling pathway mediated by a member of GPCR, PAR1. Activation of PAR1 by thrombin stimulates NEDD4-2 E3 ligase activity to ubiquitinates PAR1, thus recruiting TAB2 and TAB1 adaptor proteins and triggering p38 auto-activation at endosomes (11-13). This unique pathway has also been shown sufficient to induce inflammatory responses in endothelial cells, including barrier dysfunction and pro-inflammatory cytokine expression.

With an effort to identify the potential regulators of such signaling pathway, we screened 96 human DUBs in and found that CYLD is a DUB that may be responsible for negatively regulating PAR1-p38 signaling axis in endothelial cells (200). Upon CYLD depletion, we found that endothelial cells exhibited exacerbated barrier disruption and IL-6 expression. In fact, this is not the first evidence suggesting that protein ubiquitination can regulate barrier function and other inflammatory responses (218,219). However, most studies focus on the roles of ubiquitination in

tumor necrosis factor (TNF)-stimulated signaling pathways, cytoskeleton dynamics regulated by Rac1-RhoA small GTPases, and stability of intercellular junction proteins. CYLD has been found to regulate microtubule/tubulin integrity and endothelial barrier function (186,220,221), but the substrate of CYLD and their physiological relevance were to be identified. Here, we show that CYLD is directly linked to regulation of PAR1 ubiquitination, demonstrating a new role of DUB to help maintain homeostasis of endothelial inflammatory response. Interestingly, the elevated ubiquitination did not result in suppressed PAR1 total expression nor surface expression, suggesting that the ubiquitination configuration that was regulated by CYLD may not be responsible for PAR1 instability.

Despite the fact that we observed the interaction between CYLD and PAR1, the exact mechanism is still unknown. Recently, Elliot et al. showed that the CAP-Gly domains at the N-terminal region of CYLD play a critical role in substrate recognition and bind to ubiquitin, whereas the ubiquitin-specific protease domain has been identified to be closer to the C-terminal. Further studies are needed to unveil the required regions of CYLD and PAR1 intracellular domain for the deubiquitination event. Also, it has been shown that CYLD may interact with TAB1 and TAB2 (222). Given that PAR1 interacts with these adaptor proteins basally (albeit further enhanced when activated) and CYLD co-associates with uncleaved, minimally-ubiquitinated PAR1, we suspect that TAB proteins might mediates PAR1-CYLD co-association and facilitates the deubiquitination of PAR1.

Additionally, due to the diffuse distribution of CYLD and the basal co-association with PAR1, it is unknown at which point during the PAR1-stimulated p38 activation CYLD become active. Two phosphorylation sites, serine 418 and serine 568 of CYLD has been identified to be important for CYLD DUB activity (223), yet it has not been shown whether PAR1 activation

would lead to phosphorylation of these two sites on CYLD. On the other hand, endothelial PAR1 activation has been shown to promote the proteolytic cleavage of CYLD by mucosa-associated lymphoid tissue lymphoma translocation protein 1 (MALT1), which inactivates CYLD (220). We did observe a slight decrease of co-association between CYLD and PAR1 (**Figure 3-5**), but it is unclear whether this was caused by the loss of PAR1 ubiquitination or cleavage of full-length CYLD. Therefore, how these parallel reactions and interactions orchestrated the PAR1 deubiquitination to regulate p38 kinase activity remains to be further investigated.

Figures

Figure 3-1. CYLD regulates thrombin-induced, PAR1-stimulated p38 signaling.

A & D, Immunoblot of thrombin-stimulated signaling in EA.hy926 cells that were seeded, transfected with nonspecific (siNS) or CYLD-specific siRNAs (siCYLD #7 and siCYLD #8), and stimulated with 10 nM α-thrombin for up to 60 minutes. Cell lysates were immunoblotted with indicated antibodies.

B & E, Thrombin-induced p38 phosphorylation shown in panel (A) and (D), respectively. The integrated intensity of phosphorylated p38 species is divided by the integrated intensity of total p38. These ratios are normalized to the average of each replicate, then expressed as fractions over the average of siNS, 0 min control group. (N = 3)

C & F, Thrombin-induced ERK1/2 phosphorylation shown in panel (A) and (D), respectively. The integrated intensity of phosphorylated ERK1/2 species is divided by the integrated intensity of total ERK1/2. These ratios are normalized to the average of each replicate, then expressed as fractions over the average of siNS, 0 min control group. (N = 3)

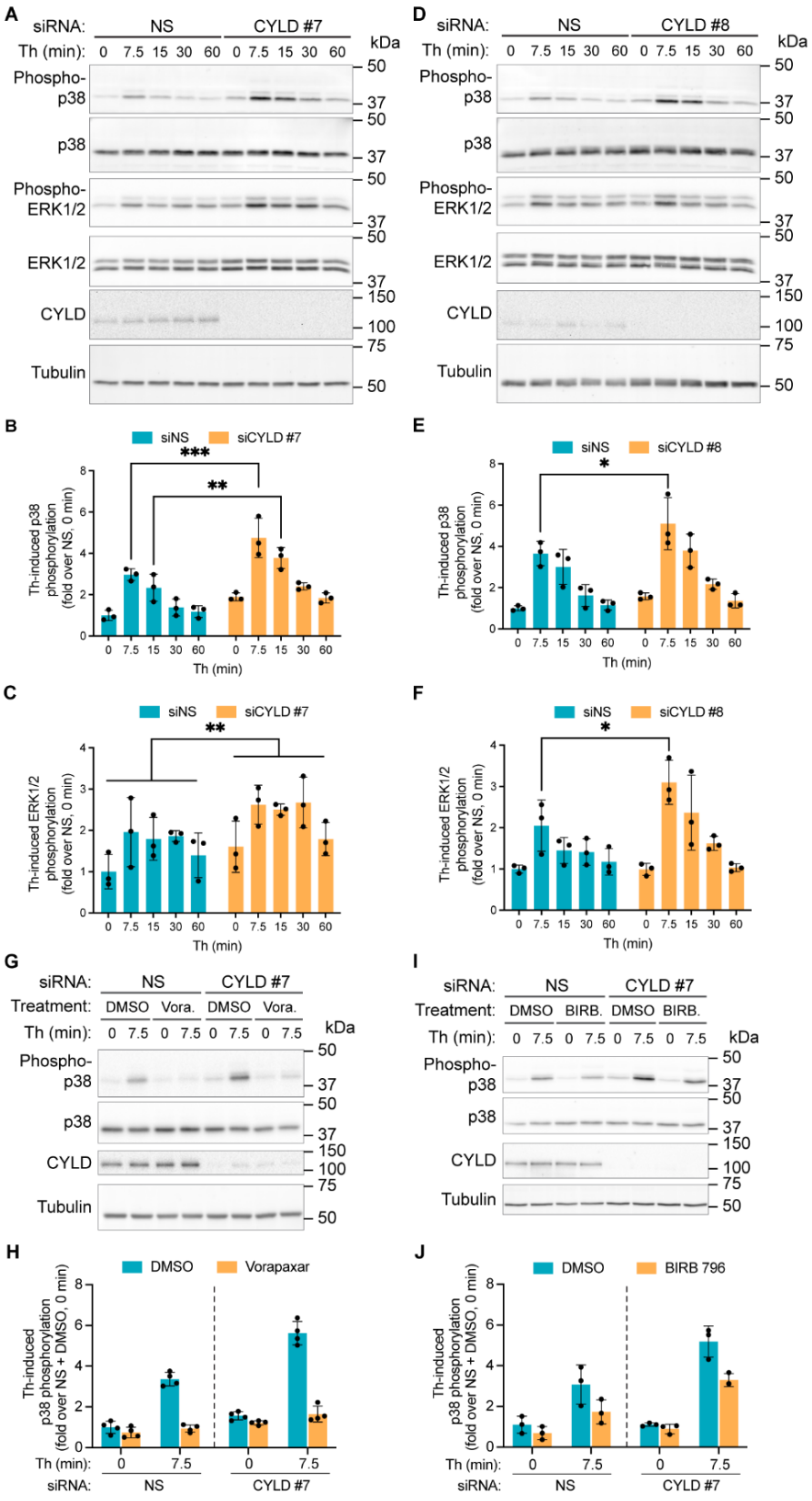
G, Immunoblots of cell lysates of EA.hy926 cells that were seeded, transfected with non-specific (siNS) or CYLD-specific siRNA (siCYLD #7). These cells are treated with either DMSO (vehicle) or vorapaxar during starvation and stimulated with 10 nM α-thrombin (+ DMSO or vorapaxar) for 7.5 minutes.

H, Thrombin-induced p38 phosphorylation shown in panel (G). The integrated intensity of phosphorylated p38 species is divided by the integrated intensity of total p38. These ratios are normalized to the average of each replicate, then expressed as fractions over the average of siNS, 0 min control group. (N = 4)

I, Immunoblots of cell lysates of EA.hy926 cells that were seeded, transfected with non-specific (siNS) or CYLD-specific siRNA (siCYLD #7). These cells are treated with either DMSO (vehicle) or BIRB 796 during starvation and stimulated with 10 nM α-thrombin (+ DMSO or BIRB 796) for 7.5 minutes.

J, Thrombin-induced p38 phosphorylation shown in panel (I). The integrated intensity of phosphorylated p38 species is divided by the integrated intensity of total p38. These ratios are normalized to the average of each replicate, then expressed as fractions over the average of siNS, 0 min control group. (N = 3)

Error bar = standard deviation. Data shown in *B*, *C*, *E*, and *F* were analyzed by two-way ANOVA, followed by Šídák's post hoc test. * $p < 0.05$, ** $p < 0.01$, *** $p < 0.001$. Data shown in H and J were analyzed by three-way ANOVA. See **Supplemental Table 3-1** for full analysis results.


A
siRNA:
NS
CYLD #7
Th (min):
0 7.5 15 30 60 0 7.5 15 30 60
kDa
Phospho-p38
p38
Phospho-ERK1/2
ERK1/2
CYLD
Tubulin
50
37
150
100
75
D
CYLD #8
B
siNS
siCYLD #7
***
**
Th-induced p38 phosphorylation (fold over NS, 0 min)
Th (min)
E
*
C
Th-induced ERK1/2 phosphorylation (fold over NS, 0 min)
F
G
Treatment:
DMSO
Vora.
I
BIRB.
H
DMSO
Vorapaxar
Th-induced p38 phosphorylation (fold over NS + DMSO, 0 min)
J
BIRB 796

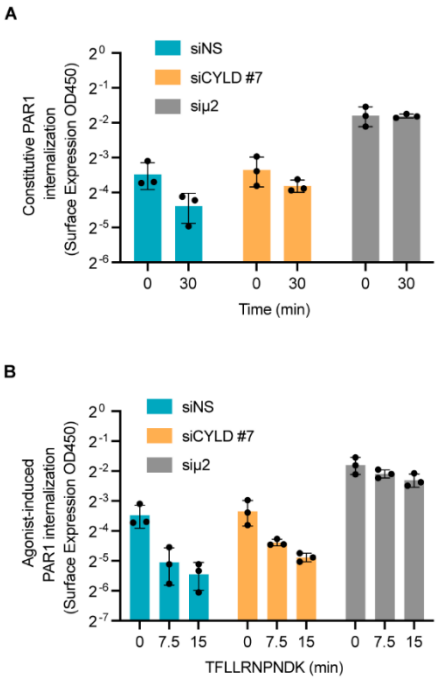


Figure 3-2. CYLD does not regulate PAR1 surface expression or internalization.

A, Remaining PAR1 expression at the surface after constitutive internalization, measured by loss-of-surface-receptor assay. EA.hy926 cells were seeded and transfected with non-specific (siNS), CYLD- (siCYLD #7), or μ2-specific siRNA (siμ2). The cells are labeled with mouse anti-PAR1 antibody (WEDE15) on ice, and either left on ice or incubated at 37°C for 30 minutes. The remaining PAR1 at cell surface is then measured by loss-of-receptor assay at 450 nm. The background OD450 (secondary antibody-only) values were averaged and subtracted from all raw OD450 readout values. Error bar = standard deviation. Multiple linear regression analysis was used to estimate the main effects of incubation duration, CYLD-knockdown, biological replicates (date), and interaction term (incubation duration×CYLD-knockdown), upon log(OD450). (N = 3). See **Supplemental Table 3-2** for full analysis results.

B, Remaining PAR1 expression at the surface after constitutive internalization, measured by loss-of-surface-receptor assay. EA.hy926 cells were seeded and transfected with non-specific (siNS), CYLD- (siCYLD #7), or μ2-specific siRNA (siμ2). The cells are labeled with mouse anti-PAR1 antibody (WEDE15) on ice, and either left on ice or treated with TFLLRNPNDK agonist-peptide incubated at 37°C for up to 15 minutes. The remaining PAR1 at cell surface is then measured by loss-of-receptor assay at 450 nm. The background OD450 (secondary antibody-only) values were averaged and subtracted from all raw OD450 readout values. Error bar = standard deviation. Multiple linear regression analysis was used to estimate the main effects of incubation duration, CYLD-knockdown, biological replicates (date), and interaction term (incubation duration×CYLD-knockdown), upon log(OD450). See **Supplemental Table 3-2** for full analysis results.

Figure 3-3. CYLD does not regulate PAR1-stimulated p38 pathway components expression, but may modulate post-translational modifications of TAB1.

A, Immunoblots of cell lysates of EA.hy926 cells that were seeded, transfected with non-specific (NS) or CYLD-specific siRNA (siCYLD #7), and stimulated with 10 nM α-thrombin for up to 60 minutes.

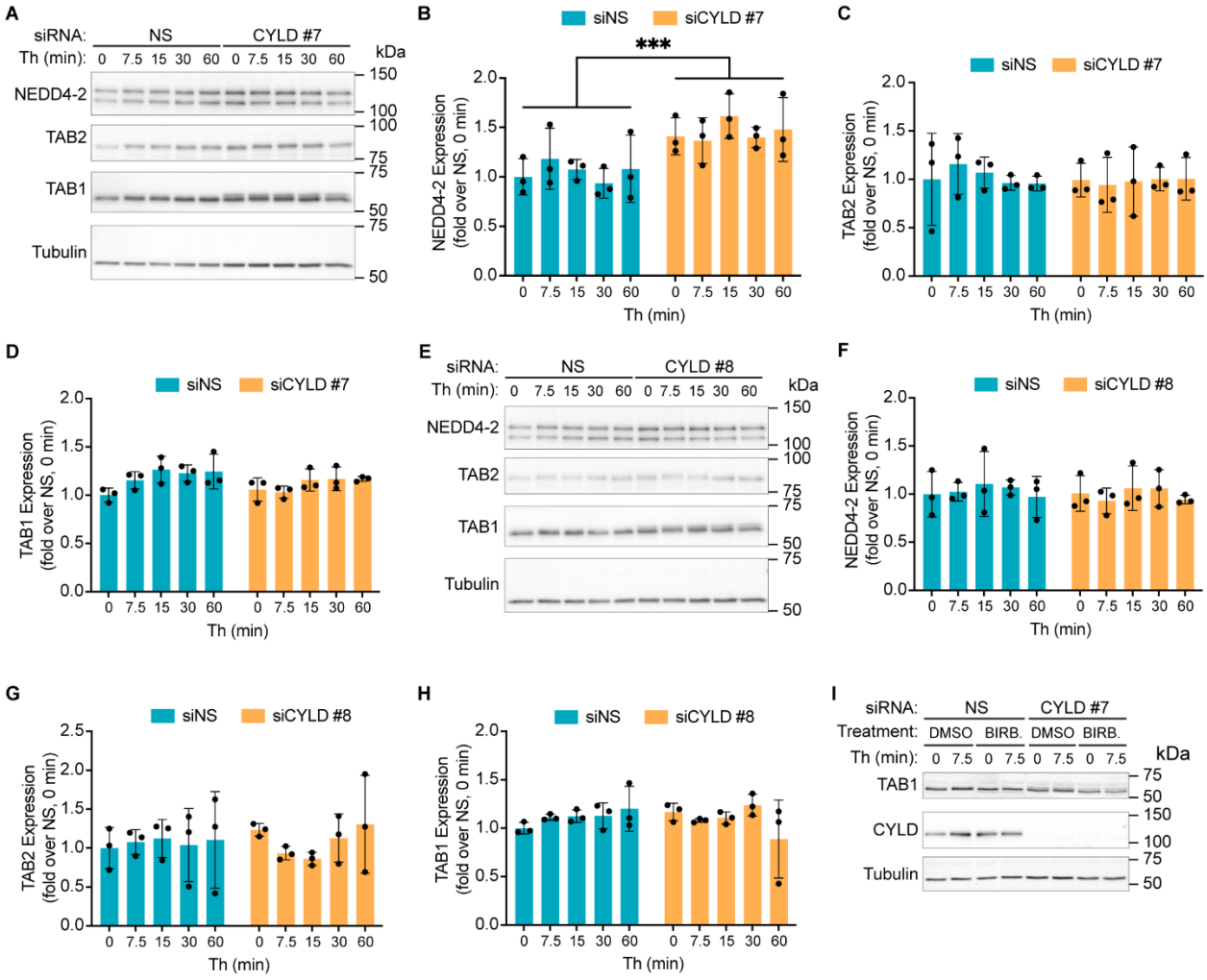
B-D, NEDD4-2 (*B*), TAB2 (*C*), and TAB1 (*D*) expression shown in panel (A). For each target protein, the integrated intensity is normalized to the average of each replicate, then expressed as a fraction over the average of NS-siRNA, 0-min control group. (N = 3)

E, Immunoblots of cell lysates of EA.hy926 cells that were seeded, transfected with non-specific (NS) or CYLD-specific siRNA (siCYLD #8), and stimulated with 10 nM α-thrombin for up to 60 minutes.

F-H, NEDD4-2 (*F*), TAB2 (*G*), and TAB1 (*H*) expression shown in panel (E). For each target protein, the integrated intensity is normalized to the average of each replicate, then expressed as a fraction over the average of NS-siRNA, 0-min control group. (N = 3)

I, Immunoblots of cell lysates of EA.hy926 cells that were seeded, transfected with non-specific (siNS) or CYLD-specific siRNA (siCYLD #7). These cells are treated with either DMSO (vehicle) or BIRB 796 during starvation and stimulated with 10 nM α-thrombin (+ DMSO or BIRB 796) for 7.5 minutes.

Error bar = standard deviation. Data shown in *B-D*, and *F-H* were analyzed by two-way ANOVA. *** $p < 0.001$. See **Supplemental Table 3-3** for full analysis results.


A
siRNA:
NS
CYLD #7
Th (min):
0 7.5 15 30 60 0 7.5 15 30 60
kDa
NEDD4-2
TAB2
TAB1
Tubulin
150
100
100
75
75
50
75
50
B
siNS
siCYLD #7
***
NEDD4-2 Expression (fold over NS, 0 min)
Th (min)
C
siNS
siCYLD #7
TAB2 Expression (fold over NS, 0 min)
Th (min)
D
siNS
siCYLD #7
TAB1 Expression (fold over NS, 0 min)
Th (min)
E
siRNA:
NS
CYLD #8
Th (min):
kDa
NEDD4-2
TAB2
TAB1
Tubulin
F
siNS
siCYLD #8
NEDD4-2 Expression (fold over NS, 0 min)
Th (min)
G
siNS
siCYLD #8
TAB2 Expression (fold over NS, 0 min)
Th (min)
H
siNS
siCYLD #8
TAB1 Expression (fold over NS, 0 min)
Th (min)
I
siRNA:
NS
CYLD #7
Treatment:
DMSO
BIRB.
DMSO
BIRB.
Th (min):
0 7.5 0 7.5 0 7.5 0 7.5
kDa
TAB1
CYLD
Tubulin

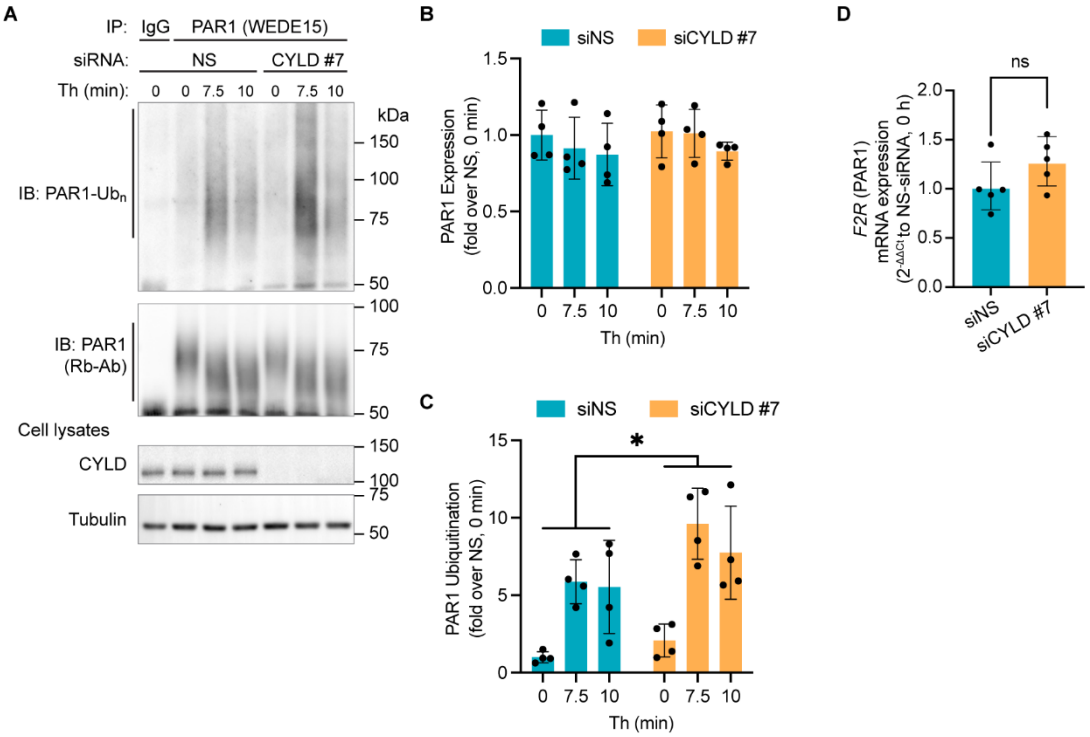


Figure 3-4. CYLD regulates thrombin-induced PAR1 ubiquitination without modulating PAR1 protein abundance.

A, Immunoblots of immunoprecipitated PAR1 using anti-PAR1 (WEDE15) antibody and protein A beads, and input lysates from EA.hy926 cells. These cells were seeded, transfected with non-specific (siNS) or CYLD-specific siRNA, and stimulated with 10 nM α-thrombin for up to 10 minutes. The PAR1-Ub_n is immunoblotted with ubiquitin-specific mouse antibody.

B, PAR1 expression shown in panel (A). The integrated intensity of PAR1 (> 55kDa in IP lysates) is normalized to the average of each replicate, then expressed as a fraction over the average of NS-siRNA, 0-min control group. (N = 4)

C, PAR1 ubiquitination shown in panel (A). The integrated intensity of ubiquitinated PAR1 (> 55 kDa in PAR1-Ub_n blot) is divided by total PAR1 expression (> 55kDa in PAR1 blot). These ratios are then normalized to the average of each replicate, then expressed as a fraction over the average of NS-siRNA, 0-min control group. (N = 4)

D, *F2R* (PAR1) mRNA expression in EA.hy926 cells that were transfected with non-specific (siNS) or CYLD-specific siRNA (siCYLD #7). (N = 5)

Error bar = standard deviation. Data shown in *B* and *C* were analyzed by two-way ANOVA. * $p < 0.05$. Data show in *D* were analyzed by two-tailed unpaired Student's *t* test. ns, not significant. See **Supplemental Table 3-4** for full analysis results.

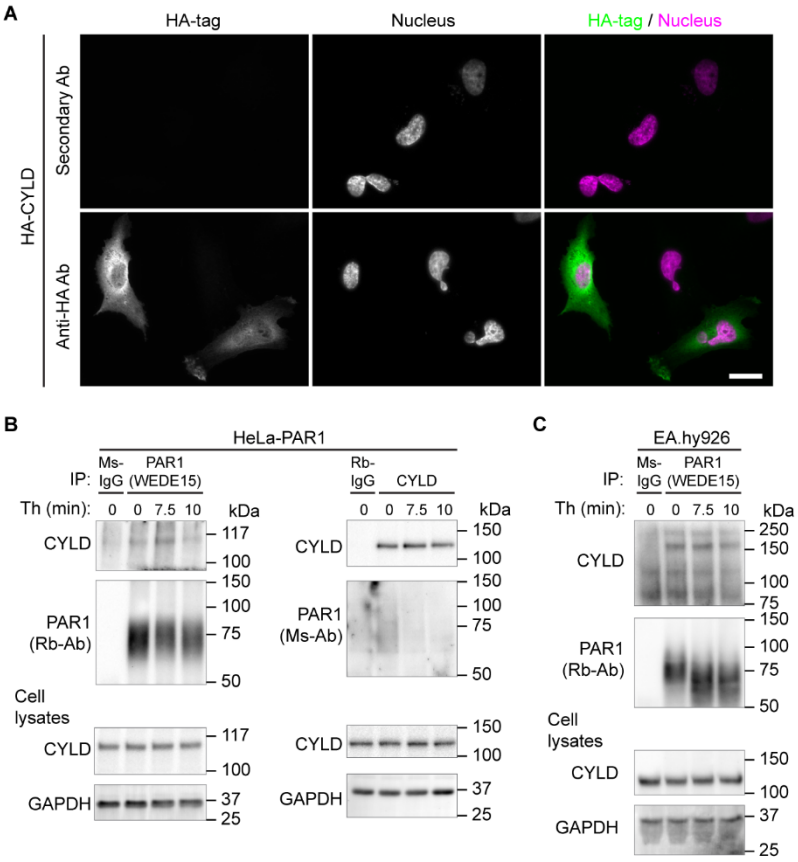


Figure 3-5. CYLD is localized to cytoplasm in endothelial cells and may interact with PAR1.

A, Immunofluorescence of HA-tagged CYLD in EA.hy926 cells. Cells were seeded, grown, and transfected with pDEST-3xHA-CYLD (WT) plasmid. After fixation, primary and secondary antibodies are used to probe localization of HA-CYLD. Scale bar = 20 μm.

B, Immunoblots of proteins enriched with immunoprecipitation, using anti-PAR1 (WEDE15) or anti-CYLD antibodies, and input lysates from HeLa-PAR1 cells.

C, Immunoblots of proteins enriched with immunoprecipitation using anti-PAR1 (WEDE15) antibody, and input lysates from EA.hy926 cells.

Figure 3-6. Thrombin induced phosphorylation of p38 kinase activity biosensors at endosomes and nuclei.

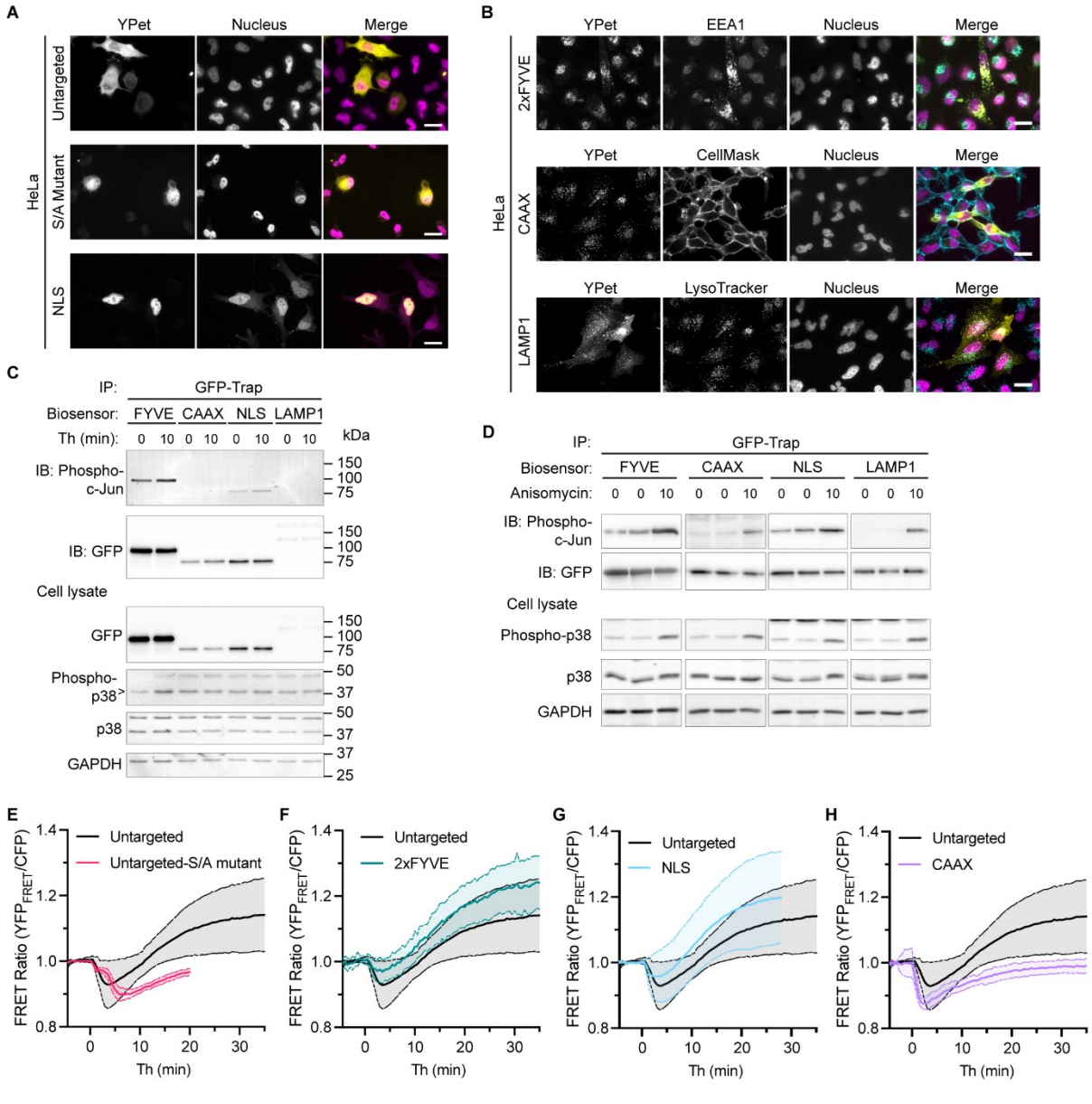
A, Confocal microscopy images of HeLa cell that were transfected with plasmids encoding the untargeted, S/A mutant, and NLS-tagged PerKy-EV p38 activity biosensors. Cells were fixed and stained with RedDot-2 nuclear stain. Scale bar = 20 μm.

B, Confocal microscopy images of HeLa cell that were transfected with plasmids encoding the 2xFYVE-, CAAX-tagged, and LAMP1-recombinant PerKy-EV p38 activity biosensors. CellMask plasma membrane stain was added to cells expressing CAAX-tagged p38 biosensor. LysoTracker lysosome stain was added to cells expressing LAMP1-recombinant p38 biosensor. Cells were then fixed and stained with RedDot-2 nuclear stain. For cells expressing 2xFYVE-tagged p38 biosensor, anti-EEA1 and secondary antibodies were used to label early endosomes. Scale bar = 20 μm.

C, Immunoblots of immunoprecipitated PerKy-EV p38 biosensors with GFP-Trap beads and input cell lysates. Phospho-c-Jun antibody was used to probe the substrate region of the biosensors. GFP antibody was used to probe the YPet that is part of the biosensors. Cells were stimulated with 10 nM α-thrombin for 10 minutes.

D, Immunoblots of immunoprecipitated PerKy-EV p38 biosensors with GFP-Trap beads and input cell lysates. Phospho-c-Jun antibody was used to probe the substrate region of the biosensors. GFP antibody was used to probe the YPet that is part of the biosensors. Cells were stimulated with 5 μM anisomycin for 10 minutes.

E-H, FRET ratio recorded from live-cell images of HeLa cells transfected with the untargeted ,S/A mutant, endosomal (2xFYVE), plasma membrane (CAAX), and nuclear (NLS) variants of p38 biosensor. Cells were stimulated with 10 nM α-thrombin. The solid line represents the average FRET ratio of at least 3 cells. The dotted line and the shaded area represent the standard deviation at each timepoint.


A
YPet
Nucleus
Merge
HeLa
Untargeted
S/A Mutant
NLS
B
YPet
EEA1
Nucleus
Merge
2xFYVE
YPet
CellMask
Nucleus
Merge
CAAX
YPet
LysoTracker
Nucleus
Merge
LAMP1
C
IP:
GFP-Trap
Biosensor:
FYVE
CAAX
NLS
LAMP1
Th (min):
0 10 0 10 0 10 0 10
kDa
IB: Phospho-c-Jun
150
100
75
IB: GFP
150
100
75
Cell lysate
GFP
150
100
75
Phospho-p38
50
37
p38
50
37
GAPDH
37
25
D
IP:
GFP-Trap
Biosensor:
FYVE
CAAX
NLS
LAMP1
Anisomycin:
0 0 10 0 0 10 0 0 10 0 0 10
IB: Phospho-c-Jun
IB: GFP
Cell lysate
Phospho-p38
p38
GAPDH
E
Untargeted
Untargeted-S/A mutant
FRET Ratio (YFP FRET/CFP)
1.4
1.2
1.0
0.8
0 10 20 30
Th (min)
F
Untargeted
2xFYVE
FRET Ratio (YFP FRET/CFP)
1.4
1.2
1.0
0.8
0 10 20 30
Th (min)
G
Untargeted
NLS
FRET Ratio (YFP FRET/CFP)
1.4
1.2
1.0
0.8
0 10 20 30
Th (min)
H
Untargeted
CAAX
FRET Ratio (YFP FRET/CFP)
1.4
1.2
1.0
0.8
0 10 20 30
Th (min)

Material and Methods

Reagents and Antibodies

Vorapaxar (SCH 530348, catalog no. 1755) was purchased from Axon MedChem (Groningen, Netherlands). BIRB 796 (catalog no. 506172) was purchased from Sigma-Aldrich (Irvine, CA). Human α-Thrombin was obtained from Enzyme Research Laboratories (catalog no. HT1002a, South Bend, IN). TFLLRNPNDK peptide agonist for PAR1 was synthesized at the Tufts University Core Facility (Boston, MA). Subquinocin (catalog no. E942-0252) was obtained from ChemDiv (San Diego, CA). Lambda protein phosphatase and supplied buffers (catalog no. P0753) was purchased from New England Biolabs (Ipswich, MA).

Antibodies recognizing CYLD (catalog no. 8426), p38 MAPK (catalog no. 9212), phospho-p38 MAPK (catalog no. 4511), p44/42 MAPK ERK1/2 (catalog no. 9102), phospho-p44/42 MAPK ERK1/2 (catalog no. 9106), NEDD4L (catalog no. 4013), TAB1(catalog no. 3226), TAB2 (catalog no. 3745), EEA1 (catalog no. 3288), and phospho-c-Jun (serine 63) were purchased from Cell Signaling Technology (Danvers, MA). Mouse monoclonal anti-PAR1 WEDE15 was purified from hybridoma as previously described (212). Rabbit polyclonal C5433 anti-PAR1 antibody was described previously (202). Mouse anti-ubiquitin antibody (P4D1, catalog no. sc-8017) was purchased from Santa Cruz Biotechnology (Dallas, TX). Anti-HA.11 epitope tag antibody (catalog no. MMS-101R) was purchased from BioLegend (San Diego, CA). Rat monoclonal GFP antibody (catalog no. 3H9) was purchased from Proteintech (Rosemont, IL). Horseradish peroxidase (HRP)-conjugated goat-anti rabbit (catalog no. 1706515), HRP-conjugated goat-anti mouse (catalog no. 1706516), StarBright Blue 520-conjugated goat anti-mouse (catalog no. 12005867), StarBright Blue 700-conjugated goat anti-rabbit (catalog no. 12004162), hFAB Rhodamine Tubulin (catalog no. 12004166), and hFAB Rhodamine Tubulin

(catalog no. 12004168) were purchased from BioRad (Hercules, CA).

AllStars negative control non-specific siRNA (catalog no. 1027281) was purchased from Qiagen (Hilden, Germany). CYLD-specific siRNA #7 (catalog no. J-004609-07; 5'- GGA GAG UAC UUG AAG AUG U -3') and #8 (catalog no. J-004609-08; 5'- GAA GGU UGG AGA AAC AAU A -3') were purchased from Horizon Discovery (Waterbeach, UK).

Cell culture and transfection

HeLa cells were generously provided by Dr. Jin Zhang's laboratory. These cells were maintained in Dulbecco's Modified Eagle's Medium (DMEM) with low glucose (catalog no. 11885084, Thermo Fisher Scientific, Waltham, MA) added with 10% FBS (catalog no. FB-01, Omega Scientific, Vista, CA), at 37°C with 5% CO_2. Human umbilical vein endothelial cell (HUVEC)-derived EA.hy926 cells were obtained from American Type Culture Collection (ATCC) (Manassas, VA) and maintained per ATCC instructions. These cells were grown in DMEM with high glucose (catalog no. 10-013-CV, Corning, Corning, NY) and 10% FBS, at 37°C with 8% CO_2. All cell culture were used between P2 and P10 and routinely tested for mycoplasma contamination using PCR-based Venor GeM Mycoplasma detection kit (catalog no. MP0025, Sigma-Aldrich, Irvine, CA).

For siRNA transfection in EA.hy926 cells, TransIT-X2 Dynamic Delivery System (catalog no. MIR 6004, Mirus Bio, Madison, WI) was used according to manufacturer's instructions. In brief, siRNA and the TransIT-X2 reagent were separately diluted in Opti-MEM I Reduced Serum Medium (catalog no. 31985062, Thermo Fisher Scientific, Waltham, MA) and then mixed, followed by 20-minute incubation. The incubated mixture is then added to the cell in fresh media drop-wise while the culture vessel being gently rocked, to achieve 28 nM siRNA in the final volume. For DNA transfection in EA.hy926 cells, Lipofectamine 3000 Transfection Reagent

(catalog no. L3000015, Thermo Fisher Scientific, Waltham, MA) was used per manufacturer's instructions. Similarly, the DNA of needed amount was diluted in Opti-MEM and mixed with the included P3000 reagent, while the Lipofectamine 3000 reagent was diluted separately. The two mixtures were then mixed gently and incubated for 15 minutes. The incubated mixture was then added to the cells drop-wise while rocking. 6 hours after the transfection, the cells were washed once with PBS and fresh media was added, in order to minimize cytotoxicity.

DNA delivery in HeLa cells was done with similar techniques using polyethylenimine (PEI). DNA and PEI were diluted separately, mixed, and incubated for 20 minutes. The mixture was added drop-wise to the cells.

Signaling Assays and Immunoblotting

EA.hy926 cells were seeded in 48-well plates at the density of 4.8×10^4 cells per well. After the cells adhered to the plate, they were transfected with siRNA at 28 nM and incubated for 48 hours. Then, these cells were starved with DMEM + 0.4% FBS overnight and further starved with DMEM + BSA + $CaCl_2$ for 1 hour before the agonist stimulation. To stimulate the cells with PAR1 agonist, 10 nM α-thrombin was added to the cells for various times and were subsequently lysed directly in 2X Laemmli Sample Buffer + DTT, followed by boiling at 95°C for 5 minutes. Cell lysates of equal amount were resolved in polyacrylamide gels by SDS-PAGE and transferred to 0.45 μm low fluorescence-PVDF membranes using Trans-Blot Turbo Transfer System (BioRad, Hercules, CA). The membranes were then blocked with 5% BSA/TBST for 1 hour and immunoblotted with antibodies. Membranes were developed by either epifluorescence or chemiluminescence, depending on the secondary antibodies used. Images of blots were acquired with ChemiDoc Imaging System (BioRad, Hercules, CA), and quantified by densitometry using NIH Fiji software (224) or Image Lab 6.1 (BioRad, Hercules, CA).

Loss-of-receptor assay

In four 24-well plates, EA.hy926 cells were seeded at 9.0×10^4 cells per well and transfected as described above. Surface cohort PAR1 was labeled with mouse anti-PAR1 (WEDE15) antibody (except the secondary-only control group) diluted to 1:500 in DMEM + BS + $CaCl_2$ starvation media at 4ºC for an hour. The unbound antibody was washed out with cold starvation buffer before the PAR1 stimulation. The control plate was kept on ice, one plate was incubated for 30 minutes at 37ºC to measure constitutive internalization. The two other plates were treated with 100 mM TFLLRNPNDK agonist peptide for 7.5 minutes and 15 minutes. All plates were washed with PBS and added with cold 4% (w/v) paraformaldehyde (PFA)/PBS to fix the cells. The remaining PAR1 surface cohort was labeled with HRP-conjugated goat anti-mouse IgG secondary antibody (diluted at 1:1000) for 1 hour at room temperature (20-22ºC). Cells were gently washed with PBS and incubated in TMB substrate solution (catalog no. 34022, Thermo Scientific, Waltham, MA) for up to 30 minutes. Equal volume of developed TMB solution from each well was transferred to a 96-well plate and mixed with 1 N HCl. Optical density at OD 450 nm of each well was measured with a SpectraMax ABS Plus Microplate Reader (Molecular Devices, San Jose, CA).

Detection of protein ubiquitination

In 100-mm petri dishes, EA.hy926 cells were seeded at 1.0×10^6 cells each and were transfected with siRNA. After 48 hours, the cells were starved with DMEM + 0.4% FBS overnight. Cells were serum-starved with DMEM + BSA + $CaCl_2$ for 1 hour and stimulated with 10 nM thrombin for various times. Then, the cells were lysed with lysis buffer supplemented with protease and deubiquitinase inhibitors (50 mM Tris pH 8.0, 150 mM NaCl, 1% [v/v] NP-40, 5 mM EDTA, 0.5% [w/v] sodium deoxycholate, 0.1% [w/v] SDS, 1 µg/mL leupeptin, 1 µg/mL aprotinin, 1

μg/mL pepstatin, 10 μg/mL benzamidine, 1 μg/mL TPI, 50 μM PR619, 20 mM NEM, 3 mM *o*-phenanthroline) on ice. The crude lysates were sheared using 22-gauge needles and centrifuged at 14,000 rpm for 20 min at 4°C to remove insoluble proteins. Protein concentrations in clarified lysates were equalized with lysis buffer using a BCA protein assay (Thermo Fisher Scientific, Waltham, MA). Mouse anti-PAR1 (WEDE15) or anti-TAB1 antibody and BSA-blocked protein A beads (catalog no. 17078001, Cytiva, Marlborough, MA) were mixed to the lysates for 2-16 hours at 4°C. Beads were washed with lysis buffer and eluted with 2X Laemmli Sample Buffer + DTT and boiled for 5 min at 95ºC. Samples were immunoblotted with anti-ubiquitin and anti-PAR1 (C5433) antibodies as describe above, except the PVDF membrane was transferred with Mini Trans-Blot Cell (BioRad, Hercules, CA) at 0.2 A for 120 minutes.

Co-immunoprecipitation

In 100-mm petri dishes, EA.hy926 or HeLa-PAR1 cells were seeded at 1.0×10^6 cells per dish or 5.0×10^6 cells per dish, respectively. Cells were starved, stimulated with 10 nM thrombin and lysed with lysis buffer supplemented with protease and phosphatase inhibitors (50 mM Tris pH 7.4, 100 mM NaCl, 1% [v/v] Triton X-100, 5 mM EDTA, 50 mM NaF, 10 mM NaPP, 10 mM β-Glycerophosphate, 1 μg/mL leupeptin, 1 μg/mL aprotinin, 1 μg/mL pepstatin, 10 μg/mL benzamidine, 1 μg/mL PMSF, 1 μg/mL TPI, 2 mM Na_3VO_4, 20 mM NEM). Lysates were sheared, clarified, and equalized as described above. Anti-PAR1 (WEDE15) or anti-CYLD antibodies, and BSA-blocked protein A beads or protein G beads (catalog no. 11719416001, Sigma-Aldrich [Roche], St. Louis, MO) were mixed with the lysates and incubated at 4°C overnight. The beads were washed with lysis buffer and eluted with 2X Laemmli Sample Buffer + DTT. The lysates were boiled for 5 minutes at 50°C and 5 minutes at 95°C. Immunoblot technique was used to analyze proteins eluted from the beads.

Real-time quantitative polymerase chain reaction

In a 24-well plate, EA.hy926 cells were seeded at 9×10^4 cells per well. Cells were transfected with siRNA for 72 hours and subsequently lysed with TRIzol reagent (catalog no. 15596026, Thermo Fisher Scientific, Waltham, MA). RNA was isolated from these lysates using Direct-zol RNA Miniprep Plus Kit (catalog no. R2072, Zymo Research, Irvine, CA) and quantified with Nanodrop Lite spectrophotometer (Thermo Fisher Scientific, Waltham, MA). Equalized amount of total RNA was used for cDNA synthesis reaction using SuperScript IV VILO Master Mix with ezDNase enzyme kit (catalog no. 111766050, Thermo Fisher Scientific, Waltham, MA). The real-time quantitative PCR was carried out by a QuantStudio 3 Real-Time PCR System with TaqMan Fast Advanced Master Mix (catalog no. 4444964, Thermo Fisher Scientific, Waltham, MA). TaqMan Gene Expression Probes for F2R (catalog no. Hs05045041_s1) and 18S (catalog no. Hs03003631_g1, primer-limited) were also obtained from Thermo Fisher Scientific (Waltham, MA). Messenger RNA transcript expression was analyzed using the comparative CT (threshold cycle) method, and normalized to 18S ribosomal RNA expression. The difference in gene expression was expressed as $2^{-\Delta\Delta Ct}$ to the non-specific siRNA-transfected group.

Immunofluorescence

To over-express HA-tagged CYLD, EA.hy926 cells were seeded at 6×10^4 cells per well in a 12-well plate and grown on coverslips (catalog no. 1943-10012A, Bellco Glass, Vineland, NJ) overnight. These cells were transfected with 300 ng pDEST-3xHA-CYLD (WT) plasmid, which was a gift from Stephen Elledge (185). These transfected cells were fixed with 4% (w/v) paraformaldehyde (PFA)/PBS for 20 minutes at room temperature (20-22°C) and permeabilized with 0.2% (v/v) Triton X-100/PBS + 2% BSA for 20 minutes. Mouse anti-HA.11 primary antibody (1:1000) and goat anti-Mouse IgG (H+L) conjugated to Alexa Fluor 488 (catalog no. A-11001,

Thermo Fisher Scientific) secondary antibody (1:500) were used to label HA-tagged CYLD; each was incubated for 1 hour at room temperature. Hoechst 33342 (catalog no. 62249, Thermo Fisher Scientific) was used at 1:2000 dilution to label nuclei. After washes, the stained coverslips were mounted with FluorSave Reagent (catalog no. 345789, Sigma-Aldrich [Calbiochem], Irvine, CA).

For visualizing the PerKy-EV p38 activity biosensor variants, HeLa cells were seeded in 12-wells with fibronectin-coated coverslips at 5×10^4 cells per well. When applicable, LysoTracker Red DND-99 (catalog no. L7528, Thermo Fisher Scientific), RedDot-2 Far-Red Nuclear Stain (catalog no. 40061, Biotium, Fremont, CA), and CellMask Plasma Membrane Stains (catalog no. C10046, Thermo Fisher Scientific), EEA1 antibody were used to label various organelles. These coverslips were fixed and mounted as described above.

Confocal microscopy and image acquisition were conducted using an Olympus IX81 microscope with IX2-DSU spinning disc, CoolSNAP HQ2 CCD Camera (Andor, Belfast, UK), and a PlanApo 60× 1.40 NA oil objective lens (Olympus) installed. Three or more fields of view from each coverslip were acquired with MetaMorph software (MDS Analytical Technologies, Sunnyvale, CA) at multiple focal planes (z-stack). Images were processed and prepared using NIH Fiji software and ScientiFig plugin (224,225).

Live-cell FRET imaging

PerKy-EV p38 activity biosensor plasmid derived from Taichiro Tomida *et al.* (214) was a gift from Jin Zhang. Subcellular sorting motifs/domains were added to the N- or C-terminal of the biosensor construct, which consists of CFP, WW domain (from PIN1), EV linker, p38 docking region (from MEF2A), kinase substrate region (from c-Jun), and YPet sequences.

HeLa cells were seeded at 3×10^4 cells in 35-mm petri dishes with 14 mm micro-well #1.5 cover glass (catalog no. D35-14-1.5-N, Cellvis, Mountain View, CA). These cells were transfected

with PerKy p38 activity biosensor plasmids and incubated for 48-72 hours. They were starved with DMEM + BSA + $CaCl_2$ for 1 hour and changed to 1X HBSS + 0.1% (w/v) BSA + 20 mM HEPES + 2mg/mL glucose for imaging.

Live-cell image acquisition was performed with a AxioObserverZ1 microscope (Zeiss) equipped with a Photometrics Evolve EMCCD camera, Plan-APOCHROMAT 40X/1.4 NA oil lens (Zeiss), stage-top incubator (Pecon, Germany), and FRET-compatible filter sets. Images were acquired using MetaFluor (MDS Analytical Technologies, Sunnyvale, CA) and analyzed by MetaFluor or CellProfiler 4 (226). In brief, the raw images were stabilized with rigid registration methods if needed, then regions of interest (ROIs) were either manually drawn or automatically assigned by segmentation methods. The average intensity of the ROIs at each color channel are subtracted by the background intensity of that channel and plotted by time. The FRET readout is defined as YFP_{FRET}/CFP_{Epi} ratio per cell. FRET ratio is normalized to the averaged ratio of baseline (before stimulation) by division.

Detection of biosensor phosphorylation

HeLa cells were seeded at 3.5×10^5 cells per dish in 60-mm petri dishes and transfected with 1500 ng PerKy-EV p38 biosensor plasmid. Cells were starved and stimulated with 10 nM thrombin or 5 μM anisomysin for various times. Stimulated cells were lysed with lysis buffer supplemented with protease and phosphatase inhibitors (10 mM Tris pH 7.5, 150 mM NaCl, 0.5% [v/v] NP-40, 5 mM EDTA, 10 mM NaF, 2 mM NaPP, 10 mM β-Glycerophosphate, 1 μg/mL leupeptin, 1 μg/mL aprotinin, 1 μg/mL pepstatin, 10 μg/mL benzamidine, 1 μg/mL PMSF, 1 μg/mL TPI, 2 mM Na_3VO_4). Lysates were sheared and clarified as described above. GFP-trap agarose (Proteintech, Rosemont, IL) beads were used to enrich the over-expressed biosensor in the lysates according to manufacturer's instructions. In brief, all lysates were diluted with Dilution

Buffer (lysis buffer without NP-40 detergent) and mixed with Dilution Buffer-equilibrated GFP-Trap beads for at least 1 hour at 4°C. The beads were then washed with Wash Buffer (lysis buffer with low NP-40 concentration) and eluted with 2X Laemmli Sample Buffer + DTT. The lysates were boiled for 5 minutes at 95°C. Immunoblot was performed to evaluate the expression and phosphorylation of the biosensors using rat anti-GFP and rabbit anti-phospho-c-Jun (ser63) antibodies.

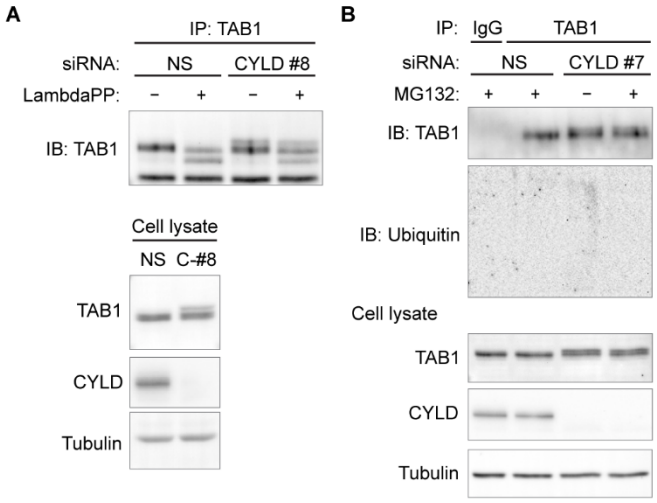
Statistical Analysis

Data were analyzed using Prism 10.2 statistical software (GraphPad Software, La Jolla, CA) and Microsoft Excel. Statistical analysis methods are indicated in the figure legends. Detailed statistical analysis results are included in Supplemental Information.

Acknowledgements

We thank Jin Zhang and Sohum Mehta for their helpful advice and technical assistance.

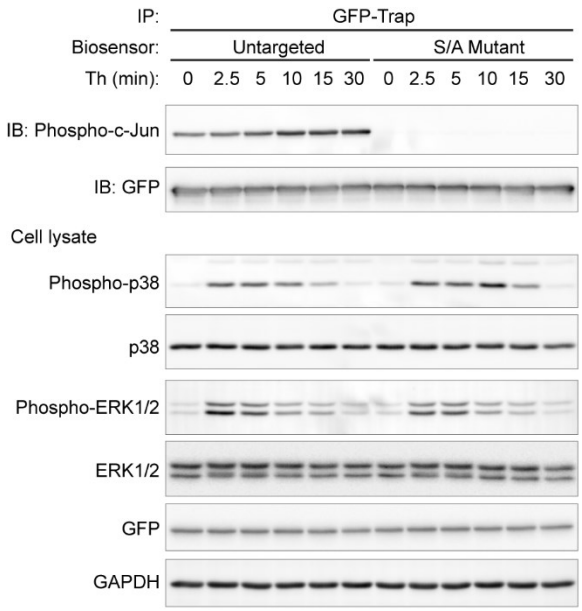
Supplemental Information



Supplemental Figure 3-1. TAB1 post-translational modification.

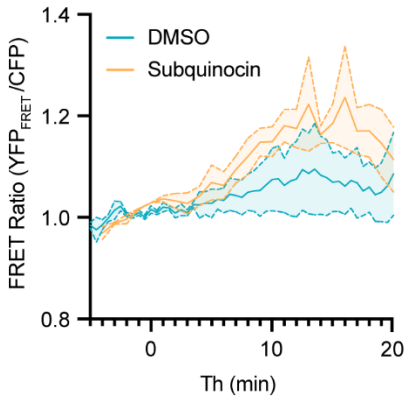
A, Immunoblots of immunoprecipitated TAB1 and total cell lysates from the cells that were transfected with non-specific (NS) or CYLD-specific (CYLD #8) siRNA. TAB1 from the lysates was immobilized by anti-TAB1 antibody and protein A beads. Lambda protein phosphatase was used to dephosphorylated immobilized proteins. The immobilized proteins were eluted and immunoblotted by TAB1 antibody.

B, Immunoblots of immunoprecipitated TAB1 and total cell lysates from the cells that were transfected with non-specific (NS) or CYLD-specific (CYLD #8) siRNA and treated with 10 μM MG132 proteasome inhibitor for 30 minutes. The eluted proteins were immunoblotted by TAB1 and ubiquitin antibodies.



Supplemental Figure 3-2. PerKy-EV p38 activity biosensor was phosphorylated when stimulated by thrombin.

Immunoblots of immunoprecipitated untargeted and S/A mutant PerKy-EV p38 biosensors with GFP-Trap beads and input cell lysates. Phospho-c-Jun antibody was used to probe the substrate region of the biosensors. GFP antibody was used to probe the YPet that is part of the biosensors. Cells were stimulated with 10 nM α-thrombin for up to 30 minutes.



Supplemental Figure 3-3. CYLD may regulate p38 kinase activity at endosomes.

FRET ratio recorded from live-cell images of EA.hy926 cells transfected with the endosomal (2xFYVE) p38 biosensor. Cells were pre-incubated with 40 μM subquinocin or DMSO for 2 hours, and stimulated with 10 nM α-thrombin. The solid line represents the average FRET ratio of at least 3 cells. The dotted line and the shaded area represent the standard deviation at each timepoint.

Supplemental Table 3-1. ANOVA results for Figure 3-1.

Panel B: p38 phosphorylation

- Two-way ANOVA

Source of variation	SS	DF	MS	F (DFn, DFd)	P value
Interaction	1.2	4	0.2999	F (4, 20) = 1.418	0.2643
Time	27.03	4	6.757	F (4, 20) = 31.95	<0.0001
siRNA	10.12	1	10.12	F (1, 20) = 47.84	<0.0001
Residual	4.229	20	0.2115		

- Post hoc multiple comparisons

Time	Mean 1	Mean 2	Mean Diff.	SE of diff.	N1	N2	t	DF	Adjusted P Value
siCYLD #7 - siNS									
0	1.896	1	0.8963	0.3755	3	3	2.387	20	0.1277
7.5	4.751	2.969	1.783	0.3755	3	3	4.747	20	0.0006
15	3.776	2.337	1.439	0.3755	3	3	3.833	20	0.0052
30	2.406	1.38	1.026	0.3755	3	3	2.733	20	0.0624
60	1.843	1.18	0.6631	0.3755	3	3	1.766	20	0.3851

Panel C: ERK1/2 phosphorylation

- Two-way ANOVA

Source of variation	SS	DF	MS	F (DFn, DFd)	P value
Interaction	0.1452	4	0.03629	F (4, 20) = 0.1383	0.9661
Time	4.801	4	1.2	F (4, 20) = 4.573	0.0087
siRNA	3.027	1	3.027	F (1, 20) = 11.53	0.0029
Residual	5.249	20	0.2625		

- Post hoc multiple comparisons

Time	Mean 1	Mean 2	Mean Diff.	SE of diff.	N1	N2	t	DF	Adjusted P Value
siCYLD #7 - siNS									
0	1.603	1	0.6034	0.4183	3	3	1.442	20	0.5932
7.5	2.622	1.957	0.665	0.4183	3	3	1.59	20	0.4945
15	2.502	1.797	0.7051	0.4183	3	3	1.686	20	0.4333
30	2.674	1.863	0.8108	0.4183	3	3	1.938	20	0.2924
60	1.788	1.396	0.392	0.4183	3	3	0.9371	20	0.8925

(continued)

Supplemental Table 3-1. ANOVA results for Figure 3-1. (continue)

Panel E: p38 phosphorylation

- Two-way ANOVA

Source of variation	SS	DF	MS	F (DFn, DFd)	P value
Interaction	1.286	4	0.3216	F (4, 20) = 0.8301	0.5217
Time	46.12	4	11.53	F (4, 20) = 29.76	<0.0001
siRNA	3.818	1	3.818	F (1, 20) = 9.854	0.0052
Residual	7.749	20	0.3874		

- Post hoc multiple comparisons

Time	Mean 1	Mean 2	Mean Diff.	SE of diff.	N1	N2	t	DF	Adjusted P Value
siCYLD #8 - siNS									
0	1.579	1	0.5786	0.5082	3	3	1.138	20	0.7904
7.5	5.104	3.651	1.453	0.5082	3	3	2.859	20	0.0476
15	3.791	3.008	0.7827	0.5082	3	3	1.54	20	0.5275
30	2.171	1.62	0.5509	0.5082	3	3	1.084	20	0.8212
60	1.361	1.158	0.2022	0.5082	3	3	0.3979	20	0.9974

Panel F: ERK1/2 phosphorylation

- Two-way ANOVA

Source of variation	SS	DF	MS	F (DFn, DFd)	P value
Interaction	1.774	4	0.4434	F (4, 20) = 2.368	0.0873
Time	9.969	4	2.492	F (4, 20) = 13.31	<0.0001
siRNA	1.227	1	1.227	F (1, 20) = 6.554	0.0187
Residual	3.745	20	0.1873		

- Post hoc multiple comparisons

Time	Mean 1	Mean 2	Mean Diff.	SE of diff.	N1	N2	t	DF	Adjusted P Value
siCYLD #8 - siNS									
0	0.9908	1	-0.0092	0.3533	3	3	0.02604	20	>0.9999
7.5	3.099	2.051	1.049	0.3533	3	3	2.968	20	0.0375
15	2.366	1.45	0.9153	0.3533	3	3	2.59	20	0.0844
30	1.622	1.413	0.2088	0.3533	3	3	0.5909	20	0.9837
60	1.034	1.175	-0.1408	0.3533	3	3	0.3985	20	0.9973

(continued)

Supplemental Table 3-1. ANOVA results for Figure 3-1. (continue)

Panel H: p38 phosphorylation - Two-way ANOVA					
Source of variation	SS	DF	MS	F (DFn, DFd)	P value
Thrombin	24.81	1	24.81	F (1, 24) = 238.4	<0.0001
siRNA	8.018	1	8.018	F (1, 24) = 77.06	<0.0001
Vorapaxar	24.49	1	24.49	F (1, 24) = 235.4	<0.0001
Thrombin x siRNA	1.858	1	1.858	F (1, 24) = 17.85	0.0003
Thrombin x Vorapaxar	16.83	1	16.83	F (1, 24) = 161.8	<0.0001
siRNA x Vorapaxar	1.35	1	1.35	F (1, 24) = 12.97	0.0014
Thrombin x siRNA x Vorapaxar	1.07	1	1.07	F (1, 24) = 10.29	0.0038
Residual	2.497	24	0.104		
Panel J: p38 phosphorylation - Two-way ANOVA					
Source of variation	SS	DF	MS	F (DFn, DFd)	P value
Thrombin	33.8	1	33.8	F (1, 16) = 116.9	<0.0001
siRNA	5.647	1	5.647	F (1, 16) = 19.53	0.0004
BIRB 796	5.585	1	5.585	F (1, 16) = 19.31	0.0005
Thrombin x siRNA	4.507	1	4.507	F (1, 16) = 15.58	0.0012
Thrombin x BIRB 796	2.532	1	2.532	F (1, 16) = 8.757	0.0092
siRNA x BIRB 796	0.04699	1	0.04699	F (1, 16) = 0.1625	0.6922
Thrombin x siRNA x BIRB 796	0.2113	1	0.2113	F (1, 16) = 0.7307	0.4053
Residual	4.627	16	0.2892		

Supplemental Table 3-2. ANOVA results for Figure 3-2.

Panel A: Constitutive internalization of PAR1

- Multiple linear regression
- Log-transformed OD450 value (based on the assumption that the relationship between incubation duration and PAR1 surface expression is multiplicative)
- log_OD450 ~ Intercept + siRNA + Duration + Replicate + siRNA : Duration

siNS versus siCYLD #7

Independent variable	Estimate	Standard error	|t|	P value
Intercept	-1.09	0.07628	14.29	<0.0001
siRNA[siCYLD #7]	0.0357	0.08808	0.4053	0.6993
Time	-0.009321	0.002936	3.175	0.0192
Rep[2]	-0.001075	0.07628	0.01409	0.9892
Rep[3]	0.1036	0.07628	1.358	0.2234
siRNA[siCYLD #7] : Time	0.005051	0.004152	1.217	0.2694

$R^2 = 0.7488$

F (DFn, DFd) = 3.576

siNS versus siμ2

Independent variable	Estimate	Standard error	|t|	P value
Intercept	-1.115	0.05421	20.57	<0.0001
siRNA[siμ2]	0.5084	0.0626	8.121	0.0002
Duration	-0.009321	0.002087	4.467	0.0042
Replicate[2]	0.03835	0.05421	0.7074	0.5058
Replicate[3]	0.1394	0.05421	2.572	0.0422
siRNA[siμ2] : Duration	0.009427	0.002951	3.195	0.0187

$R^2 = 0.9759$

F (DFn, DFd) = 48.51

Panel B: Agonist-induced internalization of PAR1

- Multiple linear regression
- Log-transformed OD450 value (based on the assumption that the relationship between treatment duration and PAR1 surface expression is multiplicative)
- log_OD450 ~ Intercept + siRNA + Duration + Replicate + siRNA : Duration

siNS versus siCYLD #7

Independent variable	Estimate	Standard error	|t|	P value
Intercept	-1.086	0.08662	12.54	<0.0001
siRNA[siUSP34]	0.07434	0.1035	0.718	0.4865
Duration	-0.04003	0.007561	5.294	0.0002
Replicate[2]	-0.08617	0.0802	1.074	0.3037
Replicate[3]	-0.01353	0.0802	0.1688	0.8688
siRNA[siUSP34] : Duration	0.009949	0.01069	0.9304	0.3705

$R^2 = 0.8076$

F (DFn, DFd) = 10.07

(continued)

Supplemental Table 3-2. ANOVA results for Figure 3-2. (continue)

siNS versus siμ2				
Independent variable	Estimate	Standard error	|t|	P value
Intercept	-1.101	0.08249	13.35	<0.0001
siRNA[siμ2]	0.5694	0.09859	5.775	<0.0001
Duration	-0.04003	0.0072	5.559	0.0001
Replicate[2]	-0.06998	0.07637	0.9164	0.3775
Replicate[3]	0.01487	0.07637	0.1947	0.8489
siRNA[siμ2] : Duration	0.03015	0.01018	2.961	0.0119
$R^2 = 0.9426$ F (DFn, DFd) = 39.39				

Supplemental Table 3-3. ANOVA results for Figure 3-3.

Panel B: expression of NEDD4-2					
- Two-way ANOVA					
Source of variation	SS	DF	MS	F (DFn, DFd)	P value
Interaction	0.1055	4	0.02638	F (4, 20) = 0.4949	0.7396
Time	0.1158	4	0.02895	F (4, 20) = 0.5432	0.7059
siRNA	1.194	1	1.194	F (1, 20) = 22.40	0.0001
Residual	1.066	20	0.0533		
Panel C: expression of TAB2					
- Two-way ANOVA					
Source of variation	SS	DF	MS	F (DFn, DFd)	P value
Interaction	0.07324	4	0.01831	F (4, 20) = 0.2754	0.8904
Time	0.02106	4	0.005266	F (4, 20) = 0.07920	0.9878
siRNA	0.01533	1	0.01533	F (1, 20) = 0.2306	0.6363
Residual	1.33	20	0.06649		
Panel D: expression of TAB1					
- Two-way ANOVA					
Source of variation	SS	DF	MS	F (DFn, DFd)	P value
Interaction	0.03064	4	0.00766	F (4, 20) = 0.6406	0.6397
Time	0.1617	4	0.04041	F (4, 20) = 3.380	0.0288
siRNA	0.02803	1	0.02803	F (1, 20) = 2.344	0.1414
Residual	0.2391	20	0.01196		
Panel F: expression of NEDD4-2					
- Two-way ANOVA					
Source of variation	SS	DF	MS	F (DFn, DFd)	P value
Interaction	0.00924	4	0.00231	F (4, 20) = 0.06175	0.9924
Time	0.07261	4	0.01815	F (4, 20) = 0.4853	0.7464
siRNA	0.008167	1	0.008167	F (1, 20) = 0.2183	0.6454
Residual	0.7481	20	0.03741		
Panel G: expression of TAB2					
- Two-way ANOVA					
Source of variation	SS	DF	MS	F (DFn, DFd)	P value
Interaction	0.2852	4	0.0713	F (4, 20) = 0.5587	0.6952
Time	0.1823	4	0.04558	F (4, 20) = 0.3571	0.8361
siRNA	0.004306	1	0.004306	F (1, 20) = 0.03373	0.8561
Residual	2.553	20	0.1276		

(continued)

Supplemental Table 3-3. ANOVA results for Figure 3-3.**Supplemental Table 3-2. ANOVA results for Figure 3-2.** (continue)

Panel H: expression of TAB1 - Two-way ANOVA					
Source of variation	SS	DF	MS	F (DFn, DFd)	P value
Interaction	0.2058	4	0.05144	F (4, 20) = 1.920	0.1463
Time	0.06244	4	0.01561	F (4, 20) = 0.5828	0.6786
siRNA	0.002202	1	0.002202	F (1, 20) = 0.08219	0.7773
Residual	0.5357	20	0.02679		

Supplemental Table 3-4. ANOVA results for Figure 3-4.

Panel B: expression of PAR1

- Two-way ANOVA

Source of variation	SS	DF	MS	F (DFn, DFd)	P value
Interaction	0.007336	2	0.003668	F (2, 18) = 0.1315	0.8777
Time	0.06698	2	0.03349	F (2, 18) = 1.200	0.3241
siRNA	0.01341	1	0.01341	F (1, 18) = 0.4806	0.4970
Residual	0.5022	18	0.0279		

Panel C: PAR1 ubiquitination

- Two-way ANOVA

Source of variation	SS	DF	MS	F (DFn, DFd)	P value
Interaction	7.113	2	3.556	F (2, 18) = 0.8035	0.4632
Time	175.2	2	87.59	F (2, 18) = 19.79	<0.0001
siRNA	32.97	1	32.97	F (1, 18) = 7.447	0.0138
Residual	79.68	18	4.426		

Panel D: mRNA expression of *F2R* (PAR1)

- ΔΔCt (siCYLD #7 - siNS)
- two-tailed unpaired Student's t test

Mean [NS] = 0.000
Mean [siUSP34] = -0.3279
t = 1.629
Degree of freedom = 8
P value = 0.1420

Chapter 4 CONCLUSIONS

The vascular endothelium is critical for regulating blood flow, clotting and inflammation to maintain homeostasis of the circulation system. Endothelial dysfunction has been linked to both acute and chronic disorders, such as sepsis and atherosclerosis, and is a major risk factor for cardiovascular diseases (CVD) (227-230). GPCRs and downstream signaling pathways which are controlled by these receptors are involved in endothelial functions and vascular inflammation, thus making them potential pharmaceutical targets for CVD therapies (229,231,232). Of the many physiologically relevant GPCRs, this dissertation focuses on protease-activated receptor 1 (PAR1) and a unique pro-inflammatory signaling pathway that contributes to two important inflammation responses, including barrier function and cytokine expression.

It has been established that thrombin-activated PAR1 can mediate cellular signaling via the receptor ubiquitination and subsequent protein recruitment to induce auto-activation of p38 MAPK at endosomes (11,12). This PAR1-mediated p38 MAPK signaling axis was found to be independent from the canonical RhoA-myosin light chain (MLC) pathway and plays a role in promoting barrier disruption and cytokine expression in endothelial cells (11,13,131). Although some of the mediators, such as the E3 ligase responsible for thrombin-induced PAR1 ubiquitination as well as the adaptor proteins, TAB1 and TAB2, have been identified, it was unclear how the p38 MAPK signal is regulated. This dissertation started with the identification of the deubiquitinase (DUB) which regulates thrombin-stimulated p38 MAPK signaling, followed by two arms of further investigation of the mechanisms by which the two DUBs identified from the comprehensive screen.

To identify the DUB(s) which may regulate thrombin-induced p38 activation, we individually inhibited expression of the 96 human DUBs in two model systems: HeLa cells and

EA.hy926 endothelial cells. As shown in the Chapter 1, we found several DUBs, namely CYLD, USP34, USP47, and USP51 prolonged the thrombin-induced p38 phosphorylation, which is indicative of the p38 auto-phosphorylation activity. We then showed that CYLD and USP34 specifically regulate p38 phosphorylation in HeLa cells, while they may be implicated in distinct endothelial responses. CYLD was found to regulate thrombin-induced endothelial permeability. Interestingly, CYLD and USP34 regulate IL-6 pro-inflammatory cytokine expression differentially, suggesting that they may integrate into PAR1-p38 signaling axis distinctly.

In Chapter 2, we further investigated the role of USP34 in the PAR1-mediated signaling. We showed that the increase of p38 phosphorylation requires PAR1 activation and p38 auto-phosphorylation activity. While USP34 was not found to regulate PAR1 ubiquitination, it plays a role in down-regulating PAR1 surface and total expression. Furthermore, we revealed that USP34 regulates PAR1 protein expression not by affecting its stability, but rather by modulating the *F2R* (PAR1) mRNA expression. Interestingly, depletion of USP34 also affected *F2RL1* (PAR2) expression. We also showed that USP34 is localized to nucleus and cytoplasm in endothelial cells by both biochemical and imaging approaches. Together with these observations and that USP34 regulates IL-6 expression, we hypothesized that USP34 may be active at the nucleus and regulates either transcription factors or histone thus affecting multiple gene expression.

On the other hand, in Chapter 3, we showed that CYLD regulates thrombin-induced p38 and ERK1/2 phosphorylation. Unlike USP34, CYLD was not shown to regulate PAR1 surface nor total expression. Instead, CYLD was shown to regulate PAR1 ubiquitination, regardless of PAR1 activation, suggesting that CYLD may constitutively control PAR1 ubiquitination. This was confirmed by the co-immunoprecipitation experiment, which showed that CYLD co-associates with PAR1 basally in HeLa and endothelial cells. In order to better understand whether CYLD

regulates PAR1-mediated p38 activation at specific subcellular compartments, we developed a series of FRET-based p38 kinase activity reporter, PerKy-EV biosensor and localization-targeted variants. By over-expressing these biosensors in HeLa cells, we showed that all these reporters were phosphorylated when we activated p38 with anisomycin. In contrast, when the cells were stimulated with thrombin, only the endosomal (2xFYVE) and nuclear (NLS) variants were phosphorylated. Additionally, we observed p38 activity at endosomes and nuclei but not at plasma membrane by live-cell FRET imaging. These data showed that thrombin-stimulated p38 activity is localized to the endosomes and nuclei. However, whether CYLD regulates p38 activity at these subcellular compartments is to be further investigated.

Overall, this dissertation demonstrated that two DUBs, CYLD and USP34, regulate PAR1-mediated signaling by two distinct mechanisms. These findings provide a novel understanding of how GPCR and GPCR-stimulated signaling pathways are regulated by DUBs. My work suggests an important role of USP34 mediating pro-inflammatory cytokine and GPCR expression, thus it may be a therapeutic target for vascular inflammation. Moreover, while the detailed mechanisms by which CYLD interplays with the characterized components that control cell morphology and cell-cell junctions remain to be investigated, this dissertation shows that CYLD is implicated in the regulation of endothelial barrier function and CYLD may play a protective role against endothelial hyperpermeability. These conclusions demonstrated GPCR-regulating DUBs may be crucial in maintaining vascular homeostasis.

REFERENCES

1. Patwardhan, A., Cheng, N., and Trejo, J. (2021) Post-Translational Modifications of G Protein-Coupled Receptors Control Cellular Signaling Dynamics in Space and Time. *Pharmacol Rev* **73**, 120-151

2. Soh, U. J., Dores, M. R., Chen, B., and Trejo, J. (2010) Signal transduction by protease-activated receptors. *Br J Pharmacol* **160**, 191-203

3. Hauser, A. S., Attwood, M. M., Rask-Andersen, M., Schiöth, H. B., and Gloriam, D. E. (2017) Trends in GPCR drug discovery: new agents, targets and indications. *Nature Reviews Drug Discovery* **16**, 829-842

4. Sriram, K., and Insel, P. A. (2018) G Protein-Coupled Receptors as Targets for Approved Drugs: How Many Targets and How Many Drugs? *Molecular Pharmacology* **93**, 251-258

5. Patwardhan, A., Cheng, N., and Trejo, J. (2021) Post-Translational Modifications of G Protein–Coupled Receptors Control Cellular Signaling Dynamics in Space and Time. *Pharmacological Reviews* **73**, 120-151

6. Hislop, J. N., and von Zastrow, M. (2011) Role of Ubiquitination in Endocytic Trafficking of G-Protein-Coupled Receptors. *Traffic* **12**, 137-148

7. Terrell, J., Shih, S., Dunn, R., and Hicke, L. (1998) A Function for Monoubiquitination in the Internalization of a G Protein–Coupled Receptor. *Molecular cell* **1**, 193-202

8. Shenoy, S. K., McDonald, P. H., Kohout, T. A., and Lefkowitz, R. J. (2001) Regulation of receptor fate by ubiquitination of activated beta 2-adrenergic receptor and beta-arrestin. *Science* **294**, 1307-1313

9. Marchese, A., Raiborg, C., Santini, F., Keen, J. H., Stenmark, H., and Benovic, J. L. (2003) The E3 Ubiquitin Ligase AIP4 Mediates Ubiquitination and Sorting of the G Protein-Coupled Receptor CXCR4. *Dev. Cell* **5**, 709-722

10. Jacob, C., Cottrell, G. S., Gehringer, D., Schmidlin, F., Grady, E. F., and Bunnett, N. W. (2005) c-Cbl mediates ubiquitination, degradation, and down-regulation of human protease-activated receptor 2. *J Biol Chem* **280**, 16076-16087

11. Grimsey, N. J., Aguilar, B., Smith, T. H., Le, P., Soohoo, A. L., Puthenveedu, M. A., Nizet, V., and Trejo, J. (2015) Ubiquitin plays an atypical role in GPCR-induced p38 MAP kinase activation on endosomes. *The Journal of Cell Biology* **210**, 1117-1131

12. Grimsey, N. J., Narala, R., Rada, C. C., Mehta, S., Stephens, B. S., Kufareva, I., Lapek, J., Gonzalez, D. J., Handel, T. M., Zhang, J., and Trejo, J. (2018) A Tyrosine Switch on NEDD4-2 E3 Ligase Transmits GPCR Inflammatory Signaling. *Cell Reports* **24**, 3312-3323.e3315

13. Grimsey, N. J., Lin, Y., Narala, R., Rada, C. C., Mejia-Pena, H., and Trejo, J. (2019) G protein–coupled receptors activate p38 MAPK via a non-canonical TAB1–TAB2– and TAB1–TAB3–dependent pathway in endothelial cells. *Journal of Biological Chemistry* **294**, 5867-5878

14. Kaur, S., Chen, Y., and Shenoy, S. K. (2020) Agonist-activated glucagon receptors are deubiquitinated at early endosomes by two distinct deubiquitinases to facilitate Rab4a-dependent recycling. *J Biol Chem* **295**, 16630-16642

15. Kaur, S., Sokrat, B., Capozzi, M. E., El, K., Bai, Y., Jazic, A., Han, B., Krishna Kumar, K., D'Alessio, D. A., Campbell, J. E., Bouvier, M., and Shenoy, S. K. (2023) The ubiquitination status of the glucagon receptor determines signal bias. *J Biol Chem* **299**, 104690

16. Snyder, N. A., and Silva, G. M. (2021) Deubiquitinating enzymes (DUBs): Regulation, homeostasis, and oxidative stress response. *Journal of Biological Chemistry* **297**

17. Love, K. R., Catic, A., Schlieker, C., and Ploegh, H. L. (2007) Mechanisms, biology and inhibitors of deubiquitinating enzymes. *Nature Chemical Biology* **3**, 697-705

18. Leznicki, P., and Kulathu, Y. (2017) Mechanisms of regulation and diversification of deubiquitylating enzyme function. *Journal of Cell Science* **130**, 1997-2006

19. Mevissen, T. E. T., and Komander, D. (2017) Mechanisms of Deubiquitinase Specificity and Regulation. *Annual review of biochemistry* **86**, 159-192

20. Clague, M. J., Urbé, S., and Komander, D. (2019) Breaking the chains: deubiquitylating enzyme specificity begets function. *Nat. Rev. Mol. Cell Biol.* **20**, 338-352

21. Komander, D., and Rape, M. (2012) The Ubiquitin Code. *Annual Review of Biochemistry* **81**, 203-229

22. Oh, E., Akopian, D., and Rape, M. (2018) Principles of Ubiquitin-Dependent Signaling. *Annu Rev Cell Dev Biol* **34**, 137-162

23. Chen, Y., Zhou, D., Yao, Y., Sun, Y., Yao, F., and Ma, L. (2022) Monoubiquitination in Homeostasis and Cancer. *Int J Mol Sci* **23**

24. Passmore, L. A., and Barford, D. (2004) Getting into position: the catalytic mechanisms of protein ubiquitylation. *Biochem J* **379**, 513-525

25. Kelsall, I. R. (2022) Non-lysine ubiquitylation: Doing things differently. *Frontiers in Molecular Biosciences* **9**

26. Mallette, F. A., and Richard, S. (2012) K48-linked ubiquitination and protein degradation regulate 53BP1 recruitment at DNA damage sites. *Cell Research* **22**, 1221-1223

27. Jacobson, A. D., Zhang, N. Y., Xu, P., Han, K. J., Noone, S., Peng, J., and Liu, C. W. (2009) The lysine 48 and lysine 63 ubiquitin conjugates are processed differently by the 26 s proteasome. *J Biol Chem* **284**, 35485-35494

28. Xu, P., Duong, D. M., Seyfried, N. T., Cheng, D., Xie, Y., Robert, J., Rush, J., Hochstrasser, M., Finley, D., and Peng, J. (2009) Quantitative Proteomics Reveals the Function of Unconventional Ubiquitin Chains in Proteasomal Degradation. *Cell* **137**, 133-145

29. Cao, L., Liu, X., Zheng, B., Xing, C., and Liu, J. (2022) Role of K63-linked ubiquitination in cancer. *Cell Death Discovery* **8**, 410

30. Puangmalai, N., Sengupta, U., Bhatt, N., Gaikwad, S., Montalbano, M., Bhuyan, A., Garcia, S., McAllen, S., Sonawane, M., Jerez, C., Zhao, Y., and Kayed, R. (2022) Lysine 63-linked ubiquitination of tau oligomers contributes to the pathogenesis of Alzheimer's disease. *J Biol Chem* **298**, 101766

31. Yin, X., Liu, Q., Liu, F., Tian, X., Yan, T., Han, J., and Jiang, S. (2022) Emerging Roles of Non-proteolytic Ubiquitination in Tumorigenesis. *Frontiers in Cell and Developmental Biology* **10**

32. Deng, L., Meng, T., Chen, L., Wei, W., and Wang, P. (2020) The role of ubiquitination in tumorigenesis and targeted drug discovery. *Signal Transduction and Targeted Therapy* **5**, 11

33. Elu, N., Osinalde, N., Ramirez, J., Presa, N., Rodriguez, J. A., Prieto, G., and Mayor, U. (2022) Identification of substrates for human deubiquitinating enzymes (DUBs): An up-to-date review and a case study for neurodevelopmental disorders. *Seminars in Cell & Developmental Biology*

34. Newton, K., and Gitlin, A. D. (2022) Deubiquitinases in cell death and inflammation. *Biochemical Journal* **479**, 1103-1119

35. Park, C. W., and Ryu, K. Y. (2014) Cellular ubiquitin pool dynamics and homeostasis. *BMB Rep* **47**, 475-482

36. Suresh, H. G., Pascoe, N., and Andrews, B. (2020) The structure and function of deubiquitinases: lessons from budding yeast. *Open Biol* **10**, 200279

37. Zeng, C., Zhao, C., Ge, F., Li, Y., Cao, J., Ying, M., Lu, J., He, Q., Yang, B., Dai, X., and Zhu, H. (2020) Machado-Joseph Deubiquitinases: From Cellular Functions to Potential Therapy Targets. *Front Pharmacol* **11**, 1311

38. Caba, C., Mohammadzadeh, A., and Tong, Y. (2022) On the Study of Deubiquitinases: Using the Right Tools for the Job. *Biomolecules*. 10.3390/biom12050703

39. Sowa, M. E., Bennett, E. J., Gygi, S. P., and Harper, J. W. (2009) Defining the Human Deubiquitinating Enzyme Interaction Landscape. *Cell* **138**, 389-403

40. Millard, S. M., and Wood, S. A. (2006) Riding the DUBway: regulation of protein trafficking by deubiquitylating enzymes. *J Cell Biol* **173**, 463-468

41. Clague, M. J., and Urbé, S. (2006) Endocytosis: the DUB version. *Trends Cell Biol* **16**, 551-559

42. Berlin, I., Schwartz, H., and Nash, P. D. (2010) Regulation of epidermal growth factor receptor ubiquitination and trafficking by the USP8·STAM complex. *J Biol Chem* **285**, 34909-34921

43. Hurley, J. H., and Stenmark, H. (2011) Molecular mechanisms of ubiquitin-dependent membrane traffic. *Annu Rev Biophys* **40**, 119-142

44. Grou, C. P., Pinto, M. P., Mendes, A. V., Domingues, P., and Azevedo, J. E. (2015) The de novo synthesis of ubiquitin: identification of deubiquitinases acting on ubiquitin precursors. *Scientific Reports* **5**, 12836

45. Piper, R. C., Dikic, I., and Lukacs, G. L. (2014) Ubiquitin-dependent sorting in endocytosis. *Cold Spring Harb Perspect Biol* **6**

46. Fujita, H., Iwabu, Y., Tokunaga, K., and Tanaka, Y. (2013) Membrane-associated RING-CH (MARCH) 8 mediates the ubiquitination and lysosomal degradation of the transferrin receptor. *J Cell Sci* **126**, 2798-2809

47. Haglund, K., Sigismund, S., Polo, S., Szymkiewicz, I., Di Fiore, P. P., and Dikic, I. (2003) Multiple monoubiquitination of RTKs is sufficient for their endocytosis and degradation. *Nat Cell Biol* **5**, 461-466

48. de Poot, S. A. H., Tian, G., and Finley, D. (2017) Meddling with Fate: The Proteasomal Deubiquitinating Enzymes. *J Mol Biol* **429**, 3525-3545

49. Verma, R., Aravind, L., Oania, R., McDonald, W. H., Yates, J. R., 3rd, Koonin, E. V., and Deshaies, R. J. (2002) Role of Rpn11 metalloprotease in deubiquitination and degradation by the 26S proteasome. *Science* **298**, 611-615

50. Balut, C. M., Loch, C. M., and Devor, D. C. (2011) Role of ubiquitylation and USP8-dependent deubiquitylation in the endocytosis and lysosomal targeting of plasma membrane KCa3.1. *FASEB J* **25**, 3938-3948

51. Sapmaz, A., Berlin, I., Bos, E., Wijdeven, R. H., Janssen, H., Konietzny, R., Akkermans, J. J., Erson-Bensan, A. E., Koning, R. I., Kessler, B. M., Neefjes, J., and Ovaa, H. (2019) USP32 regulates late endosomal transport and recycling through deubiquitylation of Rab7. *Nat Commun* **10**, 1454

52. Wright, M. H., Berlin, I., and Nash, P. D. (2011) Regulation of endocytic sorting by ESCRT-DUB-mediated deubiquitination. *Cell Biochem Biophys* **60**, 39-46

53. Kee, Y., and Huang, T. T. (2016) Role of Deubiquitinating Enzymes in DNA Repair. *Mol Cell Biol* **36**, 524-544

54. He, M., Zhou, Z., Shah, A. A., Zou, H., Tao, J., Chen, Q., and Wan, Y. (2016) The emerging role of deubiquitinating enzymes in genomic integrity, diseases, and therapeutics. *Cell Biosci* **6**, 62

55. Sarkari, F., La Delfa, A., Arrowsmith, C. H., Frappier, L., Sheng, Y., and Saridakis, V. (2010) Further insight into substrate recognition by USP7: structural and biochemical analysis of the HdmX and Hdm2 interactions with USP7. *J Mol Biol* **402**, 825-837

56. Lee, K. K., Florens, L., Swanson, S. K., Washburn, M. P., and Workman, J. L. (2005) The deubiquitylation activity of Ubp8 is dependent upon Sgf11 and its association with the SAGA complex. *Mol Cell Biol* **25**, 1173-1182

57. Parsons, J. L., Dianova, II, Khoronenkova, S. V., Edelmann, M. J., Kessler, B. M., and Dianov, G. L. (2011) USP47 is a deubiquitylating enzyme that regulates base excision repair by controlling steady-state levels of DNA polymerase β. *Molecular cell* **41**, 609-615

58. Kapadia, B. B., and Gartenhaus, R. B. (2019) DUBbing Down Translation: The Functional Interaction of Deubiquitinases with the Translational Machinery. *Mol Cancer Ther* **18**, 1475-1483

59. Garshott, D. M., Sundaramoorthy, E., Leonard, M., and Bennett, E. J. (2020) Distinct regulatory ribosomal ubiquitylation events are reversible and hierarchically organized. *Elife* **9**

60. Courtois, G. (2008) Tumor suppressor CYLD: negative regulation of NF-kappaB signaling and more. *Cell Mol Life Sci* **65**, 1123-1132

61. Sun, S. C. (2008) Deubiquitylation and regulation of the immune response. *Nat Rev Immunol* **8**, 501-511

62. Sun, Q., Zhang, J., Li, X., Yang, G., Cheng, S., Guo, D., Zhang, Q., Sun, F., Zhao, F., Yang, D., Wang, S., Wang, T., Liu, S., Zou, L., Zhang, Y., and Liu, H. (2022) The ubiquitin-specific protease 8 antagonizes melatonin-induced endocytic degradation of MT(1) receptor to promote lung adenocarcinoma growth. *J Adv Res* **41**, 1-12

63. Boone, D. L., Turer, E. E., Lee, E. G., Ahmad, R. C., Wheeler, M. T., Tsui, C., Hurley, P., Chien, M., Chai, S., Hitotsumatsu, O., McNally, E., Pickart, C., and Ma, A. (2004) The ubiquitin-modifying enzyme A20 is required for termination of Toll-like receptor responses. *Nat Immunol* **5**, 1052-1060

64. Wertz, I. E., O'Rourke, K. M., Zhou, H., Eby, M., Aravind, L., Seshagiri, S., Wu, P., Wiesmann, C., Baker, R., Boone, D. L., Ma, A., Koonin, E. V., and Dixit, V. M. (2004) De-ubiquitination and ubiquitin ligase domains of A20 downregulate NF-kappaB signalling. *Nature* **430**, 694-699

65. Enesa, K., Zakkar, M., Chaudhury, H., Luong le, A., Rawlinson, L., Mason, J. C., Haskard, D. O., Dean, J. L., and Evans, P. C. (2008) NF-kappaB suppression by the deubiquitinating enzyme Cezanne: a novel negative feedback loop in pro-inflammatory signaling. *J Biol Chem* **283**, 7036-7045

66. Sun, W., Tan, X., Shi, Y., Xu, G., Mao, R., Gu, X., Fan, Y., Yu, Y., Burlingame, S., Zhang, H., Rednam, S. P., Lu, X., Zhang, T., Fu, S., Cao, G., Qin, J., and Yang, J. (2010) USP11 negatively regulates TNFalpha-induced NF-kappaB activation by targeting on IkappaBalpha. *Cell Signal* **22**, 386-394

67. Izzi, L., and Attisano, L. (2004) Regulation of the TGFbeta signalling pathway by ubiquitin-mediated degradation. *Oncogene* **23**, 2071-2078

68. Dupont, S., Mamidi, A., Cordenonsi, M., Montagner, M., Zacchigna, L., Adorno, M., Martello, G., Stinchfield, M. J., Soligo, S., Morsut, L., Inui, M., Moro, S., Modena, N., Argenton, F., Newfeld, S. J., and Piccolo, S. (2009) FAM/USP9x, a deubiquitinating enzyme essential for TGFbeta signaling, controls Smad4 monoubiquitination. *Cell* **136**, 123-135

69. Wicks, S. J., Haros, K., Maillard, M., Song, L., Cohen, R. E., Dijke, P. T., and Chantry, A. (2005) The deubiquitinating enzyme UCH37 interacts with Smads and regulates TGF-beta signalling. *Oncogene* **24**, 8080-8084

70. Huang, X., Langelotz, C., Hetfeld-Pechoc, B. K., Schwenk, W., and Dubiel, W. (2009) The COP9 signalosome mediates beta-catenin degradation by deneddylation and blocks adenomatous polyposis coli destruction via USP15. *J Mol Biol* **391**, 691-702

71. Li, M., Chen, D., Shiloh, A., Luo, J., Nikolaev, A. Y., Qin, J., and Gu, W. (2002) Deubiquitination of p53 by HAUSP is an important pathway for p53 stabilization. *Nature* **416**, 648-653

72. Cummins, J. M., and Vogelstein, B. (2004) HAUSP is required for p53 destabilization. *Cell Cycle* **3**, 689-692

73. Murray, R. Z., Jolly, L. A., and Wood, S. A. (2004) The FAM deubiquitylating enzyme localizes to multiple points of protein trafficking in epithelia, where it associates with E-cadherin and beta-catenin. *Mol Biol Cell* **15**, 1591-1599

74. Zhang, Z., Du, J., Wang, S., Shao, L., Jin, K., Li, F., Wei, B., Ding, W., Fu, P., van Dam, H., Wang, A., Jin, J., Ding, C., Yang, B., Zheng, M., Feng, X. H., Guan, K. L., and Zhang, L. (2019) OTUB2 Promotes Cancer Metastasis via Hippo-Independent Activation of YAP and TAZ. *Mol Cell* **73**, 7-21 e27

75. Yao, F., Zhou, Z., Kim, J., Hang, Q., Xiao, Z., Ton, B. N., Chang, L., Liu, N., Zeng, L., Wang, W., Wang, Y., Zhang, P., Hu, X., Su, X., Liang, H., Sun, Y., and Ma, L. (2018) SKP2- and OTUD1-regulated non-proteolytic ubiquitination of YAP promotes YAP nuclear localization and activity. *Nat Commun* **9**, 2269

76. Zhao, B., Li, L., Lu, Q., Wang, L. H., Liu, C. Y., Lei, Q., and Guan, K. L. (2011) Angiomotin is a novel Hippo pathway component that inhibits YAP oncoprotein. *Genes Dev* **25**, 51-63

77. Toloczko, A., Guo, F., Yuen, H. F., Wen, Q., Wood, S. A., Ong, Y. S., Chan, P. Y., Shaik, A. A., Gunaratne, J., Dunne, M. J., Hong, W., and Chan, S. W. (2017) Deubiquitinating Enzyme USP9X Suppresses Tumor Growth via LATS Kinase and Core Components of the Hippo Pathway. *Cancer Res* **77**, 4921-4933

78. Reyes-Turcu, F. E., Ventii, K. H., and Wilkinson, K. D. (2009) Regulation and cellular roles of ubiquitin-specific deubiquitinating enzymes. *Annu Rev Biochem* **78**, 363-397

79. Zhang, E., Shen, B., Mu, X., Qin, Y., Zhang, F., Liu, Y., Xiao, J., Zhang, P., Wang, C., Tan, M., and Fan, Y. (2016) Ubiquitin-specific protease 11 (USP11) functions as a tumor suppressor through deubiquitinating and stabilizing VGLL4 protein. *Am J Cancer Res* **6**, 2901-2909

80. Mohseni, M., Sun, J., Lau, A., Curtis, S., Goldsmith, J., Fox, V. L., Wei, C., Frazier, M., Samson, O., Wong, K. K., Kim, C., and Camargo, F. D. (2014) A genetic screen identifies an LKB1-MARK signalling axis controlling the Hippo-YAP pathway. *Nat Cell Biol* **16**, 108-117

81. Durcan, T. M., and Fon, E. A. (2015) The three 'P's of mitophagy: PARKIN, PINK1, and post-translational modifications. *Genes Dev* **29**, 989-999

82. Bingol, B., Tea, J. S., Phu, L., Reichelt, M., Bakalarski, C. E., Song, Q., Foreman, O., Kirkpatrick, D. S., and Sheng, M. (2014) The mitochondrial deubiquitinase USP30 opposes parkin-mediated mitophagy. *Nature* **510**, 370-375

83. Combaret, L., Adegoke, O. A., Bedard, N., Baracos, V., Attaix, D., and Wing, S. S. (2005) USP19 is a ubiquitin-specific protease regulated in rat skeletal muscle during catabolic states. *Am J Physiol Endocrinol Metab* **288**, E693-700

84. Hassink, G. C., Zhao, B., Sompallae, R., Altun, M., Gastaldello, S., Zinin, N. V., Masucci, M. G., and Lindsten, K. (2009) The ER-resident ubiquitin-specific protease 19 participates in the UPR and rescues ERAD substrates. *EMBO Rep* **10**, 755-761

85. Denuc, A., Bosch-Comas, A., Gonzàlez-Duarte, R., and Marfany, G. (2009) The UBA-UIM domains of the USP25 regulate the enzyme ubiquitination state and modulate substrate recognition. *PLoS One* **4**, e5571

86. Meray, R. K., and Lansbury, P. T., Jr. (2007) Reversible monoubiquitination regulates the Parkinson disease-associated ubiquitin hydrolase UCH-L1. *J Biol Chem* **282**, 10567-10575

87. Huang, X., Summers, M. K., Pham, V., Lill, J. R., Liu, J., Lee, G., Kirkpatrick, D. S., Jackson, P. K., Fang, G., and Dixit, V. M. (2011) Deubiquitinase USP37 is activated by CDK2 to antagonize APC(CDH1) and promote S phase entry. *Mol Cell* **42**, 511-523

88. Huang, T. T., Nijman, S. M., Mirchandani, K. D., Galardy, P. J., Cohn, M. A., Haas, W., Gygi, S. P., Ploegh, H. L., Bernards, R., and D'Andrea, A. D. (2006) Regulation of monoubiquitinated PCNA by DUB autocleavage. *Nat Cell Biol* **8**, 339-347

89. Hutti, J. E., Shen, R. R., Abbott, D. W., Zhou, A. Y., Sprott, K. M., Asara, J. M., Hahn, W. C., and Cantley, L. C. (2009) Phosphorylation of the tumor suppressor CYLD by the breast cancer oncogene IKKepsilon promotes cell transformation. *Mol Cell* **34**, 461-472

90. Fotedar, A., Cannella, D., Fitzgerald, P., Rousselle, T., Gupta, S., Dorée, M., and Fotedar, R. (1996) Role for cyclin A-dependent kinase in DNA replication in human S phase cell extracts. *J Biol Chem* **271**, 31627-31637

91. Koulich, E., Li, X., and DeMartino, G. N. (2008) Relative structural and functional roles of multiple deubiquitylating proteins associated with mammalian 26S proteasome. *Mol Biol Cell* **19**, 1072-1082

92. Cotto-Rios, X. M., Jones, M. J., and Huang, T. T. (2011) Insights into phosphorylation-dependent mechanisms regulating USP1 protein stability during the cell cycle. *Cell Cycle* **10**, 4009-4016

93. Shembade, N., and Harhaj, E. W. (2012) Regulation of NF-κB signaling by the A20 deubiquitinase. *Cell Mol Immunol* **9**, 123-130

94. Huang, O. W., Ma, X., Yin, J., Flinders, J., Maurer, T., Kayagaki, N., Phung, Q., Bosanac, I., Arnott, D., Dixit, V. M., Hymowitz, S. G., Starovasnik, M. A., and Cochran, A. G. (2012) Phosphorylation-dependent activity of the deubiquitinase DUBA. *Nat Struct Mol Biol* **19**, 171-175

95. Xu, D., Shan, B., Lee, B. H., Zhu, K., Zhang, T., Sun, H., Liu, M., Shi, L., Liang, W., Qian, L., Xiao, J., Wang, L., Pan, L., Finley, D., and Yuan, J. (2015) Phosphorylation and activation of ubiquitin-specific protease-14 by Akt regulates the ubiquitin-proteasome system. *Elife* **4**, e10510

96. Cai, S. Y., Babbitt, R. W., and Marchesi, V. T. (1999) A mutant deubiquitinating enzyme (Ubp-M) associates with mitotic chromosomes and blocks cell division. *Proc Natl Acad Sci U S A* **96**, 2828-2833

97. Joo, H. Y., Zhai, L., Yang, C., Nie, S., Erdjument-Bromage, H., Tempst, P., Chang, C., and Wang, H. (2007) Regulation of cell cycle progression and gene expression by H2A deubiquitination. *Nature* **449**, 1068-1072

98. Meijer, I. M., Kerperien, J., Sotoca, A. M., van Zoelen, E. J., and van Leeuwen, J. E. (2013) The Usp8 deubiquitination enzyme is post-translationally modified by tyrosine and serine phosphorylation. *Cell Signal* **25**, 919-930

99. Herhaus, L., Perez-Oliva, A. B., Cozza, G., Gourlay, R., Weidlich, S., Campbell, D. G., Pinna, L. A., and Sapkota, G. P. (2015) Casein kinase 2 (CK2) phosphorylates the deubiquitylase OTUB1 at Ser16 to trigger its nuclear localization. *Sci Signal* **8**, ra35

100. Zhang, L., Zhou, F., Drabsch, Y., Gao, R., Snaar-Jagalska, B. E., Mickanin, C., Huang, H., Sheppard, K. A., Porter, J. A., Lu, C. X., and ten Dijke, P. (2012) USP4 is regulated by AKT phosphorylation and directly deubiquitylates TGF-β type I receptor. *Nat Cell Biol* **14**, 717-726

101. Yuan, J., Luo, K., Zhang, L., Cheville, J. C., and Lou, Z. (2010) USP10 regulates p53 localization and stability by deubiquitinating p53. *Cell* **140**, 384-396

102. Mueller, T., Breuer, P., Schmitt, I., Walter, J., Evert, B. O., and Wüllner, U. (2009) CK2-dependent phosphorylation determines cellular localization and stability of ataxin-3. *Hum Mol Genet* **18**, 3334-3343

103. Shen, C., Ye, Y., Robertson, S. E., Lau, A. W., Mak, D. O., and Chou, M. M. (2005) Calcium/calmodulin regulates ubiquitination of the ubiquitin-specific protease TRE17/USP6. *J Biol Chem* **280**, 35967-35973

104. Gersch, M., Gladkova, C., Schubert, A. F., Michel, M. A., Maslen, S., and Komander, D. (2017) Mechanism and regulation of the Lys6-selective deubiquitinase USP30. *Nat Struct Mol Biol* **24**, 920-930

105. Mashtalir, N., Daou, S., Barbour, H., Sen, N. N., Gagnon, J., Hammond-Martel, I., Dar, H. H., Therrien, M., and Affar el, B. (2014) Autodeubiquitination protects the tumor suppressor BAP1 from cytoplasmic sequestration mediated by the atypical ubiquitin ligase UBE2O. *Mol Cell* **54**, 392-406

106. Meulmeester, E., Kunze, M., Hsiao, H. H., Urlaub, H., and Melchior, F. (2008) Mechanism and consequences for paralog-specific sumoylation of ubiquitin-specific protease 25. *Mol Cell* **30**, 610-619

107. Kobayashi, T., Masoumi, K. C., and Massoumi, R. (2015) Deubiquitinating activity of CYLD is impaired by SUMOylation in neuroblastoma cells. *Oncogene* **34**, 2251-2260

108. Cohn, M. A., Kowal, P., Yang, K., Haas, W., Huang, T. T., Gygi, S. P., and D'Andrea, A. D. (2007) A UAF1-containing multisubunit protein complex regulates the Fanconi anemia pathway. *Mol Cell* **28**, 786-797

109. Cohn, M. A., Kee, Y., Haas, W., Gygi, S. P., and D'Andrea, A. D. (2009) UAF1 is a subunit of multiple deubiquitinating enzyme complexes. *J Biol Chem* **284**, 5343-5351

110. Velasco, K., Zhao, B., Callegari, S., Altun, M., Liu, H., Hassink, G., Masucci, M. G., and Lindsten, K. (2013) An N-terminal SIAH-interacting motif regulates the stability of the ubiquitin specific protease (USP)-19. *Biochemical and Biophysical Research Communications* **433**, 390-395

111. Milojevic, T., Reiterer, V., Stefan, E., Korkhov, V. M., Dorostkar, M. M., Ducza, E., Ogris, E., Boehm, S., Freissmuth, M., and Nanoff, C. (2006) The ubiquitin-specific protease Usp4 regulates the cell surface level of the A2A receptor. *Mol Pharmacol* **69**, 1083-1094

112. Mukai, A., Yamamoto-Hino, M., Awano, W., Watanabe, W., Komada, M., and Goto, S. (2010) Balanced ubiquitylation and deubiquitylation of Frizzled regulate cellular responsiveness to Wg/Wnt. *EMBO J.* **29**, 2114-2125

113. Shenoy, S. K., Modi, A. S., Shukla, A. K., Xiao, K., Berthouze, M., Ahn, S., Wilkinson, K. D., Miller, W. E., and Lefkowitz, R. J. (2009) Beta-arrestin-dependent signaling and trafficking of 7-transmembrane receptors is reciprocally regulated by the deubiquitinase USP33 and the E3 ligase Mdm2. *Proceedings of the National Academy of Sciences of the United States of America* **106**, 6650-6655

114. Berthouze, M., Venkataramanan, V., Li, Y., and Shenoy, S. K. (2009) The deubiquitinases USP33 and USP20 coordinate beta2 adrenergic receptor recycling and resensitization. *EMBO J* **28**, 1684-1696

115. Kommaddi, R. P., Jean-Charles, P. Y., and Shenoy, S. K. (2015) Phosphorylation of the deubiquitinase USP20 by protein kinase A regulates post-endocytic trafficking of β2 adrenergic receptors to autophagosomes during physiological stress. *J Biol Chem* **290**, 8888-8903

116. Yu, S. M., Jean-Charles, P. Y., Abraham, D. M., Kaur, S., Gareri, C., Mao, L., Rockman, H. A., and Shenoy, S. K. (2019) The deubiquitinase ubiquitin-specific protease 20 is a positive modulator of myocardial beta(1)-adrenergic receptor expression and signaling. *J Biol Chem* **294**, 2500-2518

117. Hasdemir, B., Murphy, J. E., Cottrell, G. S., and Bunnett, N. W. (2009) Endosomal deubiquitinating enzymes control ubiquitination and down-regulation of protease-activated receptor 2. *J. Biol. Chem.* **284**, 28453-28466

118. Lahaie, N., Kralikova, M., Prezeau, L., Blahos, J., and Bouvier, M. (2016) Post-endocytotic Deubiquitination and Degradation of the Metabotropic gamma-Aminobutyric Acid Receptor by the Ubiquitin-specific Protease 14. *J Biol Chem* **291**, 7156-7170

119. Mines, M. A., Goodwin, J. S., Limbird, L. E., Cui, F. F., and Fan, G. H. (2009) Deubiquitination of CXCR4 by USP14 is critical for both CXCL12-induced CXCR4 degradation and chemotaxis but not ERK ativation. *J Biol Chem* **284**, 5742-5752

120. Berlin, I., Higginbotham, K. M., Dise, R. S., Sierra, M. I., and Nash, P. D. (2010) The deubiquitinating enzyme USP8 promotes trafficking and degradation of the chemokine receptor 4 at the sorting endosome. *J Biol Chem* **285**, 37895-37908

121. Burton, J. C., and Grimsey, N. J. (2019) Ubiquitination as a Key Regulator of Endosomal Signaling by GPCRs. *Frontiers in Cell and Developmental Biology* **7**

122. Tsvetanova, N. G., Irannejad, R., and von Zastrow, M. (2015) G protein-coupled receptor (GPCR) signaling via heterotrimeric G proteins from endosomes. *J Biol Chem* **290**, 6689-6696

123. Mizuno, E., Iura, T., Mukai, A., Yoshimori, T., Kitamura, N., and Komada, M. (2005) Regulation of Epidermal Growth Factor Receptor Down-Regulation by UBPY-mediated Deubiquitination at Endosomes. *Molecular Biology of the Cell* **16**, 5163-5174

124. Row, P. E., Prior, I. A., McCullough, J., Clague, M. J., and Urbe, S. (2006) The ubiquitin isopeptidase UBPY regulates endosomal ubiquitin dynamics and is essential for receptor down-regulation. *J Biol Chem* **281**, 12618-12624

125. Endo, A., Fukushima, T., Takahashi, C., Tsuchiya, H., Ohtake, F., Ono, S., Ly, T., Yoshida, Y., Tanaka, K., Saeki, Y., and Komada, M. (2024) USP8 prevents aberrant NF-κB and Nrf2 activation by counteracting ubiquitin signals from endosomes. *Journal of Cell Biology* **223**

126. Wess, J., Oteng, A. B., Rivera-Gonzalez, O., Gurevich, E. V., and Gurevich, V. V. (2023) beta-Arrestins: Structure, Function, Physiology, and Pharmacological Perspectives. *Pharmacol Rev* **75**, 854-884

127. Dores, M. R., Grimsey, N. J., Mendez, F., and Trejo, J. (2016) ALIX Regulates the Ubiquitin-Independent Lysosomal Sorting of the P2Y1 Purinergic Receptor via a YPX3L Motif. *PLOS ONE* **11**, e0157587

128. Bouwmeester, T., Bauch, A., Ruffner, H., Angrand, P.-O., Bergamini, G., Croughton, K., Cruciat, C., Eberhard, D., Gagneur, J., Ghidelli, S., Hopf, C., Huhse, B., Mangano, R., Michon, A.-M., Schirle, M., Schlegl, J., Schwab, M., Stein, M. A., Bauer, A., Casari, G., Drewes, G., Gavin, A.-C., Jackson, D. B., Joberty, G., Neubauer, G., Rick, J., Kuster, B., and Superti-Furga, G. (2004) A physical and functional map of the human TNF-α/NF-κB signal transduction pathway. *Nature Cell Biology* **6**, 97-105

129. Ge, B., Gram, H., Di Padova, F., Huang, B., New, L., Ulevitch, R. J., Luo, Y., and Han, J. (2002) MAPKK-Independent Activation of p38α Mediated by TAB1-Dependent Autophosphorylation of p38α. *Science* **295**, 1291-1294

130. De Nicola, G. F., Martin, E. D., Chaikuad, A., Bassi, R., Clark, J., Martino, L., Verma, S., Sicard, P., Tata, R., Atkinson, R. A., Knapp, S., Conte, M. R., and Marber, M. S. (2013) Mechanism and consequence of the autoactivation of p38α mitogen-activated protein kinase promoted by TAB1. *Nature Structural & Molecular Biology* **20**, 1182-1190

131. Rada, C. C., Mejia-Pena, H., Grimsey, N. J., Canto Cordova, I., Olson, J., Wozniak, J. M., Gonzalez, D. J., Nizet, V., and Trejo, J. (2021) Heat shock protein 27 activity is linked to endothelial barrier recovery after proinflammatory GPCR-induced disruption. *Sci Signal* **14**, eabc1044

132. Cheng, N., and Trejo, J. (2023) An siRNA library screen identifies CYLD and USP34 as deubiquitinases that regulate GPCR-p38 MAPK signaling and distinct inflammatory responses. *Journal of Biological Chemistry* **299**

133. Shao, S., Sun, Y., Zhang, Y., Tian, X., Li, Y., Tan, B., and Su, R. (2020) A20 enhances mu-opioid receptor function by inhibiting beta-arrestin2 recruitment. *Biochem Biophys Res Commun* **528**, 127-133

134. Shichi, H., Fukuoka, H., Kanzawa, M., Yamamoto, M., Yamamoto, N., Suzuki, M., Urai, S., Matsumoto, R., Kanie, K., Fujita, Y., Bando, H., Iguchi, G., Inoshita, N., Yamada, S., Takahashi, Y., and Ogawa, W. (2022) Responsiveness to DDAVP in Cushing's disease is associated with USP8 mutations through enhancing AVPR1B promoter activity. *Pituitary* **25**, 496-507

135. Yu, J., Hou, B., Huang, Y., Wang, X., Qian, Y., Liang, Y., Gu, X., Ma, Z., and Sun, Y. (2023) USP48 alleviates bone cancer pain and regulates MrgC stabilization in spinal cord neurons of male mice. *Eur J Pain* **27**, 723-734

136. Sriram, K., and Insel, P. A. (2018) G Protein-Coupled Receptors as Targets for Approved Drugs: How Many Targets and How Many Drugs? *Mol Pharmacol* **93**, 251-258

137. Hauser, A. S., Attwood, M. M., Rask-Andersen, M., Schioth, H. B., and Gloriam, D. E. (2017) Trends in GPCR drug discovery: new agents, targets and indications. *Nat Rev Drug Discov* **16**, 829-842

138. Hershko, A., and Ciechanover, A. (1998) The ubiquitin system. *Annu Rev Biochem* **67**, 425-479

139. Jean-Charles, P. Y., Snyder, J. C., and Shenoy, S. K. (2016) Chapter One - Ubiquitination and Deubiquitination of G Protein-Coupled Receptors *Prog. Mol. Bio. Transl. Sci.* **141**, 1-55

140. Kennedy, J. E., and Marchese, A. (2015) Regulation of GPCR Trafficking by Ubiquitin. *Prog Mol Biol Transl Sci* **132**, 15-38

141. Milojevic, T., Reiterer, V., Stefan, E., Korkhov, V. M., Dorostkar, M. M., Ducza, E., Ogris, E., Boehm, S., Freissmuth, M., and Nanoff, C. (2006) The Ubiquitin-Specific Protease Usp4 Regulates the Cell Surface Level of the A2a Receptor. *Mol Pharm.* **69**, 1083-1094

142. Petaja-Repo, U. E., Hogue, M., Laperriere, A., Bhalla, S., Walker, P., and Bouvier, M. (2001) Newly Synthesized Human Opioid Receptors Retained in the Endoplasmic Reticulum Are Retrotranslocated to the Cytosol, Deglycosylated, Ubiquitinated, and Degraded by the Proteasome. *J. Biol. Chem.* **276**, 4416-4423

143. Katzmann, D. J., Babst, M., and Emr, S. D. (2001) Ubiquitin-dependent sorting into the multivesicular body pathway requires the function of a conserved endosomal protein sorting complex, ESCRT-I. *Cell* **106**, 145-155

144. Grimsey, N. J., Aguilar, B., Smith, T. H., Le, P., Soohoo, A. L., Puthenveedu, M. A., Nizet, V., and Trejo, J. (2015) Ubiquitin plays an atypical role in GPCR-induced p38 MAP kinase activation on endosomes. *J. Cell Biol.* **210**, 1117-1131

145. Malik, R., Soh, U. J., Trejo, J., and Marchese, A. (2012) Novel roles for the E3 ubiquitin ligase atrophin-interacting protein 4 and signal transduction adaptor molecule 1 in G protein-coupled receptor signaling. *J Biol Chem* **287**, 9013-9027

146. Leclair, H. M., Dubois, S. M., Azzi, S., Dwyer, J., Bidere, N., and Gavard, J. (2014) Control of CXCR2 activity through its ubiquitination on K327 residue. *BMC Cell Biol* **15**, 38

147. Grimsey, N. J., Lin, Y., Narala, R., Rada, C. C., Mejia-Pena, H., and Trejo, J. (2019) G protein-coupled receptors activate p38 MAPK via a non-canonical TAB1-TAB2 and TAB1-TAB3 dependent pathway in endothelial cells. *J Biol Chem* **294**, 5867-5878

148. Grimsey, N. J., Narala, R., Rada, C. C., Mehta, S., Stephens, B. S., Kufareva, I., Lapek, J., Gonzalez, D. J., Handel, T. M., Zhang, J., and Trejo, J. (2018) A Tyrosine Switch on NEDD4-2 E3 Ligase Transmits GPCR Inflammatory Signaling. *Cell Rep* **24**, 3312-3323

149. Bouwmeester, T., Bauch, A., Ruffner, H., Angrand, P. O., Bergamini, G., Croughton, K., Cruciat, C., Eberhard, D., Gagneur, J., Ghidelli, S., Hopf, C., Huhse, B., Mangano, R., Michon, A. M., Schirle, M., Schlegl, J., Schwab, M., Stein, M. A., Bauer, A., Casari, G., Drewes, G., Gavin, A. C., Jackson, D. B., Joberty, G., Neubauer, G., Rick, J., Kuster, B., and Superti-Furga, G. (2004) A physical and functional map of the human TNF-alpha/NF-kappa B signal transduction pathway. *Nature cell biology* **6**, 97-105

150. Ge, B., Gram, H., Di Padova, F., Huang, B., New, L., Ulevitch, R. J., Luo, Y., and Han, J. (2002) MAPKK-independent activation of p38alpha mediated by TAB1-dependent autophosphorylation of p38alpha. *Science* **295**, 1291-1294

151. De Nicola, G. F., Martin, E. D., Chaikuad, A., Bassi, R., Clark, J., Martino, L., Verma, S., Sicard, P., Tata, R., Atkinson, R. A., Knapp, S., Conte, M. R., and Marber, M. S. (2013) Mechanism and consequence of the autoactivation of p38alpha mitogen-activated protein kinase promoted by TAB1. *Nat Struct Mol Biol* **20**, 1182-1190

152. Komander, D., Clague, M. J., and Urbe, S. (2009) Breaking the chains: structure and function of the deubiquitinases. *Nat Rev Mol Cell Biol* **10**, 550-563

153. Mevissen, T. E. T., and Komander, D. (2017) Mechanisms of Deubiquitinase Specificity and Regulation. *Annu Rev Biochem* **86**, 159-192

154. Lin, Y., Wozniak, J. M., Grimsey, N. J., Girada, S., Patwardhan, A., Molinar-Inglis, O., Smith, T. H., Lapek, J. D., Gonzalez, D. J., and Trejo, J. (2020) Phosphoproteomic analysis of protease-activated receptor-1 biased signaling reveals unique modulators of endothelial barrier function. *Proceedings of the National Academy of Sciences of the United States of America* **117**, 5039-5048

155. Molinar-Inglis, O., Birch, C. A., Nicholas, D., Orduna-Castillo, L., Cisneros-Aguirre, M., Patwardhan, A., Chen, B., Grimsey, N. J., Coronel, L. J., Lin, H., Gomez Menzies, P. K., Lawson, M. A., Patel, H. H., and Trejo, J. (2021) aPC/PAR1 confers endothelial anti-apoptotic activity via a discrete, beta-arrestin-2-mediated SphK1-S1PR1-Akt signaling axis. *Proc Natl Acad Sci U S A* **118**

156. Paing, M. M., Temple, B. R. S., and Trejo, J. (2004) A tyrosine-based sorting signal regulates intracellular trafficking of protease-activated receptor-1: multiple regulatory mechanisms for agonist-induced G protein-coupled receptor internalization. *J. Biol. Chem.* **279**, 21938-21947

157. Molinar-Inglis, O., Wozniak, J. M., Grimsey, N. J., Orduna-Castillo, L. B., Cheng, N., Lin, Y., Gonzalez Ramirez, M. L., Birch, C. A., Lapek, J. D., Gonzalez, D. J., and Trejo, J. (2022) Phosphoproteomic analysis of thrombin- and p38 MAPK-regulated signaling networks in endothelial cells. *J Biol Chem* **298**, 101801

158. Xu, G., Su, H., Lu, L., Liu, X., Zhao, L., Tang, B., and Ming, Z. (2022) Structural Insights into the Catalytic Mechanism and Ubiquitin Recognition of USP34. *J Mol Biol* **434**, 167634

159. Snyder, N. A., and Silva, G. M. (2021) Deubiquitinating enzymes (DUBs): Regulation, homeostasis, and oxidative stress response. *J Biol Chem* **297**, 101077

160. Lange, S. M., Armstrong, L. A., and Kulathu, Y. (2022) Deubiquitinases: From mechanisms to their inhibition by small molecules. *Mol Cell* **82**, 15-29

161. Hornbeck, P. V., Zhang, B., Murray, B., Kornhauser, J. M., Latham, V., and Skrzypek, E. (2015) PhosphoSitePlus, 2014: mutations, PTMs and recalibrations. *Nucleic Acids Res* **43**, D512-520

162. Reiley, W., Zhang, M., Wu, X., Granger, E., and Sun, S. C. (2005) Regulation of the deubiquitinating enzyme CYLD by IkappaB kinase gamma-dependent phosphorylation. *Mol Cell Biol* **25**, 3886-3895

163. Mu, J. J., Wang, Y., Luo, H., Leng, M., Zhang, J., Yang, T., Besusso, D., Jung, S. Y., and Qin, J. (2007) A proteomic analysis of ataxia telangiectasia-mutated (ATM)/ATM-Rad3-related (ATR) substrates identifies the ubiquitin-proteasome system as a regulator for DNA damage checkpoints. *J Biol Chem* **282**, 17330-17334

164. UniProt, C. (2023) UniProt: the Universal Protein Knowledgebase in 2023. *Nucleic Acids Res* **51**, D523-D531

165. Komander, D., Lord, C. J., Scheel, H., Swift, S., Hofmann, K., Ashworth, A., and Barford, D. (2008) The structure of the CYLD USP domain explains its specificity for Lys63-linked polyubiquitin and reveals a B box module. *Mol Cell* **29**, 451-464

166. Eguether, T., Ermolaeva, M. A., Zhao, Y., Bonnet, M. C., Jain, A., Pasparakis, M., Courtois, G., and Tassin, A. M. (2014) The deubiquitinating enzyme CYLD controls apical docking of basal bodies in ciliated epithelial cells. *Nat Commun* **5**, 4585

167. Lui, T. T., Lacroix, C., Ahmed, S. M., Goldenberg, S. J., Leach, C. A., Daulat, A. M., and Angers, S. (2011) The ubiquitin-specific protease USP34 regulates axin stability and Wnt/beta-catenin signaling. *Mol Cell Biol* **31**, 2053-2065

168. Sy, S. M., Jiang, J., O, W. S., Deng, Y., and Huen, M. S. (2013) The ubiquitin specific protease USP34 promotes ubiquitin signaling at DNA double-strand breaks. *Nucleic Acids Res* **41**, 8572-8580

169. Parsons, J. L., Dianova, II, Khoronenkova, S. V., Edelmann, M. J., Kessler, B. M., and Dianov, G. L. (2011) USP47 is a deubiquitylating enzyme that regulates base excision repair by controlling steady-state levels of DNA polymerase beta. *Mol Cell* **41**, 609-615

170. Paul, J. J., Weigel, C., Muller, T., Heller, R., Spiegel, S., and Graler, M. H. (2020) Inflammatory Conditions Disrupt Constitutive Endothelial Cell Barrier Stabilization by Alleviating Autonomous Secretion of Sphingosine 1-Phosphate. *MDPI, Cells* **9**, 928

171. Marin, V., Farnarier, C., Gres, S., Kaplanski, S., Su, M. S., Dinarello, C. A., and Kaplanski, G. (2001) The p38 mitogen-activated protein kinase pathway plays a critical role in thrombin-induced endothelial chemokine production and leukocyte recruitment. *Blood* **98**, 667-673

172. Li, Y., Chi, L., Stechschulte, D. J., and Dileepan, K. N. (2001) Histamine-induced production of interleukin-6 and interleukin-8 by human coronary artery endothelial cells is enhanced by endotoxin and tumor necrosis factor-alpha. *Microvasc Res* **61**, 253-262

173. Ding, Y., Zhang, L., Goodwin, J. S., Wang, Z., Liu, B., Zhang, J., and Fan, G. H. (2008) Plectin regulates the signaling and trafficking of the HIV-1 co-receptor CXCR4 and plays a role in HIV-1 infection. *Exp Cell Res* **314**, 590-602

174. Kato, M., Miyazawa, K., and Kitamura, N. (2000) A Deubiquitinating Enzyme UBPY Interacts with the Src Homology 3 Domain of Hrs-binding Protein via a Novel Binding Motif PX(V/I)RXXXKP. *J. Biol. Chem.* **275**, 37481-37487

175. Trompouki, E., Hatzivassiliou, E., Tsichritzis, T., Farmer, H., Ashworth, A., and Mosialos, G. (2003) CYLD is a deubiquitinating enzyme that negatively regulates NF-kappaB activation by TNFR family members. *Nature* **424**, 793-796

176. Kovalenko, A., Chable-Bessia, C., Cantarella, G., Israel, A., Wallach, D., and Courtois, G. (2003) The tumour suppressor CYLD negatively regulates NF-kappaB signalling by deubiquitination. *Nature* **424**, 801-805

177. Harhaj, E. W., and Dixit, V. M. (2012) Regulation of NF-kappaB by deubiquitinases. *Immunol Rev* **246**, 107-124

178. Rahman, A., True, A. L., Anwar, K. N., Ye, R. D., Voyno-Yasenetskaya, T. A., and Malik, A. B. (2002) Galpha(q) and Gbetagamma regulate PAR-1 signaling of thrombin-induced NF-kappaB activation and ICAM-1 transcription in endothelial cells. *Circ Res* **91**, 398-405

179. Minami, T., Abid, M. R., Zhang, J., King, G., Kodama, T., and Aird, W. C. (2003) Thrombin stimulation of vascular adhesion molecule-1 in endothelial cells is mediated by protein kinase C (PKC)-delta-NF-kappa B and PKC-zeta-GATA signaling pathways. *J Biol Chem* **278**, 6976-6984

180. Klei, L. R., Hu, D., Panek, R., Alfano, D. N., Bridwell, R. E., Bailey, K. M., Oravecz-Wilson, K. I., Concel, V. J., Hess, E. M., Van Beek, M., Delekta, P. C., Gu, S., Watkins, S. C., Ting, A. T., Gough, P. J., Foley, K. P., Bertin, J., McAllister-Lucas, L. M., and Lucas, P. C. (2016) MALT1 Protease Activation Triggers Acute Disruption of Endothelial Barrier Integrity via CYLD Cleavage. *Cell Rep* **17**, 221-232

181. Wu, X., Fukushima, H., North, B. J., Nagaoka, Y., Nagashima, K., Deng, F., Okabe, K., Inuzuka, H., and Wei, W. (2014) SCFbeta-TRCP regulates osteoclastogenesis via promoting CYLD ubiquitination. *Oncotarget* **5**, 4211-4221

182. Leggett, D. S., Hanna, J., Borodovsky, A., Crosas, B., Schmidt, M., Baker, R. T., Walz, T., Ploegh, H., and Finley, D. (2002) Multiple associated proteins regulate proteasome structure and function. *Mol Cell* **10**, 495-507

183. Vander Linden, R. T., Hemmis, C. W., Schmitt, B., Ndoja, A., Whitby, F. G., Robinson, H., Cohen, R. E., Yao, T., and Hill, C. P. (2015) Structural basis for the activation and inhibition of the UCH37 deubiquitylase. *Mol Cell* **57**, 901-911

184. Urbe, S., Liu, H., Hayes, S. D., Heride, C., Rigden, D. J., and Clague, M. J. (2012) Systematic survey of deubiquitinase localization identifies USP21 as a regulator of centrosome- and microtubule-associated functions. *Mol Biol Cell* **23**, 1095-1103

185. Stegmeier, F., Sowa, M. E., Nalepa, G., Gygi, S. P., Harper, J. W., and Elledge, S. J. (2007) The tumor suppressor CYLD regulates entry into mitosis. *Proc Natl Acad Sci U S A* **104**, 8869-8874

186. Gao, J., Huo, L., Sun, X., Liu, M., Li, D., Dong, J. T., and Zhou, J. (2008) The tumor suppressor CYLD regulates microtubule dynamics and plays a role in cell migration. *J Biol Chem* **283**, 8802-8809

187. Lee, S., Park, S., Lee, H., Han, S., Song, J. M., Han, D., and Suh, Y. H. (2019) Nedd4 E3 ligase and beta-arrestins regulate ubiquitination, trafficking, and stability of the mGlu7 receptor. *Elife* **8**

188. Zhang, Q., Xiao, K., Liu, H., Song, L., McGarvey, J. C., Sneddon, W. B., Bisello, A., and Friedman, P. A. (2018) Site-specific polyubiquitination differentially regulates parathyroid hormone receptor-initiated MAPK signaling and cell proliferation. *J Biol Chem* **293**, 5556-5571

189. Groer, C. E., Schmid, C. L., Jaeger, A. M., and Bohn, L. M. (2011) Agonist-directed interactions with specific beta-arrestins determine mu-opioid receptor trafficking, ubiquitination, and dephosphorylation. *J Biol Chem* **286**, 31731-31741

190. Shenoy, S. K., and Lefkowitz, R. J. (2005) Receptor-specific ubiquitination of beta-arrestin directs assembly and targeting of seven-transmembrane receptor signalosomes. *The Journal of biological chemistry* **280**, 15315-15324

191. Shenoy, S. K., Xiao, K., Venkataramanan, V., Snyder, P. M., Freedman, N. J., and Weissman, A. M. (2008) Nedd4 mediates agonist-dependent ubiquitination, lysosomal targeting, and degradation of the beta2-adrenergic receptor. *J Biol Chem* **283**, 22166-22176

192. Han, S. O., Xiao, K., Kim, J., Wu, J. H., Wisler, J. W., Nakamura, N., Freedman, N. J., and Shenoy, S. K. (2012) MARCH2 promotes endocytosis and lysosomal sorting of carvedilol-bound beta(2)-adrenergic receptors. *J Cell Biol* **199**, 817-830

193. Zhao, J., Cai, B., Shao, Z., Zhang, L., Zheng, Y., Ma, C., Yi, F., Liu, B., and Gao, C. (2021) TRIM26 positively regulates the inflammatory immune response through K11-linked ubiquitination of TAB1. *Cell Death Differ* **28**, 3077-3091

194. Bruce, M. C., Kanelis, V., Fouladkou, F., Debonneville, A., Staub, O., and Rotin, D. (2008) Regulation of Nedd4-2 self-ubiquitination and stability by a PY motif located within its HECT-domain. *Biochem J* **415**, 155-163

195. Ko, R., Park, H., Lee, N., Seo, J., Jeong, W., and Lee, S. Y. (2019) Glycogen Synthase Kinase 3beta Regulates Antiviral Responses of TLR3 via TRAF2-Src Axis. *J Immunol* **203**, 2990-2999

196. Dores, M. R., Chen, B., Lin, H., Soh, U. J. K., Paing, M. M., Montagne, W. A., Meerloo, T., and Trejo, J. (2012) ALIX binds a YPX3L motif of the GPCR PAR1 and mediates ubiquitin-independent ESCRT-III/MVB sorting *J. Cell Biol.* **197: 407-419**

197. Morris, D. R., Ding, Y., Ricks, T. K., Gullapalli, A., Wolfe, B. L., and Trejo, J. (2006) Protease-activated receptor-2 is essential for factor VIIa and Xa-induced signaling, migration and invasion of breast cancer cells. *Cancer Res.* **66**, 307-314

198. Lagerstrom, M. C., and Schioth, H. B. (2008) Structural diversity of G protein-coupled receptors and significance for drug discovery. *Nat Rev Drug Discov* **7**, 339-357

199. Swatek, K. N., and Komander, D. (2016) Ubiquitin modifications. *Cell Research* **26**, 399-422

200. Cheng, N., and Trejo, J. (2023) An siRNA library screen identifies CYLD and USP34 as deubiquitinases that regulate GPCR-p38 MAPK signaling and distinct inflammatory responses. *J Biol Chem* **299**, 105370

201. Russo, A., Soh, U. J. K., Paing, M. M., Arora, P., and Trejo, J. (2009) Caveolae are required for protease-selective signaling by protease-activated receptor-1. *Proceedings of the National Academy of Sciences* **106**, 6393-6397

202. Paing, M. M., Johnston, C. A., Siderovski, D. P., and Trejo, J. (2006) Clathrin Adaptor AP2 Regulates Thrombin Receptor Constitutive Internalization and Endothelial Cell Resensitization. *Mol. Cell Biol.* **26**, 3231-3242

203. Paing, M. M., Temple, B. R. S., and Trejo, J. (2004) A Tyrosine-based Sorting Signal Regulates Intracellular Trafficking of Protease-activated Receptor-1: MULTIPLE

REGULATORY MECHANISMS FOR AGONIST-INDUCED G PROTEIN-COUPLED RECEPTOR INTERNALIZATION. *Journal of Biological Chemistry* **279**, 21938-21947

204. Wolfe, B. L., Marchese, A., and Trejo, J. (2007) Ubiquitination differentially regulates clathrin-dependent internalization of protease-activated receptor-1. *The Journal of Cell Biology* **177**, 905-916

205. Chen, B., Dores, M. R., Grimsey, N., Canto, I., Barker, B. L., and Trejo, J. (2011) Adaptor Protein Complex-2 (AP-2) and Epsin-1 Mediate Protease-activated Receptor-1 Internalization via Phosphorylation- and Ubiquitination-dependent Sorting Signals. *Journal of Biological Chemistry* **286**, 40760-40770

206. Dores, M. R., Lin, H., Grimsey, N. J., Mendez, F., and Trejo, J. (2015) The α-arrestin ARRDC3 mediates ALIX ubiquitination and G protein–coupled receptor lysosomal sorting. *Molecular Biology of the Cell* **26**, 4660-4673

207. Dores, M. R., Chen, B., Lin, H., Soh, U. J. K., Paing, M. M., Montagne, W. A., Meerloo, T., and Trejo, J. (2012) ALIX binds a YPX3L motif of the GPCR PAR1 and mediates ubiquitin-independent ESCRT-III/MVB sorting. *The Journal of Cell Biology* **197**, 407-419

208. Wedegaertner, H., Bosompra, O., Kufareva, I., and Trejo, J. (2023) Divergent regulation of α-arrestin ARRDC3 function by ubiquitination. *Molecular Biology of the Cell* **34**, ar93

209. Oh, E., Kim, J. Y., Sung, D., Cho, Y., Lee, N., An, H., Kim, Y. J., Cho, T. M., and Seo, J. H. (2017) Inhibition of ubiquitin-specific protease 34 (USP34) induces epithelial-mesenchymal transition and promotes stemness in mammary epithelial cells. *Cell Signal* **36**, 230-239

210. Xu, G., Su, H., Lu, L., Liu, X., Zhao, L., Tang, B., and Ming, Z. (2022) Structural insights into the catalytic mechanism and ubiquitin recognition of USP34. *Journal of Molecular Biology*, 167634

211. García-Santisteban, I., Bañuelos, S., and Rodríguez, Jose A. (2011) A global survey of CRM1-dependent nuclear export sequences in the human deubiquitinase family. *Biochemical Journal* **441**, 209-217

212. Brass, L. F., Pizarro, S., Ahuja, M., Belmonte, E., Blanchard, N., Stadel, J. M., and Hoxie, J. A. (1994) Changes in the structure and function of the human thrombin receptor during receptor activation, internalization, and recycling. *Journal of Biological Chemistry* **269**, 2943-2952

213. Dorsam, R. T., and Gutkind, J. S. (2007) G-protein-coupled receptors and cancer. *Nature Reviews Cancer* **7**, 79-94

214. Tomida, T., Takekawa, M., and Saito, H. (2015) Oscillation of p38 activity controls efficient pro-inflammatory gene expression. *Nature Communications* **6**, 8350

215. Dores, M. R., and Trejo, J. (2019) Endo-lysosomal sorting of G-protein-coupled receptors by ubiquitin: Diverse pathways for G-protein-coupled receptor destruction and beyond. *Traffic* **20**, 101-109

216. McCann, A. P., Scott, C. J., Van Schaeybroeck, S., and Burrows, J. F. (2016) Deubiquitylating enzymes in receptor endocytosis and trafficking. *Biochemical Journal* **473**, 4507-4525

217. Smith, G. A., Fearnley, G. W., Abdul-Zani, I., Wheatcroft, S. B., Tomlinson, D. C., Harrison, M. A., and Ponnambalam, S. (2016) VEGFR2 Trafficking, Signaling and Proteolysis is Regulated by the Ubiquitin Isopeptidase USP8. *Traffic* **17**, 53-65

218. Cai, J., Culley, M. K., Zhao, Y., and Zhao, J. (2017) The role of ubiquitination and deubiquitination in the regulation of cell junctions. *Protein & Cell* **9**, 754-769

219. Majolée, J., Kovačević, I., and Hordijk, P. L. (2019) Ubiquitin-based modifications in endothelial cell–cell contact and inflammation. *Journal of Cell Science* **132**

220. Klei, Linda R., Hu, D., Panek, R., Alfano, Danielle N., Bridwell, Rachel E., Bailey, Kelly M., Oravecz-Wilson, Katherine I., Concel, Vincent J., Hess, Emily M., Van Beek, M., Delekta, Phillip C., Gu, S., Watkins, Simon C., Ting, Adrian T., Gough, Peter J., Foley, Kevin P., Bertin, J., McAllister-Lucas, Linda M., and Lucas, Peter C. (2016) MALT1 Protease Activation Triggers Acute Disruption of Endothelial Barrier Integrity via CYLD Cleavage. *Cell Reports* **17**, 221-232

221. Gao, J., Sun, L., Huo, L., Liu, M., Li, D., and Zhou, J. (2010) CYLD regulates angiogenesis by mediating vascular endothelial cell migration. *Blood* **115**, 4130-4137

222. Elliott, P. R., Leske, D., Hrdinka, M., Bagola, K., Fiil, B. K., McLaughlin, S. H., Wagstaff, J., Volkmar, N., Christianson, J. C., Kessler, B. M., Freund, S. M., Komander, D., and Gyrd-Hansen, M. (2016) SPATA2 Links CYLD to LUBAC, Activates CYLD, and Controls LUBAC Signaling. *Molecular cell* **63**, 990-1005

223. Elliott, P. R., Leske, D., Wagstaff, J., Schlicher, L., Berridge, G., Maslen, S., Timmermann, F., Ma, B., Fischer, R., Freund, S. M. V., Komander, D., and Gyrd-Hansen, M. (2021) Regulation of CYLD activity and specificity by phosphorylation and ubiquitin-binding CAP-Gly domains. *Cell Rep* **37**, 109777

224. Schindelin, J., Arganda-Carreras, I., Frise, E., Kaynig, V., Longair, M., Pietzsch, T., Preibisch, S., Rueden, C., Saalfeld, S., Schmid, B., Tinevez, J.-Y., White, D. J., Hartenstein, V., Eliceiri, K., Tomancak, P., and Cardona, A. (2012) Fiji: an open-source platform for biological-image analysis. *Nature Methods* **9**, 676-682

225. Aigouy, B., and Mirouse, V. (2013) ScientiFig: a tool to build publication-ready scientific figures. *Nature Methods* **10**, 1048-1048

226. Stirling, D. R., Swain-Bowden, M. J., Lucas, A. M., Carpenter, A. E., Cimini, B. A., and Goodman, A. (2021) CellProfiler 4: improvements in speed, utility and usability. *BMC bioinformatics* **22**, 433

227. Maneta, E., Aivalioti, E., Tual-Chalot, S., Emini Veseli, B., Gatsiou, A., Stamatelopoulos, K., and Stellos, K. (2023) Endothelial dysfunction and immunothrombosis in sepsis. *Frontiers in Immunology* **14**

228. Xu, S., Ilyas, I., Little, P. J., Li, H., Kamato, D., Zheng, X., Luo, S., Li, Z., Liu, P., Han, J., Harding, I. C., Ebong, E. E., Cameron, S. J., Stewart, A. G., and Weng, J. (2021) Endothelial Dysfunction in Atherosclerotic Cardiovascular Diseases and Beyond: From Mechanism to Pharmacotherapies. *Pharmacological Reviews* **73**, 924-967

229. Daiber, A., Steven, S., Weber, A., Shuvaev, V. V., Muzykantov, V. R., Laher, I., Li, H., Lamas, S., and Münzel, T. (2017) Targeting vascular (endothelial) dysfunction. *British Journal of Pharmacology* **174**, 1591-1619

230. Cleaver, O., and Melton, D. A. (2003) Endothelial signaling during development. *Nature Medicine* **9**, 661-668

231. Li, Y., Li, B., Chen, W.-D., and Wang, Y.-D. (2023) Role of G-protein coupled receptors in cardiovascular diseases. *Frontiers in Cardiovascular Medicine* **10**

232. Wang, J., Gareri, C., and Rockman, H. A. (2018) G-Protein–Coupled Receptors in Heart Disease. *Circulation Research* **123**, 716-735